


7-27-2011

Miniature Mass Spectrometry: RF Amplitude Control System Design

Matthew Allen Kirleis
matt.kirleis@gmail.com

Follow this and additional works at: <http://docs.lib.purdue.edu/techmasters>

 Part of the [Analytical Chemistry Commons](#), [Electrical and Electronics Commons](#), and the [Signal Processing Commons](#)

Kirleis, Matthew Allen, "Miniature Mass Spectrometry: RF Amplitude Control System Design" (2011). *College of Technology Masters Theses*. Paper 50.
<http://docs.lib.purdue.edu/techmasters/50>

This document has been made available through Purdue e-Pubs, a service of the Purdue University Libraries. Please contact epubs@purdue.edu for additional information.

PURDUE UNIVERSITY
GRADUATE SCHOOL
Thesis/Dissertation Acceptance

This is to certify that the thesis/dissertation prepared

By Matthew Allen Kirleis

Entitled

Miniature Mass Spectrometry: RF Amplitude Control System Design

For the degree of Master of Science

Is approved by the final examining committee:

Jeffrey J. Evans

Chair

Zheng Ouyang

John P. Denton

To the best of my knowledge and as understood by the student in the *Research Integrity and Copyright Disclaimer (Graduate School Form 20)*, this thesis/dissertation adheres to the provisions of Purdue University's "Policy on Integrity in Research" and the use of copyrighted material.

Approved by Major Professor(s): Jeffrey J. Evans

Approved by: James L. Mohler

Head of the Graduate Program

7/22/2011

Date

**PURDUE UNIVERSITY
GRADUATE SCHOOL**

Research Integrity and Copyright Disclaimer

Title of Thesis/Dissertation:

Miniature Mass Spectrometry: RF Amplitude Control System Design

For the degree of Master of Science

I certify that in the preparation of this thesis, I have observed the provisions of *Purdue University Executive Memorandum No. C-22*, September 6, 1991, *Policy on Integrity in Research*.*

Further, I certify that this work is free of plagiarism and all materials appearing in this thesis/dissertation have been properly quoted and attributed.

I certify that all copyrighted material incorporated into this thesis/dissertation is in compliance with the United States' copyright law and that I have received written permission from the copyright owners for my use of their work, which is beyond the scope of the law. I agree to indemnify and save harmless Purdue University from any and all claims that may be asserted or that may arise from any copyright violation.

Matthew Allen Kirleis

Printed Name and Signature of Candidate

07/22/2011

Date (month/day/year)

*Located at http://www.purdue.edu/policies/pages/teach_res_outreach/c_22.html

MINIATURE MASS SPECTROMETRY: RF AMPLITUDE CONTROL SYSTEM
DESIGN

A Thesis

Submitted to the Faculty

of

Purdue University

by

Matthew Allen Kirleis

In Partial Fulfillment of the

Requirements for the Degree

of

Master of Science

August 2011

Purdue University

West Lafayette, Indiana

ACKNOWLEDGMENTS

There are too many people and experiences to list that have culminated to this point, but I will try to do my best. I first want to thank my new wife, Katie, for the support and listening to things she never knew she would care about. To my mother for the unconditional support and for being a great Mom. A thank you to my faculty committee, especially Prof. Jeffrey J. Evans for the reviews and meeting time during the course of my graduate studies. A special thanks goes to Frank Boudreau for continual support, direction, leadership and knowledge he brought on a day to day basis. I would like to thank Prof. R. Graham Cooks and Prof. Zheng Ouyang for the opportunity to work at Aston Labs and for their patience and trust during the design of the electronics used in this research. Additional insightful reviews were done by Nick Charipar, Dr. Alberto Piqué, Katie Masterson, Katie Kirleis, Frank Boudreau, and Dr. Robert Noll.

TABLE OF CONTENTS

	Page
LIST OF TABLES	v
LIST OF FIGURES	vi
ABSTRACT	ix
CHAPTER 1. INTRODUCTION	1
1.1. Scope	7
1.2. Significance	8
1.3. Research Question	9
1.4. Limitations	9
1.5. Delimitations	10
1.6. Assumptions	10
1.7. Summary	10
CHAPTER 2. LITERATURE REVIEW	12
2.1. Ionization and Sampling	12
2.1.1. Low Temperature Plasma (LTP)	13
2.1.2. Atmospheric Pressure Chemical Ionization (APCI)	13
2.1.3. Nano Electrospray Ionization	13
2.1.4. Paper Spray	14
2.1.5. Discontinuous Atmospheric Pressure Interface (DAPI)	14
2.2. Mass Analysis	15
2.2.1. Mass Analyzers	15
2.2.2. RF Trapping Signal	17
2.2.3. AC Signal (Resonant Excitation)	19
2.2.4. Electron Multiplier	20
2.2.5. Scan Function	20
2.3. Miniature Instruments	21
2.3.1. Mini 10	21
2.3.2. Mini 11 and Mini 11.5	22
2.4. Summary	22
CHAPTER 3. FRAMEWORK AND METHODOLOGY	24
3.1. Testing Methodology	24
3.2. Sample Set	27
3.3. Summary	28
CHAPTER 4. EXPERIMENTS AND RESULTS	29
4.1. Design and Construction	29
4.1.1. Data Acquisition Electronics	32

	Page
4.1.2. Feedback Circuit.....	36
4.1.3. Instrument Hardware and Vacuum	38
4.2. Simulation.....	40
4.3. Results	46
4.3.1. AC and RF Signal Generation Analysis	46
4.3.2. Controller Comparison	48
4.3.3. Spectra	51
4.3.4. Cost Analysis	68
4.4. Summary	69
CHAPTER 5. CONCLUSIONS	70
5.1. Future Work.....	72
LIST OF REFERENCES	73
APPENDIX	79

LIST OF TABLES

Table	Page
Table 4-1 – Digital Controller Cost on Mini 12 electronics	68
Table 4-2 – Analog Controller Cost on Mini 12 electronics	68

LIST OF FIGURES

Figure	Page
Figure 1-1 – Mass Spectrometer Block Diagram	1
Figure 1-2 – Exploded View of the inside of the Mini 11.5 (Rendering created by Tsung-Chi Chen, Purdue University)	3
Figure 1-3 - Compounds consisting of Carbon, Hydrogen, Nitrogen, Oxygen between m/z 180.0 and 180.2 (Hoffmann & Stroobant, 2007, p. 246)	4
Figure 1-4 – Open Loop Response of the RF Amplification System.....	5
Figure 1-5 – Analog RF Control Block Diagram of Mini 11.5	6
Figure 2-1 DAPI interface connected to a vacuum system.....	14
Figure 2-2 Ion trap stability diagram generated experimentally (Ouyang et al., 2004).	16
Figure 2-3 Rendering of an RIT with labeled electrodes (Ouyang et al., 2004) ..	17
Figure 2-4 – Mass resolution improvement from changing the RF mixer IC from and Texas Instruments MPY634KPU to an Analog Devices AD835 (Kaplan, 2006)	19
Figure 2-5 - Typical mass scan sequence	21
Figure 3-1 - Mini MS instrument block diagram: Mini 11.5.....	26
Figure 3-2 - Mini MS instrument block diagram: Mini 12 with Mini 11.5.....	26
Figure 3-3 – Mini MS instrument block diagrams: Mini 12	27
Figure 4-1 – Scan Function used to collect experimental spectrum.	31
Figure 4-2 – Vacuum pressure reading during a scan function	31
Figure 4-3 – System Block Diagram for Mini 12 control electronics.....	32
Figure 4-4 – FPGA Block Diagram of the internal functions of the Mini 12 FPGA.....	33
Figure 4-5 – Top view (left) and bottom view (right) of the Control Board, A0BME503	34
Figure 4-6 – Top view (left) and bottom view of the Analog Interface Board, A0BME502	35
Figure 4-7 – Control board and Analog Interface board connected together.....	35
Figure 4-8 - Custom designed Mini12 instrument control interface displaying the simultaneously acquired Mass Spectra and associated RF ramp envelope.	36
Figure 4-9 – RF capacitive divider feedback circuit	37
Figure 4-10 – Plot of the RF feedback gain as a function of frequency	38
Figure 4-11 – Rendering of the RIT, ion detector and DAPI inlet as mounted in the Mini MS instrument (Rendering created by Frank Boudreau, Purdue University).....	39

Figure	Page
Figure 4-12 - Photo of the Mini11.5 chassis with the Mini12 data acquisition electronics connected to apparatus	39
Figure 4-13 – Measured Open Loop step response	40
Figure 4-14 – Plant based on measured open loop response	41
Figure 4-15 – MATLAB Simulink Simulation Diagram	42
Figure 4-16 – Resulting Simulink PID Tuning results	42
Figure 4-17 - ModelSim Simulation of the RF digital demodulation performed in the FPGA.....	44
Figure 4-18 – Reference Ramp Generator ModelSim Simulation.....	44
Figure 4-19 – Measured step response of RF amplifier using simulation results and manually tuned gains.....	45
Figure 4-20 – Measure Ramp from 0 to 85% of full scale using gains $K_p = 0$, $K_i = 4$, $K_d = 0$, $T = 1.6\mu s$	45
Figure 4-21 – Measure Ramp from 0 to 85% of full scale using gains $K_p = 4$, $K_i = 0.25$, $K_d = 4$, $T = 1.6\mu s$	46
Figure 4-22 – Data acquisition electronics frequency output accuracy	47
Figure 4-23 – Mini 11.5 and 12 AC output analysis	47
Figure 4-24 - Mini 11.5 and 12 RF output analysis	48
Figure 4-25 – Open loop response of the RF amplifier, 100ms ramp	49
Figure 4-26 – Digital controller response of the RF amplifier, 100ms ramp	50
Figure 4-27 – Analog controller response with Mini12 electronics of the RF amplifier, 100ms ramp	50
Figure 4-28 - Analog controller response with Mini11.5 electronics of the RF amplifier, 100ms ramp	51
Figure 4-29 – Example RF Resonant Frequency Analysis	52
Figure 4-30 – 10ppm nano-ESI PEG mass spectrum.....	53
Figure 4-31 – Mass Accuracy of 8 selected peaks from a 10ppm PEG sample for the Mini 12 digital controller	53
Figure 4-32 – Mass Accuracy of 8 selected peaks from a 10ppm PEG sample for the Mini 12 using the analog controller	54
Figure 4-33 – 2000 Mini 12 single scan mass spectrum from the Digital and Analog controller configurations	56
Figure 4-34 – 500 Mini 11.5 spectrum of DEET sampled at 100Ksps	56
Figure 4-35 – Mass Drift Analysis of DEET over 1 hour of operation	57
Figure 4-36 – Measured Mass Resolving Power during mass drift test.....	57
Figure 4-37 – Observed glitch in RF signal (blue line) for DEET Spectrum (red line) captured during the second scan using Mini 12 electronics and the analog controller at the start of the mass drift test.	58
Figure 4-38 - Observed glitch in RF signal (blue line) for DEET Spectrum (red line) captured using Mini 12 electronics and the analog controller after the 12 th scan captured during the mass drift test.	58
Figure 4-39 - Observed glitch not present in the RF signal (blue line) for DEET Spectrum (red line) captured using Mini 12 electronics and the digital controller after the 12th scan captured during the mass drift test.	59

Figure	Page
Figure 4-40 - Example Single Scan mass spectra of a 10ppm sample of Methyl Salicylate (m/z 153) collected with the Mini 12 electronics and analog controller.....	60
Figure 4-41 - Mass Resolving and Drift recorded using Mini 12 electronics and the analog controller for a 10ppm sample of Methyl Salicylate (m/z 153).....	60
Figure 4-42 - Example Single Scan mass spectra of a 10ppm sample of Methyl Salicylate (m/z 153) collected with the Mini 12 electronics and digital controller.....	61
Figure 4-43 - Mass Resolving and Drift recorded using Mini 12 electronics and the digital controller for a 10ppm sample of Methyl Salicylate (m/z 153)	61
Figure 4-44 - Example Single Scan mass spectra of a 10ppm sample of cocaine (m/z 304.2) collected with the Mini 12 electronics and analog controller, mass calibration correction was corrected in MATLAB	62
Figure 4-45 - Mass Resolving and Drift recorded using Mini 12 electronics and the analog controller for a 10ppm sample of Cocaine (m/z 304.2)	62
Figure 4-46 - Example Single Scan mass spectra of a 10ppm sample of Cocaine (m/z 304.2) collected with the Mini 12 electronics and digital controller	63
Figure 4-47 - Mass Resolving and Drift recorded using Mini 12 electronics and the digital controller for a 10ppm sample of Cocaine (m/z 304.2).....	63
Figure 4-48 - Example Single Scan mass spectra of a 10ppm sample of Methamphetamine (m/z 150, fragment m/z 91) collected with the Mini 12 electronics and analog controller	64
Figure 4-49 – Mass Resolving and Drift recorded using Mini 12 electronics and the analog controller for a 10ppm sample of Methamphetamine (m/z 150, fragment m/z 91)	64
Figure 4-50 – Example Single Scan mass spectra of a 10ppm sample of Methamphetamine (m/z 150, fragment m/z 91) collected with the Mini 12 electronics and digital controller	65
Figure 4-51 - Mass Resolving and Drift recorded using Mini 12 electronics and the digital controller for a 10ppm sample of Methamphetamine (m/z 150, fragment m/z 91)	65
Figure 4-52 – Mass Resolving Power Summary for both Analog and Digital Controller for compounds Methyl Salicylate, Cocaine, Methamphetamine, and DEET	66
Figure 4-53 – Mass Spectrum of isotopically labeled Tamoxifen.....	67
Figure 4-54 – Peak Valley presented as a percentage of peak intensity	67
Appendix Figure	
Figure A-1 – VHDL PID Controller Code Listing	79

ABSTRACT

Kirleis, Matthew A. M.S., Purdue University, August 2011. Miniature Mass Spectrometry: RF Amplitude Control System Design. Major Professor: Jeffrey J. Evans.

This thesis covers the methods used to construct and characterize a custom digital RF amplitude control system. Many types of mass spectrometers exist, but few have been miniaturized as much as the Mini instruments developed at Purdue University. The goal of this research was to improve upon an earlier amplitude control system consisting of analog circuits first implemented in the Mini 11.5 mass spectrometer developed at Purdue University.

A custom set of control and data acquisition electronics were developed for testing the digital and analog control systems in a Mini 11.5 mass spectrometer chassis. A MATLAB Simulink simulation was done to aid the design of the digital controller. Software code was created in C, VHDL, and Visual Basic.NET to operate and collect mass spectra. Tests were performed to compare and contrast critical performance attributes. A cost analysis was also performed.

Important findings were that the digital controller as designed was a more costly solution by a factor of 4, but created a more linear amplification than the previous Mini 11.5 analog solution. The improved linearity increased mass resolution by 0.5. Mass drift measurements showed that the RF signal from the digital controller varied between +0.6 to -0.2 m/z, but the analog solution varied between +1.7 to -0.5 m/z.

CHAPTER 1. INTRODUCTION

The field of mass spectrometry came into its own when J.J Thompson constructed the mass spectrometer (MS) in 1912 to study molecular isotopes by controlling the movement of ions with electrical and magnetic fields (Hoffmann & Stroobant, 2007, p. 6). Since then, more applications for this family of instruments have been discovered and their utility keeps increasing. Mass spectrometers can be used to identify unknown molecules from explosives (Harper et al., 2008) to proteins (Segura et al., 2009) and to determine origins of foods such as wheat (Branch, Burke, Evans, Fairman, & Wolff Briche, 2003). Other uses include atmospheric air quality monitoring, detecting illicit drugs and explosives for airport security, and food quality testing by quantifying the amount of pesticides or other toxins present (Mulligan, Talaty, & R. G. Cooks, 2006). Today's mass spectrometers are sensitive enough to measure molecular concentrations in the parts per billion range (Bruins, 1991).

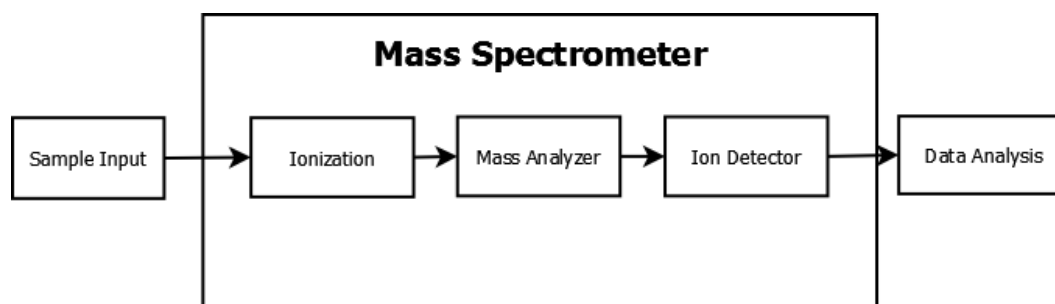


Figure 1-1 – Mass Spectrometer Block Diagram

A mass spectrometer is an instrument that is used to “weigh” molecules as they travel through its three major blocks: ionization, mass analysis, and ion detection (see Figure 1-1). To measure the masses of the compounds in a

sample, they must first be converted into ions by giving a positive or negative charge using an ionization source. Next the ions are directed into a mass analyzer and held in a quadrupolar electrical field. This field is generated by applying by applied trapping potentials referred to as r.f. voltage (RF) and a.c. voltage (AC) to an ion trap. The RF signal is the single ended dominate trapping signal ranging in the hundreds to thousands of volts peak to peak and is used to manipulate the ions inside the trap. The AC signal is a dipolar (differential) lower amplitude signal with voltages less than one hundred volts peak to peak and is used to assist the RF during mass analysis and isolate ions before mass analysis if desired.

During mass analysis the electrical trapping potentials are linearly amplitude modulated (AM) from a lower potential to higher potential amplitude with a fixed RF and AC frequency, to eject the ions according to their mass to charge ratio (m/z). The ejected ions then impact an ion detector, which produces the digitally sampled spectral signal of m/z versus voltage (sometimes referred to as intensity). The envelope of the RF ejection sequence used during amplitude modulation affects the timing of when the ions leave the trap in the mass analysis, so it must be linear and repeatable. The linearity of an MS is referred to as the mass accuracy. How well the instrument can discern between two adjacent molecular masses is called the mass resolution. The limit of detection (LOD) of the instrument is a measure of how many ions must be trapped and ejected in order to register a signal above the noise floor.

Recently, miniaturization of the mass spectrometer system from a large 500lbs plus bench top instrument to a hand portable instrument weighing in at 8.8lbs has been demonstrated by Gao, Sugiarto, Harper, R. Graham Cooks, and Ouyang, 2008. This has been done to achieve portability, reduce power, lower cost, and to expand the areas where mass spectrometers can be utilized.

One application of the technology would be for airport security inspectors or emergency first responders to carry the instrument to an inspection site. This

instrument is capable of quickly detecting the presence of explosives or deadly gases by just waving the MS over luggage or near packages, for example.

On the other hand, Ouyang and Cooks (2009) report that there is still a need to develop data analysis algorithms to “translate the raw spectral data into information needed to draw conclusions”. A key experimental parameter, over which control must be established in order to automate the data analysis is the mass accuracy of the instrument creating the data. Measured masses need to be discriminated in a reproducible fashion in order to be properly analyzed with an algorithm for automated detection (Jeffries, 2005).

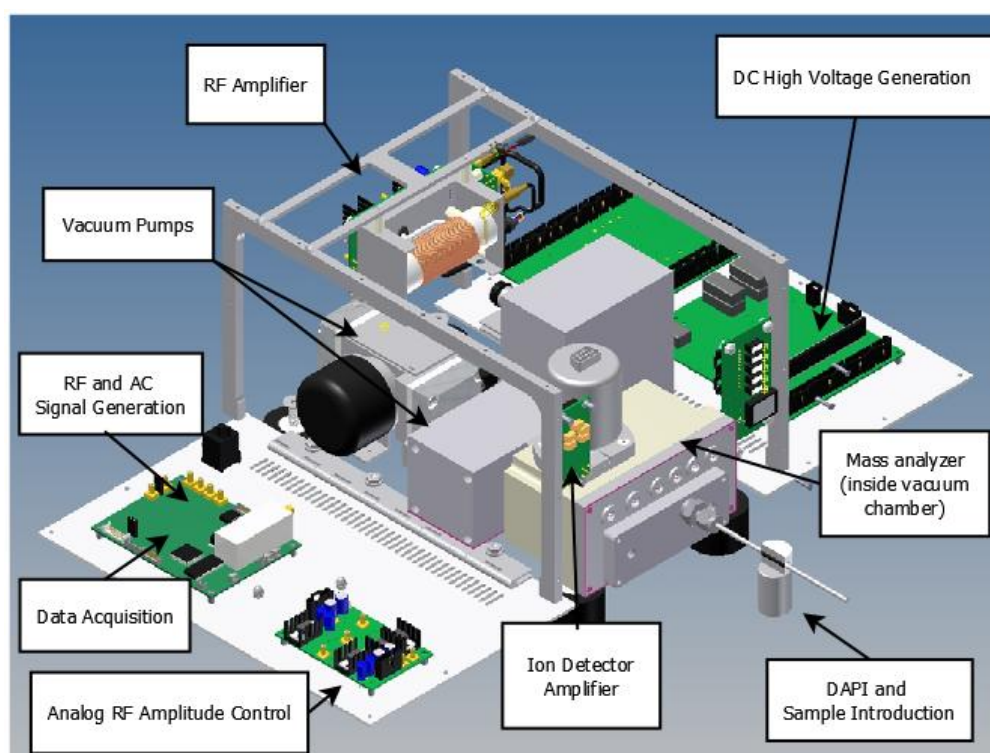


Figure 1-2 – Exploded View of the inside of the Mini 11.5 (Rendering created by Tsung-Chi Chen, Purdue University)

The latest miniature MS developed at Purdue University is the Mini 11.5 (“CAID - Center for Analytical Instrumentation Development,” n.d.). The author has worked with this instrument platform, writing user interface software and designing electronics. A rendering of the open instrument is shown in Figure 1-2,

which highlights its key elements. Ions formed from the sample enter through the Discontinuous Atmospheric Pressure Interface (DAPI), where the Rectilinear Ion Trap (RIT) mass analyzer resides in a vacuum chamber with a pressure of approximately 1×10^{-5} torr (Ouyang et al., 2004; Gao et al., 2008). Two low voltage control signals are output by the control electronics to create the RF trapping potentials. The signals are a fixed amplitude sinusoidal wave output from a Direct Digital Synthesizer (DDS) and a reference amplitude profile output by a Digital to Analog Converter (DAC). The two signals are fed into the RF amplifier where they are amplified in voltage and current. A low voltage proportional AM feedback signal of the RF signal at the ion trap electrodes is demodulated to recover the amplitude profile. The demodulated and reference amplitude profile signals are compared to determine the error between them. Using the error signal from the analog comparison, a corrected amplitude profile is input into an analog AM mixer located on the control electronics.

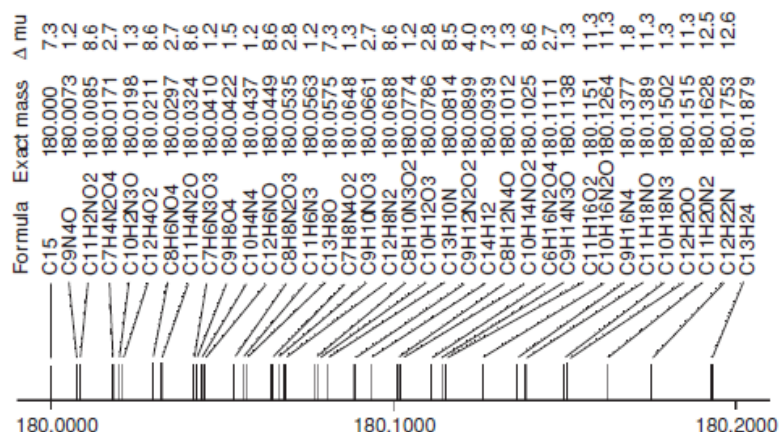


Figure 1-3 - Compounds consisting of Carbon, Hydrogen, Nitrogen, Oxygen between m/z 180.0 and 180.2 (Hoffmann & Stroobant, 2007, p. 246)

An internal study done at Purdue University of the open loop performance of the RF amplifier (Frank Boudreau, CAID) used in the Mini 11.5 found that the amplification is non-linear and results in errors of 2-3 m/z in the upper end of the instrument mass range (600 to 900 m/z). It is an error of 0.33%, but taking into

consideration of the possible number of compounds from m/z 180.0 to 180.2 containing only carbon, hydrogen, nitrogen and oxygen in Figure 1-3 the chance of correct identification is limited when the m/z reading can be 2-3 m/z in error. The non-linear response waveform was verified during this study by recording the open loop response of a 0 to full scale ramp using a Tektronics DPO4024 oscilloscope. Figure 1-4 illustrates the input reference (red) and normalized open loop demodulated amplitude profile (blue) of the full scale ramp. By comparing the input envelope of the reference ramp to the measured envelope of the feedback signal (normalized to the reference signal) it can be observed that the low mass range is also affected since low mass ions are ejected at lower voltage amplitudes. An analog RF amplitude control system to correct the linearity issues was developed recently (See Figure 1.5); however, it is susceptible to electrical component tolerance variations, temperature fluctuations and must be manually tuned by replacing parts for every MS system.

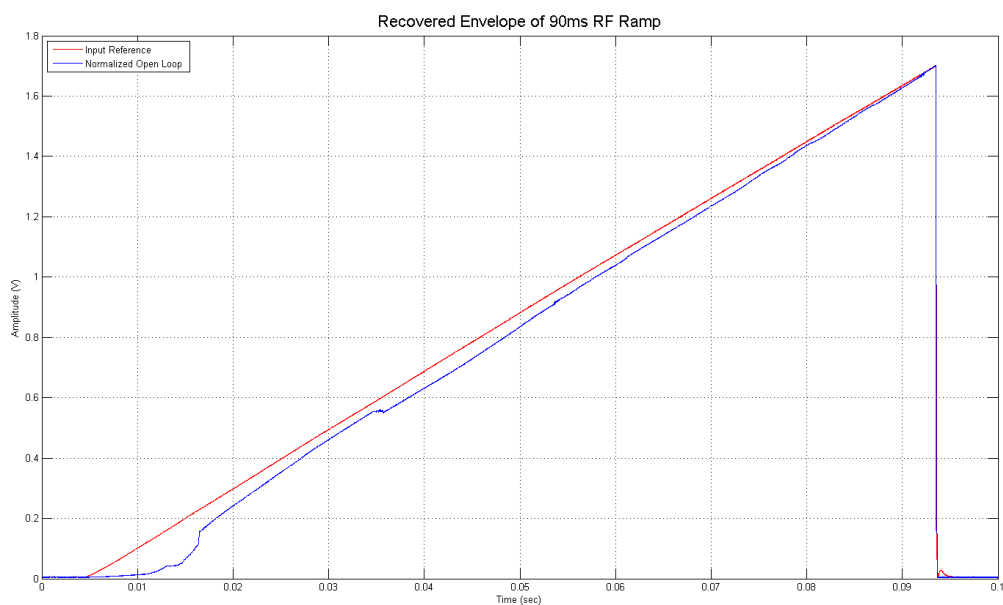


Figure 1-4 – Open Loop Response of the RF Amplification System.

The RF signal controls the trapping and timing of ions leaving the trap during a mass analysis scan for ion trap mass spectrometry (ITMS). This signal along with vacuum pressure and ion trap geometries affects mass range, mass

accuracy and mass drift (Raymond E. March, 1997). The sinusoidal RF signal is boosted to voltages greater than $4000V_{pk-pk}$ using an inductor-capacitor (LC) tank circuit operated at the resonance frequency, with the ion trap and coaxial connection cable forming the capacitive element and a hand wound air core coil constructed from common components such as magnet wire and acrylic tubing, forming the inductor part of the tank circuit. Air core hand wound inductors are often used because of their characteristics; inductance value is unaffected by current, low permeability core that saturates at higher currents, low harmonic distortion and better (Quality) Q-factor compared with magnetic or iron core inductors (Sullivan, Weidong Li, Prabhakaran, & Shanshan Lu, 2007). Unfortunately air core inductors become more susceptible to stray field radiation and are larger in physical size than magnetic core inductors.

The operating frequency of the RF signal is variable depending on the geometry of the trap used and the selected range of operation, but for the Mini 11.5 the RF frequency is designed to be a nominal 1MHz (Gao, Q. Song, Patterson, R. G. Cooks, & Ouyang, 2006). The amplitude of the RF signal determines when the trapped ions become unstable and are ejected from the ion trap, so the linearity of the envelope for this signal directly affects the mass accuracy of the instrument.

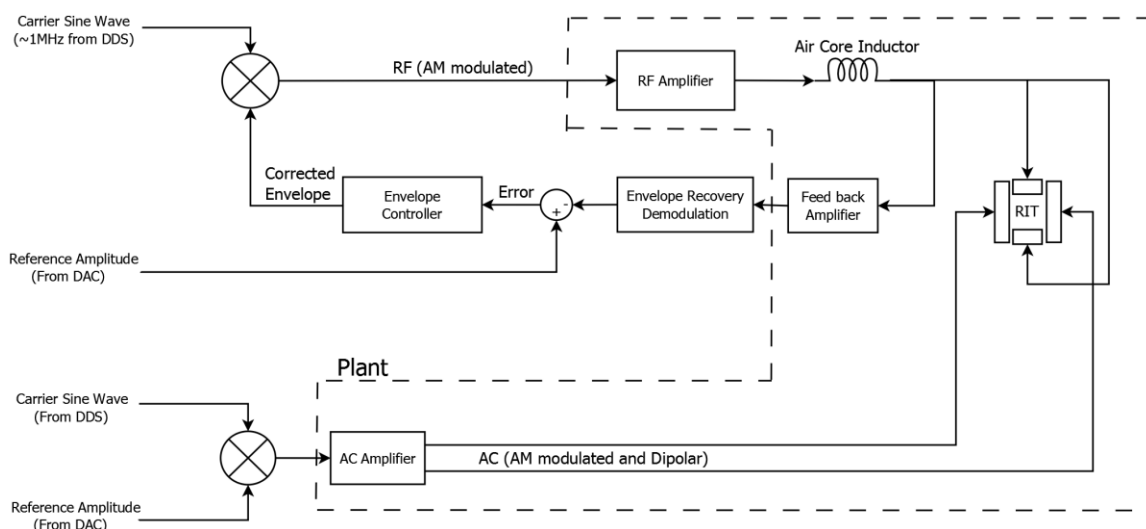


Figure 1-5 – Analog RF Control Block Diagram of Mini 11.5

The RF ramp envelope is the controlled variable which is manipulated based on the comparison of the reference signal and the measured feedback from the RF amplifier. Using control theory terminology, the plant was defined as the process of AM amplification of the RF 1MHz sinusoidal signal and the actuator was defined as the RF amplifier, RIT, air-core inductor, feedback amplifier and AC amplifier highlighted by the dashed line in Figure 1-5.

A common method used for closed loop control over a system is called Proportional – Integral – Derivative (PID) (Bennett, 1984). This method uses three terms derived from the measured error of the reference signal and the feedback signal. The proportional term is the difference between the reference and the feedback, also referred to as the error signal. The integral term is the history or sum of past errors. Finally the derivative term is the rate of change in the error signal. The sum of these signals can be used to create a new corrected signal that is inputted into the plant such that it will match the desired reference. Multiple combinations of the PID controller terms have been conceived such as PI, P, I, or PD depending on the application. The current design for ramp control is an analog circuit that uses an operational amplifier circuit to integrate the difference from the error signal and reference signal. The result of the integration forms an integrator (I) controller. Using a digital domain design with a Field Programmable Gate Array (FPGA), parts of the PID control loop can be added or removed quickly without requiring a PCB change or part change as in the case of the current analog design. This reduces the time to tune the control loop to get the controller to operate with a reduced error from the input reference signal.

1.1. Scope

Mass spectrometry instrumentation is a broad field of study with a growing number of contributors. For example, at the 2010 American Society for Mass Spectrometry (ASMS) annual conference there were over 6,500 attendees as reported by the ASMS official website. Historically, there have been many types of mass analyzers such as Fourier Transform Ion Cyclotron Resonance (FTICR)

(Marshall, 1985), time of flight (TOF) (Campana, 1987), Orbitrap (Hu et al., 2005), and ion traps (IT) (Paul, 1990). To date, the instrument type that has achieved the smallest size of 1.5 kg are mass spectrometers using ion traps as the mass analyzer. Characteristics such as low vacuum operation requirement and tandem mass spectrometry make ion traps ideal for miniature mass analysis instruments (Song et al., 2010).

Previous work done by Gao, Song, Patterson, Cooks, and Ouyang (2006) and Gao, Sugiarto, Harper, Cooks, and Ouyang (2008) in building their Mini 10 and Mini 11 instruments have led to portable instruments capable of performing *in situ* analysis with the most recent version being the Mini 11.5. All of these instruments used an $x_0 = 5\text{mm}$, $y_0 = 4\text{mm}$ by $z_0 = 40\text{mm}$ RIT, which has rectangular electrodes rather than the hyperbolic ones found in a Linear Ion Trap (LIT) (Schwartz, Senko, & Syka, 2002). This simplified geometry makes for relaxed mechanical tolerances in exchange for mass resolving power (Ouyang et al., 2004).

Miniature Mass Spectrometers are not pushing the bounds of analytical chemistry in terms of mass resolving power and LOD, but rather expand the range of applications and increase access to non-specialists users due to greater instrument portability. Because it is impractical to consider training every user of the instrument in analytical chemistry, automated processing capability must be accounted for in the system design. Instrument mass accuracy and repeatability is needed to do this. A miniature MS fitted with a digital RF control system, could achieve better performance with a reduction in circuit components, mass accuracy, mass resolving power, and mass drift.

1.2. Significance

An ultimate goal is to bring the portability and parts per billion detection (Bruins, 1991) sensitivity of the mass spectrometer instrument, a precision transducer, to the masses and improve the lives and safety of people. Resulting spectra from mass spectrometers provide useful information to a trained analyst,

such as the presence of a harmful toxin, but not to an untrained user. This is especially apparent when instrument performance variations are present in resulting data. With automatic analysis, a doctor could someday be able to precisely monitor their patient's individual reaction to a drug in order to reduce unwanted side effects and increase treatment effectiveness at a much lower cost than today. Lab results such as toxicity reports or blood analysis can take up to days before results are returned, losing critical treatment time, but miniature instruments might produce results in minutes on site.

In general, mass repeatability starts with the RF signal control system. Integration of the waveform mixer, demodulator and envelope controller sub blocks, implemented as an analog solution in the Mini 11.5, would instead benefit from a digital design contained in a FPGA if the same level of performance could be met. Such a digital solution would provide a reduction in physical part count and be a more reproducible solution.

1.3. Research Question

Can a digital demodulation and amplitude control system perform better than the current Mini 11.5 design, which uses an analog control system to control the linearity of the RF modulation?

1.4. Limitations

The following limitations are being made:

- The mass analyzer used in the instrument is an $x_0 = 5\text{mm}$, $y_0 = 4\text{mm}$ by $z_0 = 40\text{mm}$ RIT which has been used previously in the Mini 10, Mini 11 and Mini 11.5 instruments.
- The instrument under test will be limited to a Mini 11.5 outfitted with newly designed Mini 12 digital electronic boards
- The research is limited to ion trap mass spectrometer instruments.

- The research is limited to analysis of molecules with mass to charge ratios less than 1500 as reported as an upper limit for miniature instruments by Ouyang and Cook 2009
- The sensor used to measure the presence of ions will be an electron multiplier

1.5. Delimitations

The following delimitations are being made:

- Electromagnetic Compatibility (EMC) compliance will not be required.
- Vacuum system used a turbo molecular pump backed with by a diaphragm pump.

1.6. Assumptions

The following assumptions are being made:

- A miniature mass spectrometer is defined as a system with a volume under 14000cm^3 and weighing no more than 30lbs.
- The system was capable of collecting analytical data.
- The system was powered by a reliable power source – 120V AC.

1.7. Summary

This chapter covered the extents and purpose for bridging the gap in RF signal control. In the next chapter, a review of the key technologies to enable miniature mass spectrometers and how other instrument aspects affect instrument performance will be discussed. Then in Chapter Three, the method used to determine how performance was measured is discussed. It will involve a simulation model of the RF subsystem as compared to empirically collected data. The simulation model was used in the design of the control loop parameters. Then mass spectra collected from the instrument was evaluated using these

performance criteria: mass accuracy, mass drift, mass resolving power, mass resolution, linearity of the RF envelope, and system cost.

CHAPTER 2. LITERATURE REVIEW

This chapter covers important previous works that have enabled the reduction of the lab scale mass spectrometers to portable miniature instruments and the parameters that affects instrument performance.

2.1. Ionization and Sampling

Before any mass spectral generation or analyte identification can be achieved, a chemical sample must be given at least one electrical charge to become an ion. This process is called ionization. When molecules are ionized, their motion can be controlled using magnetic or electric fields. The way the ions move in the fields provides a method to differentiate each of them by mass to charge ratio and thus identify them. Ion trap mass spectrometry can only be performed within a vacuum, but can be performed at lower vacuum than all other types of mass analysis instruments (Song, et al., 2010). In order to analyze a sample it must be placed in the vacuum chamber or ionized molecules must be drawn into the instrument from atmospheric pressure. The method of ionization used to create ions must be known when comparing spectra because variations in ionization energy cause molecules to fragment differently thereby creating different spectral results. Portability and *in situ* measurements are a key part of miniaturization, so atmospheric pressure direct sampling ionization sources will be discussed.

2.1.1. Low Temperature Plasma (LTP)

Recently Harper et al. (2008) developed a new ionization method called Low Temperature Plasma that has proved to be an effective ionization source that can ionize samples in the liquid, solid, or gaseous form. The electrical design is simple, consisting of a step-up transformer, a 2-5kHz bipolar wave source, and a glass probe. Proper alignment and configuration was not critical to performance, which makes it easy for an untrained person to use. A drawback of LTP is that it is generally only able to ionize low mass molecules of less than 500m/z (Harper et al., 2008).

2.1.2. Atmospheric Pressure Chemical Ionization (APCI)

APCI was first reported by E. C. Horning, M. G. Horning, Carroll, Dzidic, & Stillwell (1973). This source is very simple to make by combining a positive or negative 3-5kV DC voltage source with a needle or piece of thin wire. The effect of having the high voltage in air will create ions of molecules in the gas phase. A drawback is that the operator mishandling of the ion source can lead to a significant shock hazard.

2.1.3. Nano Electrospray Ionization

Nano electrospray ionization (nano-ESI) is considered as “the most efficient method of introducing a liquid sample for direct analysis by mass spectrometry” (El-Faramawy, Siu, & Thomson, 2005). The source is constructed with a glass capillary that has been pulled such that the tip diameter is 1 to 10 μ m. Then 1 to 5 μ L of solution and a metal electrode is loaded into the capillary (Karas, Bahr, & Dülcks, 2000). A DC high voltage of 1500V to 2000V is applied to the electrode which and causes a Taylor cone to form that sprays the ionized droplets of the solution into the mass spectrometer.

2.1.4. Paper Spray

Recently Wang, Liu, Cooks, and Ouyang (2010) used triangular shaped chromatography paper and a +4kV DC high voltage source to directly sample biological fluids. A simple and quick procedure for dried blood spot analysis was developed. This procedure only requires a simple solvent, such as methanol, to be added to the dried blood spot to start analysis. Then a DC high voltage is applied to the base of the triangle, which drives the solvent and ions to spray off the tip of the paper. The significance of this ionization source is that it could easily be performed at a doctor's office, perhaps to monitor how a patient metabolizes a drug, without a need for a full laboratory.

2.1.5. Discontinuous Atmospheric Pressure Interface (DAPI)

After creating the ions in atmosphere, they need to be introduced into the vacuum chamber for mass analysis. Large laboratory scale mass spectrometers have multiple differential stages that are continuously pumping in order to bring the ions into the ion trap (Ouyang & Cooks, 2009). These vacuum pumps are heavy and consume hundreds of Watts to maintain the vacuum pressure.

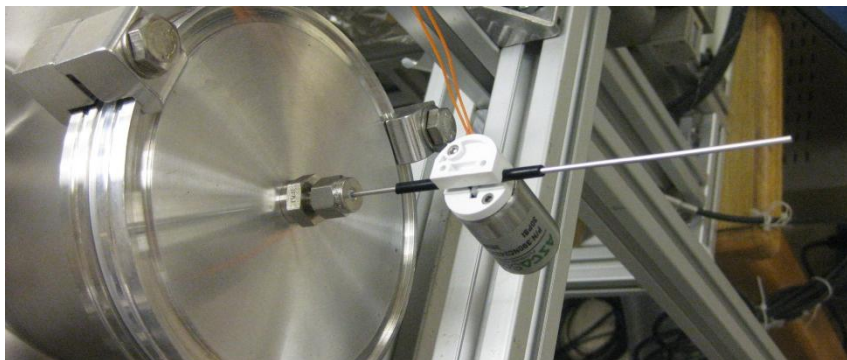


Figure 2-1 DAPI interface connected to a vacuum system.

Miniature mass spectrometers do not have the luxury of these pumps and thus a new interface was developed. This interface is called the Discontinuous Atmospheric Pressure Interface (DAPI) developed by Gao, Cooks, and Ouyang

(2008). The DAPI, pictured in Figure 2-1, consists of a pinch valve made by ASCO Scientific and two stainless steel capillary tubes. A 24Vdc (2.5W) signal is applied for 10 to 100ms to the valve in order to actuate the valve open during the ionization period. The valve returns to the closed position via an internal spring. Song et al. (2010) studied mass spectral properties at high pressures and found that mass resolution decreased, with observed peaks becoming wider, decreasing the mass resolving power of the ion trap. Mass resolving power is a ratio of the m/z value of the peak divided by the $\Delta m/z$ of the full width at half maximum of the peak. The measured masses also started to shift along the x-axis as vacuum pressure was increased, affecting the mass accuracy of the results. To isolate the effects from vacuum pressure on mass resolution, mass resolving power and mass drift from the RF signal generation, the vacuum pressure must be started at a consistent level from scan to scan.

2.2. Mass Analysis

After the samples have been successfully ionized and introduced into the vacuum chamber, mass analysis can begin inside the ion trap. To perform mass analysis using an ion trap, four main signals need to be precisely controlled with a high granularity of amplitude and frequency. The output electrical signals are called RF, AC, ion trap end cap voltage and electron multiplier voltage (Ouyang et al., 2004). While these signals are output to the trap, the electron multiplier output signal is sampled and recorded.

2.2.1. Mass Analyzers

Ion traps are designed to trap moving ions using time-dependent quadrupolar electric field potentials. A set of equations used to describe the motion of particles in these fields were developed by the French mathematician Émile Léonard Mathieu in the 1800's while studying vibrating stretched skins (Raymond E. March, 1997). The functions are known as the Mathieu equations.

The derivation of these functions is outside the scope of this literature review, but it is important to note that they are used to describe a stability region, i.e., combinations of RF and DC voltages applied to the trap electrodes where ions undergo stable repetitive motion and can thus be trapped and then removed precisely by their mass to charge ratio. Figure 2-2 depicts an experimental mapping of the stability region done by Ouyang et al. (2004) while studying the Rectilinear Ion Trap.

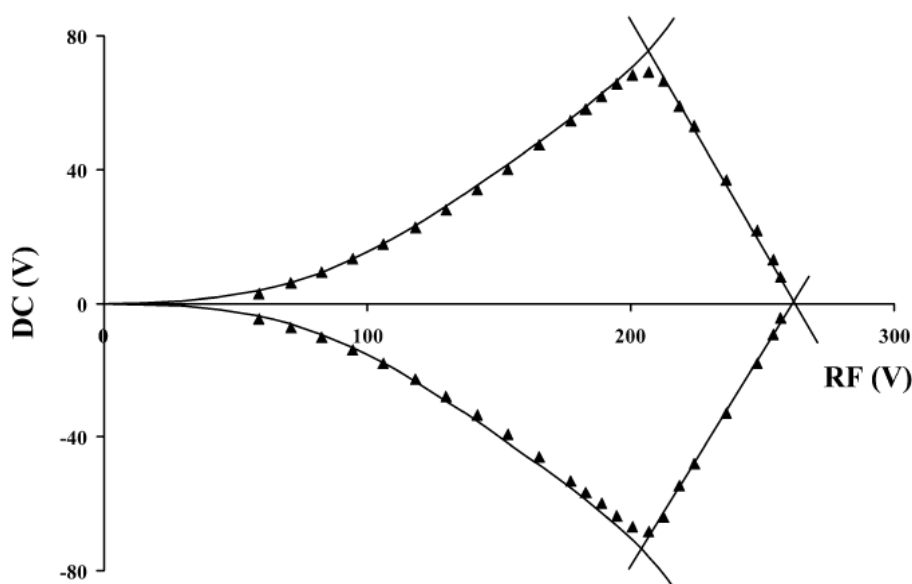


Figure 2-2 Ion trap stability diagram generated experimentally (Ouyang et al., 2004).

2.2.1.1. Rectilinear Ion Trap (RIT)

In 2004 Ouyang et al. reported a new type of mass analyzer called the RIT. The RIT was designed to be low cost, easy to assemble, and have a high trapping capacity (ability to hold ions within the trap). This ion trap, shown in Figure 2-3, consists of six rectangular electrodes that form a box shape. The RIT simplifies the complex hyperbolic surfaces of the LIT and still outperforms the simplified QIT (Cylindrical Ion Trap CIT) (Ouyang et al., 2004). This was not the first time rectangular electrodes were used to manipulate ions, but it was the first time they were used as a mass analyzer (Ouyang et al., 2004).

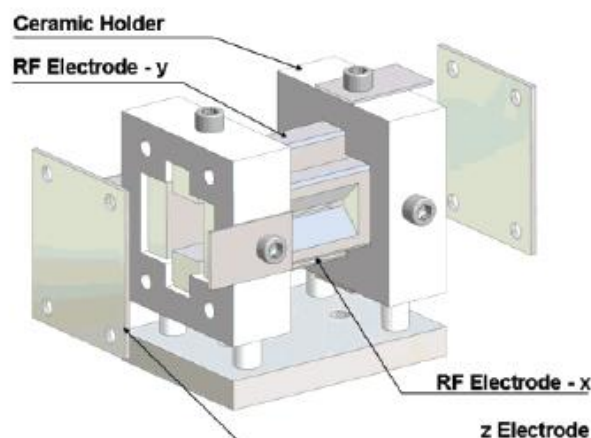


Figure 2-3 Rendering of an RIT with labeled electrodes (Ouyang et al., 2004)

Previous miniature instruments called the Mini 10 and Mini 11 have proven that the RIT is a viable mass analyzer that fulfills the needs of a miniature instrument design by achieving a mass resolution of one m/z unit (Gao et al., 2006, 2008). Unfortunately it is unclear what criteria was used to make that claim because the valley between the peaks did not reach the baseline nor a specified percentage of the valley to peak height was given. Ions as large at $1500m/z$ and as low as $60 m/z$ have been successfully analyzed on these instruments, but doing this requires different RF resonant frequencies. The attributes of an RIT are well suited for miniature instruments because of its small size (4mm by 5mm by 40mm), large trapping capacity and simple construction. This study of the RF amplitude control system will be limited to this type of ion trap.

2.2.2. RF Trapping Signal

The most critical signal applied to the ion trap is the RF signal. This signal controls mass range, potential well depth, and instrument accuracy (Raymond E. March, 1997). The sinusoidal RF signal needs to be amplified to voltages greater than 4000Vpp using a inductor-capacitor tank circuit, with the ion trap forming the

capacitor element and a hand wound air-core coil constructed from common parts such as magnet wire and acrylic tubing form the inductor part of the tank circuit. The frequency is usually established during the design of the mass analyzer and is not varied during a mass scan, but March (1997) stated that the RF frequency can be lowered to increase the mass range while forgoing the trapping of light masses. Unfortunately shifting the frequency of the RF will change the resonant tuning of the LC tank reducing the maximum voltage amplitude. Generally, the RF signal is designed to be nominally 1MHz for the RIT geometry of 4mm by 5mm (Gao et al., 2008; Jonscher & Yates, 1997; Raymond E. March, 1997; Ouyang & R. G. Cooks, 2009).

Schaefer et al. (2008) designed a unique RF control system that incorporated digital elements to replace an analog self-resonant oscillator drive circuit on an ion trap system. Their system used a FPGA to operate two DACs, one used to output a DDS waveform and the other for the envelope amplitude control. The feedback of the amplified signal was demodulated using an RMS to DC circuit so that only the envelope was sampled by the FPGA using an ADC. This allowed the amplitude controller to reside in the FPGA. The end result of the study showed that the harmonic distortion was reduced in the output RF signal thus reducing mass drifting over time. Mass drifting refers to an instrument's RF stability and can be measured by inputting a sample and collecting continuous spectra over time. It is a good indicator of the combined frequency and voltage stability of the RF signal (Schaefer et al. 2008). This work is similar to the proposed system with a digital control system, but differs with external demodulation and AM mixing done in the analog domain.

There is an important phase relationship between the AC and RF waveforms (Londry & R. E. March, 1995). If uncontrolled the recorded mass accuracy can vary by 0.25%. This is another source of error that will need to be minimized in this study.

In experiments performed by Kaplan (2006) mass resolving power was improved by simply changing the analog mixer for the RF signal generation in

Figure 2-4. Kaplan (2006) also explained that his instrument did not have feedback control the RF signal “which caused the peaks to broaden” when averaging multiple scans together.

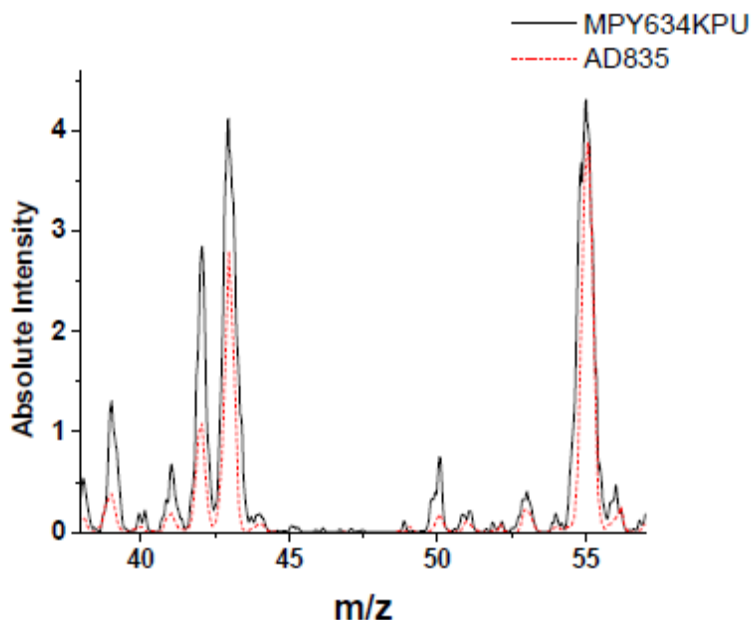


Figure 2-4 – Mass resolution improvement from changing the RF mixer IC from and Texas Instruments MPY634KPU to an Analog Devices AD835 (Kaplan, 2006)

2.2.3. AC Signal (Resonant Excitation)

Another important signal, the AC signal, is used to increase instrument resolution and perform mass isolation, but at much lower amplitudes (less than 30Vpp) than the RF signal (Jonscher & Yates, 1997). As with the RF, the AC signal is a sinusoidal wave, but is dipolar as it is applied only between the two “x”-electrodes of the RIT (Julian & R. G. Cooks, 1993). The AC signal is at most half the frequency of the RF signal.

A special kind of broadband excitation, applied to the same AC electrodes and called a Stored Waveform Inverse Fourier Transform (SWIFT) wave, is used to enhance isolation of selected ions in the trap and reject all unwanted ions (Chen, Wang, Ricca, & Marshall, 1987). Julian and Cooks (1993) used the

SWIFT wave to exclude unwanted ions from entering the trap during ionization. This is particularly useful for removing unwanted background ions from ambient ionization sources.

2.2.4. Electron Multiplier

After the ions are being ejected by the combination of the RF and AC signals, they are sent to an electron multiplier (Raymond E. March, 1997). This is the final stage of mass analysis done on the instrument. The electron multiplier output current is amplified by over 1 million, converted to voltage, sampled with an ADC and displayed digitally.

2.2.5. Scan Function

All of the previous signals are synchronized together to form a single mass scan function (Raymond E. March, 1997). Figure 2-5 is a typical example of a scan function developed for analysis on the Mini 11.5 instrument. The scan begins by opening the DAPI interface to bring in the sample ions. This action also brings in ambient air into a vacuum, raising the pressure from 1×10^{-5} torr to approximately 1×10^{-3} torr, depending on the duration of the DAPI open time. The RF voltage is operating at constant amplitude during this period to trap incoming ions. Next there is a delay period to allow the vacuum system to pump out unwanted ambient air and return the vacuum pressure to the near 1×10^{-5} torr. Then the ion detector is switched on and mass analysis begins. The RF voltage and AC voltages are linearly ramped while the processor reads the signal output from the ion detector, shown as the amplitude envelope in Figure 2-5. The increasing amplitude of the RF causes the trapped ions to move to the edges of the ion trap and ejects them in order of mass to charge ratio. The rate at which the RF and AC signals are ramped influences the mass resolving power with a slower rate (130usec/Dalton) yielding better resolution than a faster ramp rate of 60usec/Dalton (Kaiser Jr., Graham Cooks, Stafford Jr., Syka, & Hemberger,

1991). It will be important to maintain the same scan rates when collecting mass spectra data.



Figure 2-5 - Typical mass scan sequence

2.3. Miniature Instruments

Miniaturized versions of ion trap mass spectrometers have been built before, each using different electronic platforms (Gao et al., 2006, 2008; Yang, T.-Y. Kim, Hwang, Yi, & D.-H. Kim, 2008). However, the software and hardware design was not discussed in enough detail to allow reconstructing a set of design constraints. To further the advance of miniature mass spectrometry a collection of technologies and minimum electrical solutions needs to be created.

2.3.1. Mini 10

The Mini 10 was first published in 2006 by Gao et al. (2006). This was a collaboration with Griffin Analytical Instruments, where all the software, firmware and electronic control boards were provided in a closed source fashion. The instrument itself was successful at collecting data, but electrical and software design information was unknown. The mass drift of the instrument was unclear because it was not stated in Gao et al. (2006).

2.3.2. Mini 11 and Mini 11.5

Gao et al. (2008) further reduced overall size, weight and power consumption of the miniature instrument. In order to miniaturize the instrument to the 4.8kg a custom turbo pump was used (Creare, Inc., Hanover, NH) which carried a cost of \$60,000. This was impractical, so the vacuum system from the Mini 10 was fitted with the Mini 11 electronic control board. The new system was called the Mini 11.5. The author of this summary has personally worked with this instrument. The mass spectrometer control board was designed with the specific requirement of achieving a small form factor and low power consumption. Because of this, SWIFT wave generation could not be done, reducing the instruments analytical capabilities. Memory size and processor choices also limited the number of samples that could be captured to 40kBytes and the speed at which data could be downloaded from the instrument was limited to 14.4kB/s. These design tradeoffs resulted in a maximum scan length of 195ms and required 2.77 seconds to transmit the full amount of data collected, also reducing the throughput of the instrument.

2.4. Summary

In this chapter a review of the literature was conducted for mass analyzers, previous miniature mass spectrometers, ion generation and ion introduction all of which play a role in a mass spectrometer's performance. Mass accuracy is affected by vacuum pressure, AC and RF phase relationship, ion trap type and the RF signal generation. Mass resolution and mass resolving power is affected by the vacuum pressure, scan ramp rate, ion trap and RF signal generation. Mass drift is affected by RF amplitude ramp repeatability. Mass resolving power is affected by the ion trap geometry, vacuum pressure and RF signal generation. The observed mass spectrum from a molecule is affected by the ionization method used to create the ions. The effects of these phenomena

will be minimized in order to quantify the RF amplitude control system performance. Next, the method to complete this analysis will be discussed.

CHAPTER 3. FRAMEWORK AND METHODOLOGY

The purpose of creating a digitally controlled RF system was to improve the performance beyond that of the current Mini 11.5 design. A measure of this was developed using the following parameters listed below.

- Mass Accuracy – A measure of the accuracy in m/z of the reported location of a mass on the x-axis
- Mass Drift – A measure of the stability of the m/z reading over time from a single sample input.
- Mass resolving power ($m/\Delta m_{50\%}$): “The observed mass divided by the mass peak width at 50% height for a well-isolated single mass spectral peak.” (Hoffmann & Stroobant, 2007, p. 245)
- Mass resolution (either $m_2 - m_1$ in m/z or $(m_2 - m_1)/m_1$ in ppm): “The smallest difference between equal-magnitude peaks such that the valley between them is a specified fraction of either peak height.” (Hoffmann & Stroobant, 2007, p. 245)
- Linearity of RF envelope modulation.
- Total Cost – Sum of individual electrical component cost in quantities of 1000.

3.1. Testing Methodology

A digital waveform generation comparison was performed to ensure that the Mini 12 digital electronics perform as well as the Mini 11.5. Frequency spectral analysis of the digital waveforms produced by the digital electronics of the Mini 11.5 and Mini 12 electronics was done. A constant full amplitude RF

signal was measured at frequencies from 900 kHz to 1.1MHz and comparisons were made for total harmonic distortion (THD), spurious free dynamic range (SFDR) and output frequency accuracy. This was then repeated for the AC signal with frequency ranges from 100 kHz to 500 kHz. Frequency accuracy was measured with an HP 5315A universal counter.

A simulation model in MATLAB Simulink of the RF amplifier was created. Using the simulation model, a PID controller was developed and optimized. Finally a functional verification of the controller was done using the Mini 12 control electronics. Waveforms of the feedback signal were recorded with an oscilloscope and evaluated with MATLAB to measure the linearity of the RF envelope.

This research was conducted on one instrument platform, but with three different RF controlling and data acquisition setups. The instrument platform included the vacuum system, high voltage board, power distribution board, RF amplifier, ion detector amplifier board and DAPI interface. The baseline system was a system with Mini 11.5 control and data acquisition electronics shown in Figure 3-3. The next system consisted of a Mini 12 control and data acquisition electronics configured to operate the RF amplifier with the analog controller shown in Figure 3-32. This required the use of the Mini 11.5 control board as an off board mixer with DDS to maintain the minimal amount of differences. All other signals were sourced and synchronized from the Mini 12 electronics. The final configuration was the newly designed Mini12 control and data acquisition boards ran as a digital mixer and RF amplitude controller shown in Figure 3-33.

The diagram illustrates the experimental setup for the RIT ion trap. It shows the following components and their interconnections:

- Sample Ions** enter the **DAPI Interface**, which connects to the **Vacuum Chamber RIT Ion Trap**.
- The **Vacuum Chamber RIT Ion Trap** is connected to a **Turbo Pump** and a **Rough Pump**.
- The **Vacuum Chamber RIT Ion Trap** sends an **Ion Current** signal to the **Ion Detector Amplifier Board**.
- The **Ion Detector Amplifier Board** outputs a **Voltage** signal to the **Mini 12 Mass Spectrometer Controller Board (DAQ)**.
- The **RF Amplifier board** provides an **RF 5.3kVpp AM** signal to the **Vacuum Chamber RIT Ion Trap** and a **Feedback** signal to the **Mini 11.5 Mass Spectrometer Controller Board**.
- The **Mini 11.5 Mass Spectrometer Controller Board** (containing a **DDS**) provides a **Signal** to the **RF Amplifier board** and a **Correct Ref. Env.** signal to the **Mini 12 Mass Spectrometer Controller Board (DAQ)**.
- The **Mini 12 Mass Spectrometer Controller Board (DAQ)** (containing a **1.25Msps 16bit ADC**) provides a **Ref. Env.** signal to the **RF Amplifier board** and a **DAC** signal to the **High Voltage Board (HVB)**.
- The **High Voltage Board (HVB)** provides an **ADC** signal to the **Mini 12 Mass Spectrometer Controller Board (DAQ)** and a **Voltage** signal to the **Ion Detector Amplifier Board**.
- The **Power Distribution Board** provides power to the **RF Amplifier board**, **Mini 11.5 Mass Spectrometer Controller Board**, **Mini 12 Mass Spectrometer Controller Board (DAQ)**, and **High Voltage Board (HVB)**.
- The **Mini 12 Mass Spectrometer Controller Board (DAQ)** is connected to a **PC User Interface** via **Serial to Ethernet 14.4kB/s** and to a **PC Data Display Data Storage Configuration User Interface** via **USB 2.0 5MB/s**.

Figure 3-2 - Mini MS instrument block diagram: Mini 12 with Mini 11.5

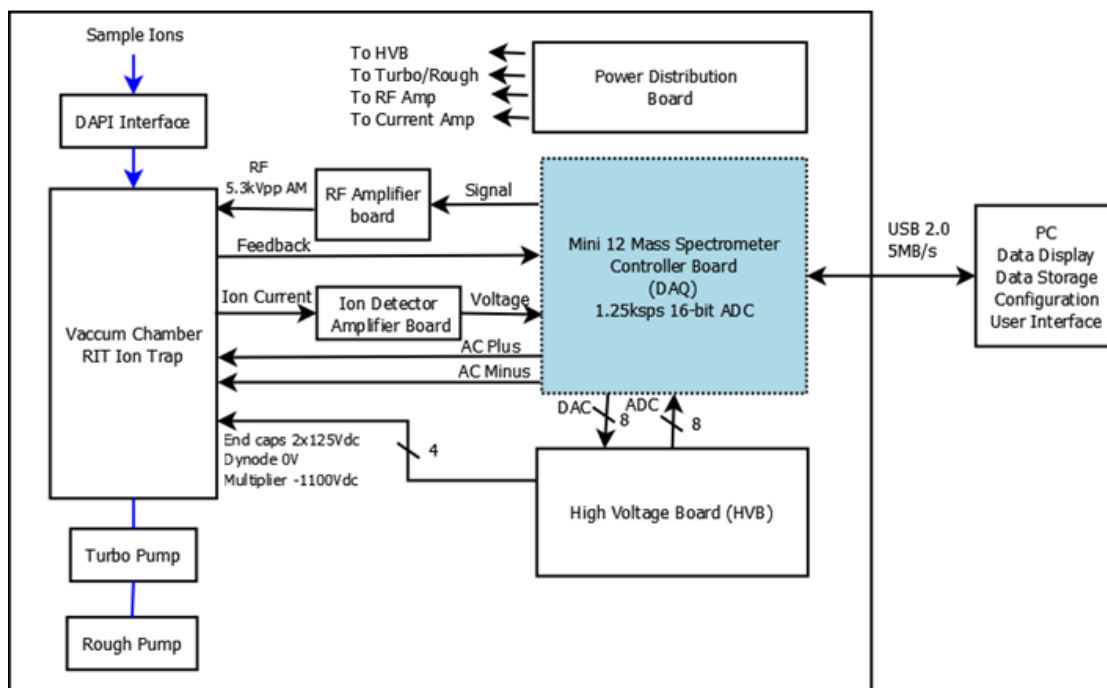


Figure 3-3 – Mini MS instrument block diagrams: Mini 12

3.2. Sample Set

Mass spectrum was measured on a Mini 11.5 chassis configured in three ways described in Section 3.1. Four chemical compounds found in previous miniature mass spectrometer literature, Gao et al., 2008, Gao et al., 2008 and Keil et al., 2007, were collected and analyzed. The compounds used were methyl salicylate, diethyltoluamide (DEET), cocaine and polyethylene glycol (PEG). These compounds did differ from those originally proposed due to the fact that three of the compounds produce m/z readings outside of the dynamic mass range of the instrument as configured during testing. The data collected by the instrument was saved to hard disk by the user interface as ADC sample reading number and the magnitude as recorded from the ion detector. In the case of the Mini 12 electronics, an additional output was the demodulated RF signal collected by the FPGA.

Frequency spectra and harmonic analysis was done using a Tektronix DPO 4032 oscilloscope. An HP 5315A universal counter was used to measure the frequency accuracy.

3.3. Summary

This chapter discussed the research methods used to complete the task of determining the performance of Mini MS using an analog controller solution versus a digital controller solution for RF amplitude control.

CHAPTER 4. EXPERIMENTS AND RESULTS

The earlier chapters discussed previous works that have led up to this research. In this chapter, the research data from the test outlined in Chapter 3 was used to attempt to determine if a digital demodulation and amplitude control system could perform better than the Mini 11.5 design, which uses an analog control system to control the linearity of the RF modulation. First, the design and construction of the system under test is discussed. Then the simulation results are given. Finally the experimentally collected data will be presented.

4.1. Design and Construction

The ion trap mass spectrometer for this research consisted of three major components: the vacuum system, an ionization source and the data acquisition electronics. The vacuum system consisted of the ion trap electrodes, an electron multiplier, a turbo molecular pump and a diaphragm pump discussed further in section 4.1.3. For this research, the vacuum system was not altered from the Mini 11.5 system. The purpose of the ionization source was to create ions of the sample. Two methods were used to ionize samples, APCI and nano-ESI. Ions were introduced into the vacuum system via the DAPI inlet. The data acquisition electronics were composed of 5 main PCBs: ion detector amplifier, high voltage board, power distribution board, RF amplifier and data acquisition board. All PCBs except the data acquisition board were kept constant during this study.

In order to create a mass spectrum, a time synchronized series of events, referred to as the scan function, took place. Previous parameters reported in the Mini 10, Mini 11 and Mini 11.5 instruments were used as a starting place for developing an optimized scan function. Exact matching parameters were not

used because geometry variation from the machining resulted in differences in the RIT electrical fields reflected in the AC and RF frequencies used. There was an optimum resonant point where the AC signal adds enough energy to the ion motion in the trap and to aid in the ejection of the ion, creating a better mass resolved spectrum. The RF, for the Mini 10, was reported as 1MHz and the AC was reported to be 350 kHz. For this experiment the RF was set to 998MHz and the AC was 351 kHz. Figure 4-1 below diagrams the scan function used. During the pre-scan, the RF signal started at level referred to as the trapping voltage. This RF amplitude was at a set where it is low enough to hold the ions in a steady motion without ejecting them.

During the ionization segment, the DAPI inlet pinch valve was opened to bring in a sample of ions from atmosphere. A spike in pressure from 1×10^{-5} torr to over 1×10^{-3} torr occurred inside the vacuum chamber during the ionization segment. Excess gas was removed during the ion cooling and pump out segment in order to achieve the best possible mass resolving power. Figure 4-2 is an oscilloscope capture of the MKS 925C vacuum pressure output (yellow trace) and the RF feedback signal (blue trace) recorded during a typical scan function.

After cooling, the AC signal was ramped up to a starting point just below where it could cause ejection and the end cap voltages were increased to 125Vdc. In the final segment called mass analysis, the RF and AC signals were simultaneously AM modulated while the ion detector signal is recorded. The result of the mass analysis segment is a single scan mass spectrum.

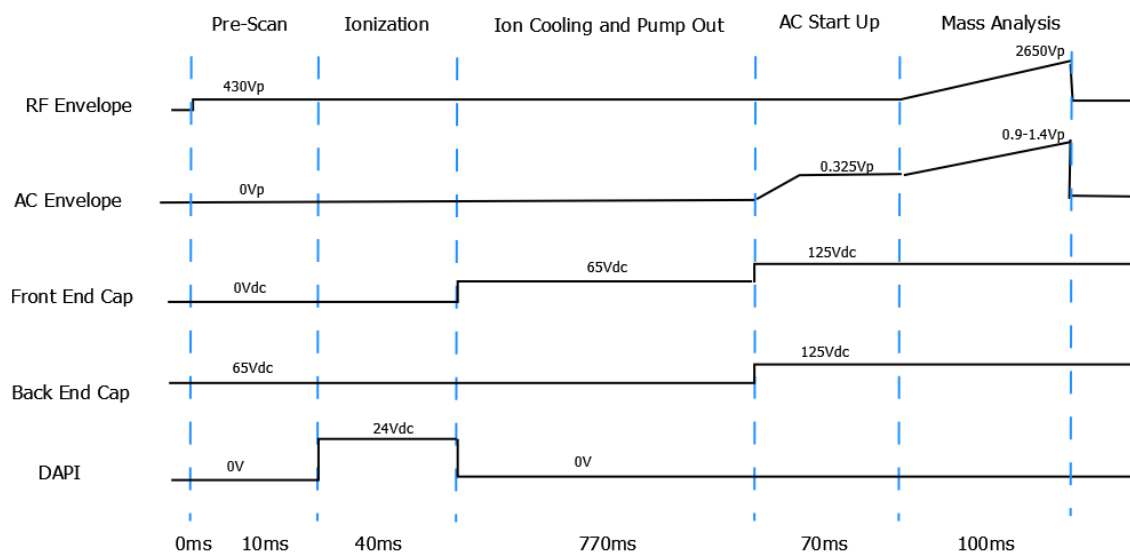


Figure 4-1 – Scan Function used to collect experimental spectrum.

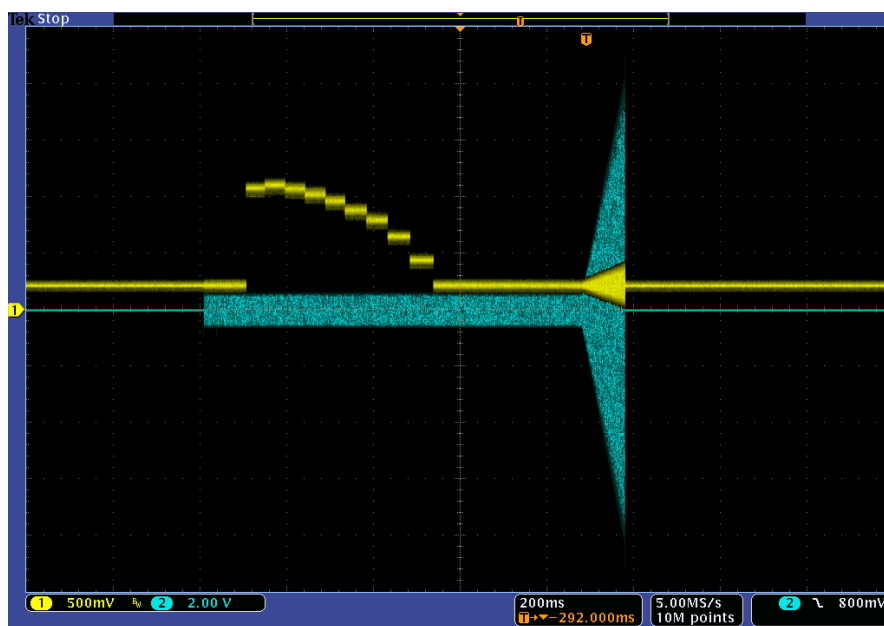


Figure 4-2 – Vacuum pressure reading during a scan function

4.1.1. Data Acquisition Electronics

A new platform for the next generation of miniature mass spectrometers at Purdue University called the Mini 12 was developed. It improves on the previous Mini 11.5 design with more processing capability and on board memory. When the platform was conceived, it was designed to operate in two modes. First, it would be able to function the same as the Mini 11.5 digital electronics board. This included creating a carrier signal of fixed amplitude and separate amplitude envelope output of the RF signal to provide to the RF amplifier and analog control electronics. The second mode of the proposed design would use the FPGA to amplitude modulate the RF signal then demodulate the feedback signal and operate a digital control loop for RF amplitude ramp correction. Figure 4-3 below shows a system diagram of the new architecture.

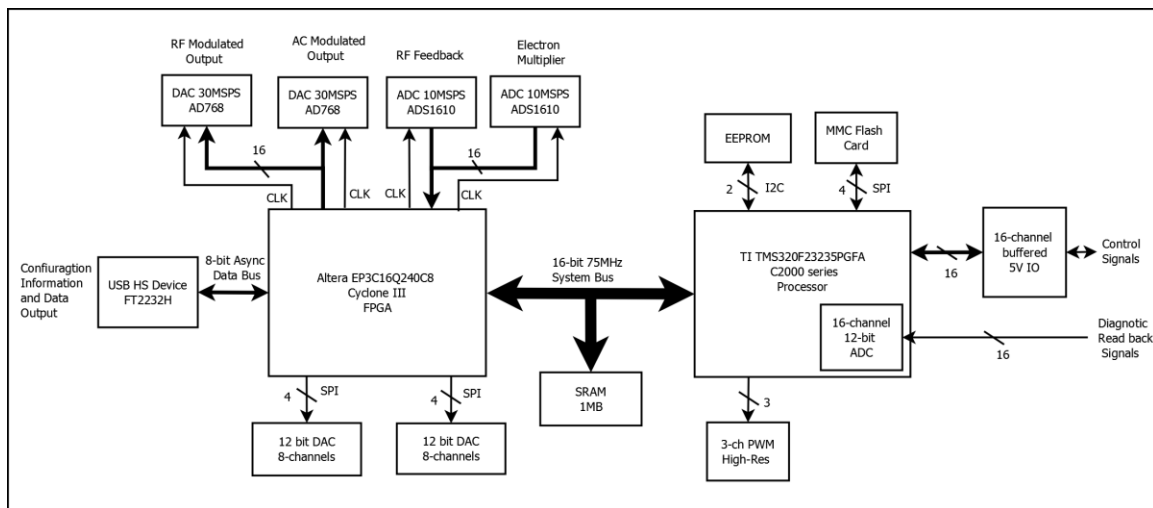


Figure 4-3 – System Block Diagram for Mini 12 control electronics

The embedded processor performed tasks associated with instrument diagnostics, communication, power management and scan function implementation. The processor was a TMS320F28235PGFA from the C2000 processor family made by Texas Instruments (TI). In total there were 48 commands that could be passed between the user interface and processor over USB 2.0. Communication packets were handled by the processor after the FPGA

translated the 8-bit USB data to the C2000 16-bit system bus. The processor code was developed using TI's Code Composer Studio v4.1 and consisted of 20,566 lines of C code. Final compiled code size was 10kB using 16kB of internal SRAM.

The FPGA ran the critical RF digital PID controller designed for this research. Additional functionality included waveform generators, two SPI interfaces, four unique parallel interfaces and direct memory access (DMA) controller. FPGA functionality (Figure 4-4) was written in VHDL and compiled using Altera's Quartus II 9.2. In total 14461 lines of VHDL code were developed for the Mini 12 design which includes the design files and the test benches created to simulate the design files. That code occupied 38% of the logic elements, 53% of the total memory bits and 39% of the multipliers available in the EP3C16Q240C8 Cyclone III FPGA made by Altera Corporation. Signals were interfaced by single ended digital logic to an analog interface board (Figure 4-6) with two 10Msps ADCs and two 30Msps DACs via a 120-pin board to board connector.

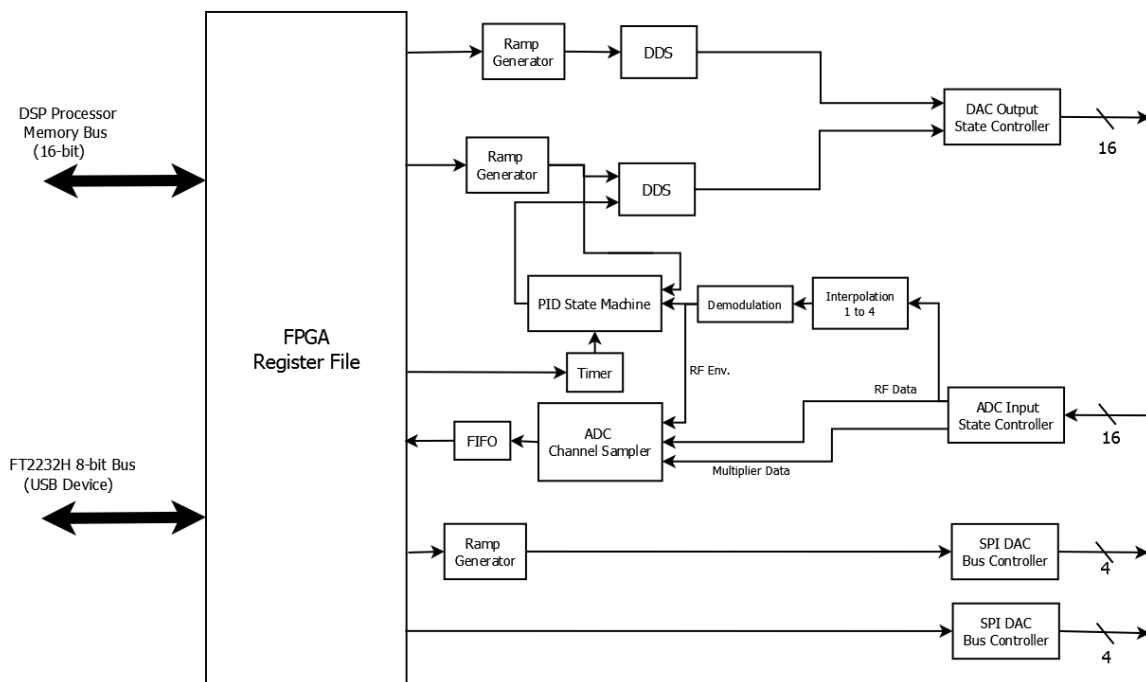


Figure 4-4 – FPGA Block Diagram of the internal functions of the Mini 12 FPGA

Below is an outline of the features made available in the Mini 12 architecture. Figure 4-5, Figure 4-6, and Figure 4-7 show where these features were mapped in the PCBs.

- A. Simultaneous output for synchronization of signals and RF digital controller
- B. Timing and Interface to the user interface
- C. RF and AC Phase Control
- D. High Speed USB 2.0 connection, up to 5Mbyte/s to capture stream data during the entire mass scan
- E. General Purpose channels of ADC, DAC and IO channels for general purpose (total 16 each)
- F. DC high voltage level controls and RF envelope output via 16 individual DAC channels
- G. Removable flash MMC Memory card slot
- H. 150MHz Texas Instruments C2000 DSP
- I. 3 high resolution pulse width modulators with external voltage input level
- J. 4.5in by 4.5in by 2in footprint
- K. Two 30MSPS Digital to Analog Converts with full 16-bit resolution
- L. Two 10MSPS Analog to Digital Converts with full 16-bit resolution
- M. 1Mbyte of SRAM

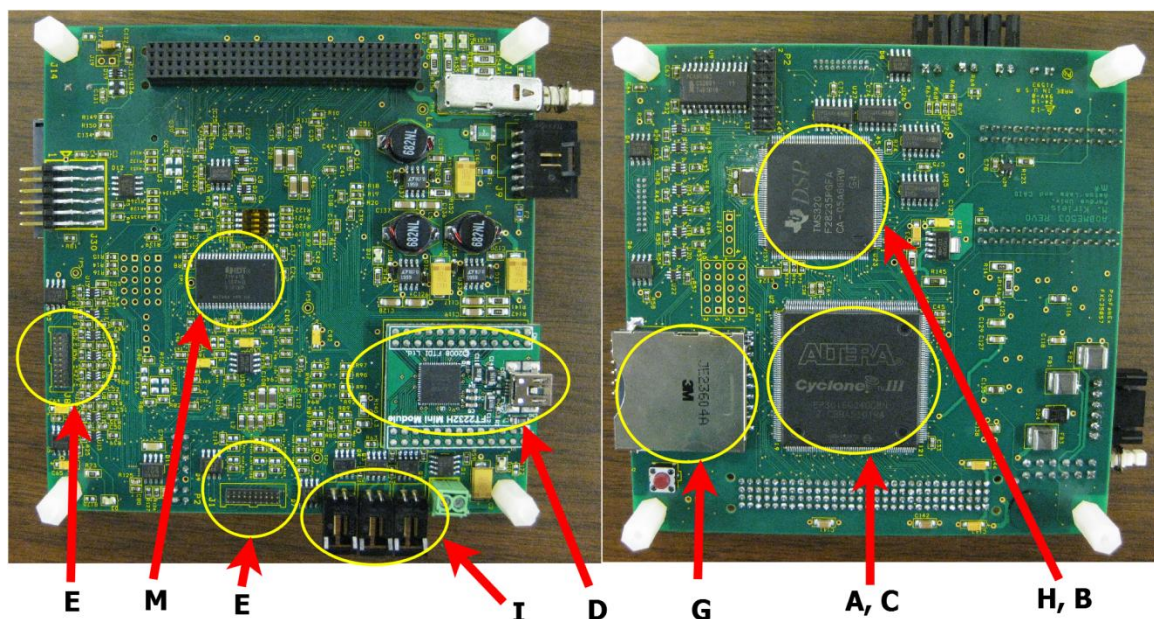


Figure 4-5 – Top view (left) and bottom view (right) of the Control Board, A0BME503

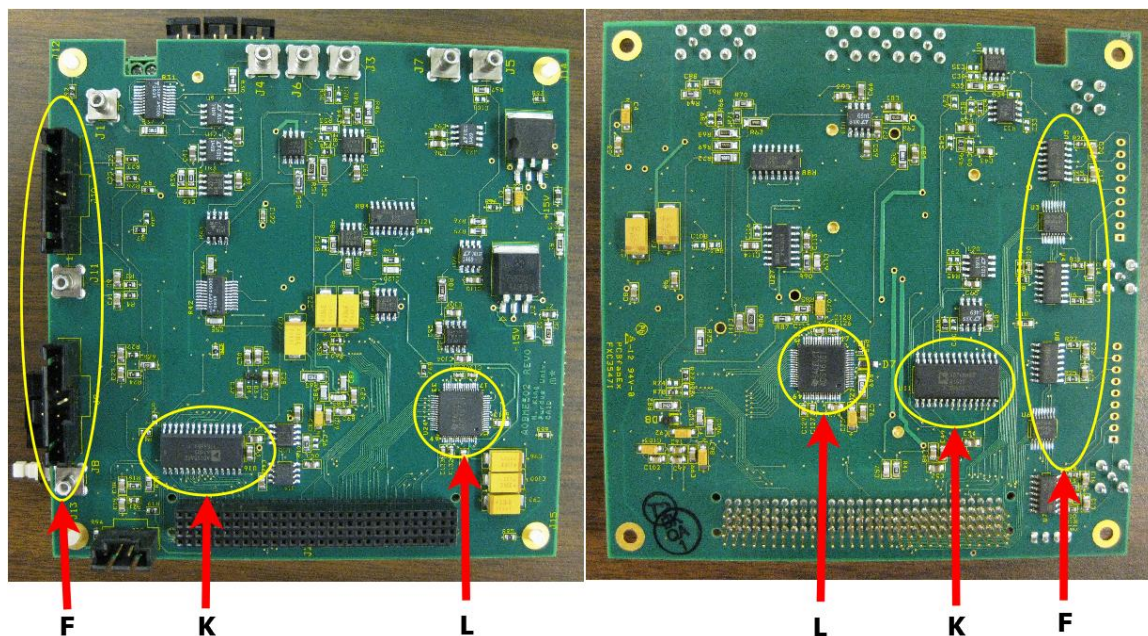


Figure 4-6 – Top view (left) and bottom view of the Analog Interface Board, A0BME502

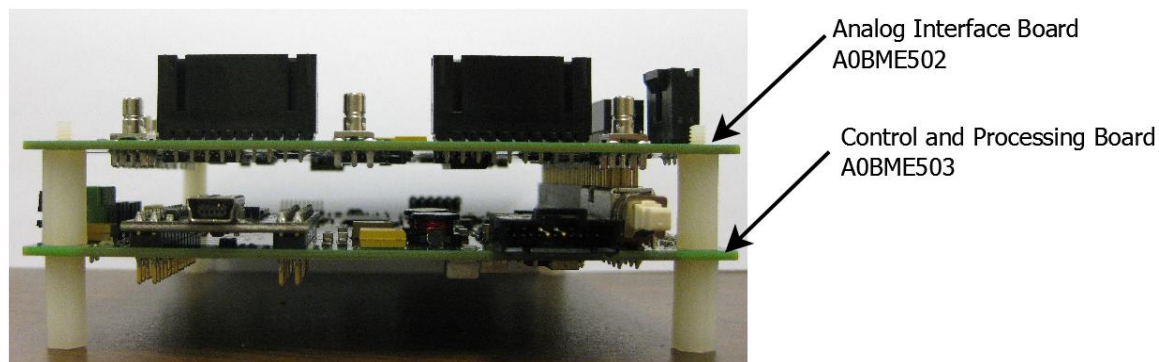


Figure 4-7 – Control board and Analog Interface board connected together

A program was developed to configure, control, collect and display data from the Mini 12 electronics. It was a Microsoft Windows based program written in Visual Basic.NET. The author wrote the Mini 11.5 user interface that consisted of 21207 lines of code. Frank Boudreau continued development of the instrument interface software for the Mini 12 bringing the final number of lines to 41440 lines

of Visual Basic.NET code. Figure 4-8 below contains a screen capture of the Mini 12 software. On the bottom part of the program the spectra results (red) and RF peaks (blue) are displayed. In the upper right hand side of the screen scan functions can be created, saved and loaded. On the upper left hand side there are tabs containing the functions to configure and control the instrument.

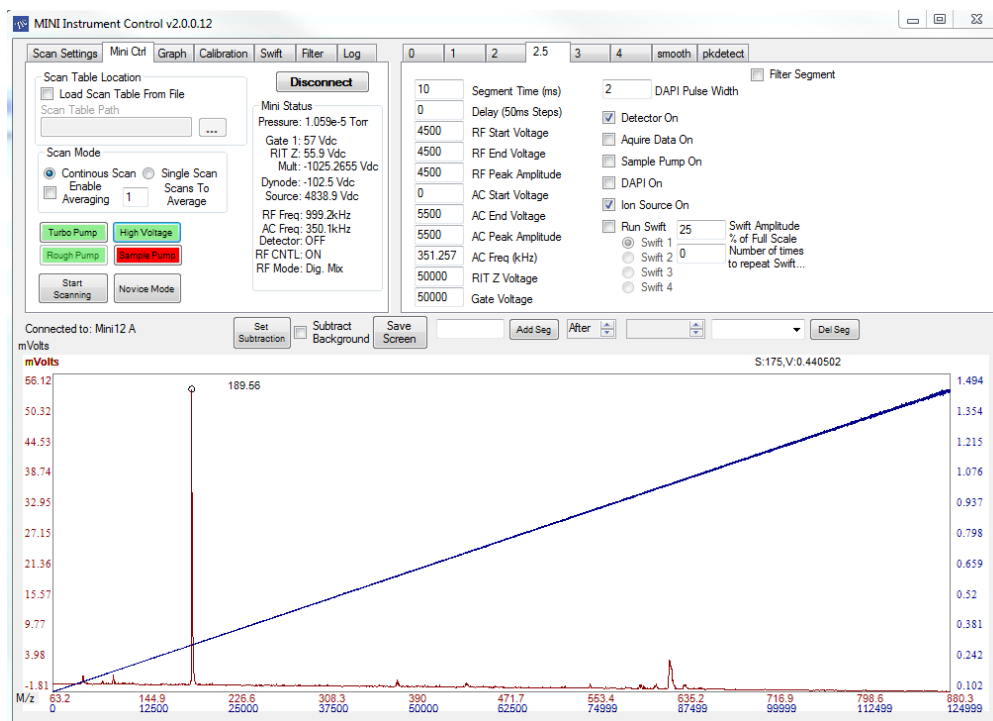


Figure 4-8 - Custom designed Mini12 instrument control interface displaying the simultaneously acquired Mass Spectra and associated RF ramp envelope.

4.1.2. Feedback Circuit

The performance of either the analog or digital control system was highly dependent on the operation of the feedback path to the controller. In the case of resonant LC tank RF amplifier, directly monitoring the over 5kV_{pp} signal directly with an ADC would not work. The solution was a capacitive divider circuit devised by Frank Boudreau (Purdue University, CAID) that creates a signal that can be proportional to the RF voltage, remain compatible with typical ADC input levels and not alter the output resonant signal. This circuit shown in Figure 4-9 was first used as the feedback measurement circuit in the Mini 11.5 analog RF controller.

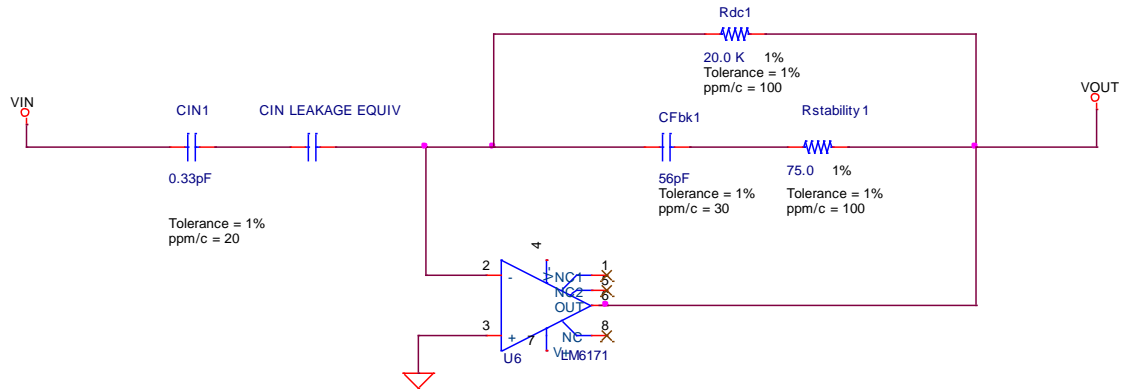


Figure 4-9 – RF capacitive divider feedback circuit

The circuit input at V_{in} was tied to the LC tank circuit directly after the air-core inductor. The C_{IN1} and C_{IN} Leakage Equiv. capacitor is in parallel with the trap and cable capacitances. The reactance of the capacitor (Eq 4-1) at the RF frequency allows for a small current to flow through the C_{in1} and C_{in} leakage to the LM6171 (National Semiconductor) virtual ground formed at pin 2 of the operational amplifier. The ratio between the C_{in1} reactance and the C_{Fbk1} reactance, $R_{stability}$, and R_{DC} (Eq 4-2) will control of the gain of the circuit (Eq 4-3). In the equations below, C_{in} is the sum of C_{in1} and C_{in} leakage. Because stray capacitances can dramatically change the gain, the mechanical design of the mounting and PCB layout is critical to consistent operation. Figure 4-10 is a plot showing the importance of the input frequency on the overall circuit gain, so the C_{fbk1} capacitor is chosen based on the nominal RF frequency. Also, the feedback signal is a 180 phase shifted from the RF signal.

$$Z_{in} = \frac{1}{2\pi f C_{in}} \quad \text{Eq 4-1}$$

$$Z_{fbk} = \frac{R_{dc}(2\pi f C_{fbk} R_{Stab} + 1)}{2\pi f C_{fbk}(R_{Stab} + R_{dc}) + 1} \quad \text{Eq 4-2}$$

$$\frac{Z_{fbk}}{Z_{in}} = \frac{2\pi f R_{dc} C_{in} (2\pi f R_{stab} C_{fbk} + 1)}{2\pi f C_{in} (R_{stab} + R_{dc}) + 1}$$

Eq 4-3

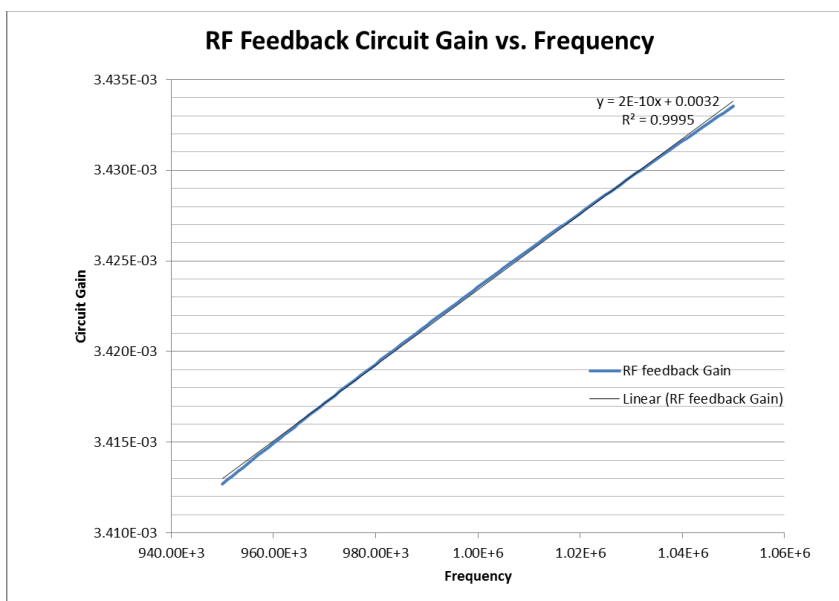


Figure 4-10 – Plot of the RF feedback gain as a function of frequency

4.1.3. Instrument Hardware and Vacuum

Testing of the Mini 12 was done using a Mini 11.5 chassis that included the vacuum system (Figure 4-12). The vacuum system consisted of a Pfeiffer HiPace 10 (TC110) turbomolecular pump, KNF (1220-N84.0-9.00) diaphragm pump, custom machined RIT, Detech 2300 electron multiplier (ion detector), and a custom machined vacuum chamber to house the RIT and electron multiplier. Figure 4-11 is a rendering done of the positioning of the RIT, electron multiplier and DAPI inlet.

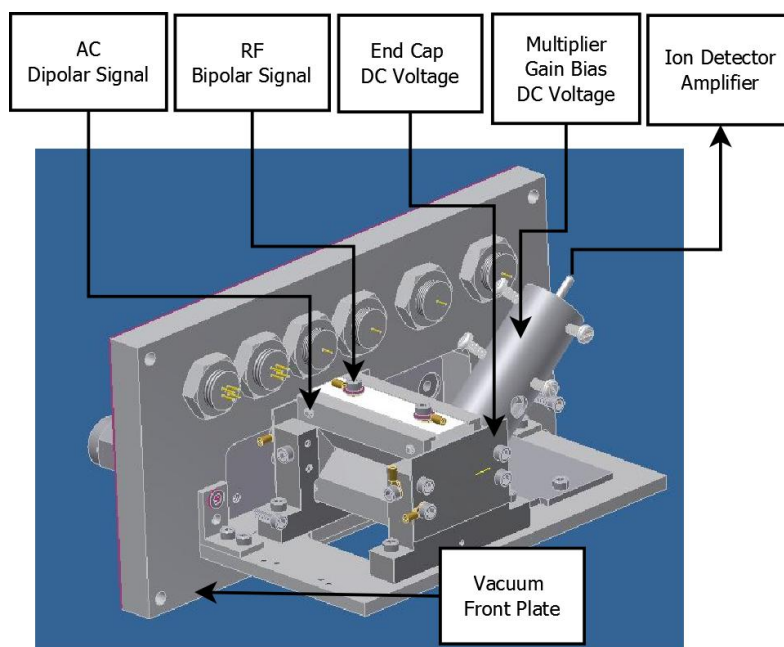


Figure 4-11 – Rendering of the RIT, ion detector and DAPI inlet as mounted in the Mini MS instrument (Rendering created by Frank Boudreau, Purdue University)

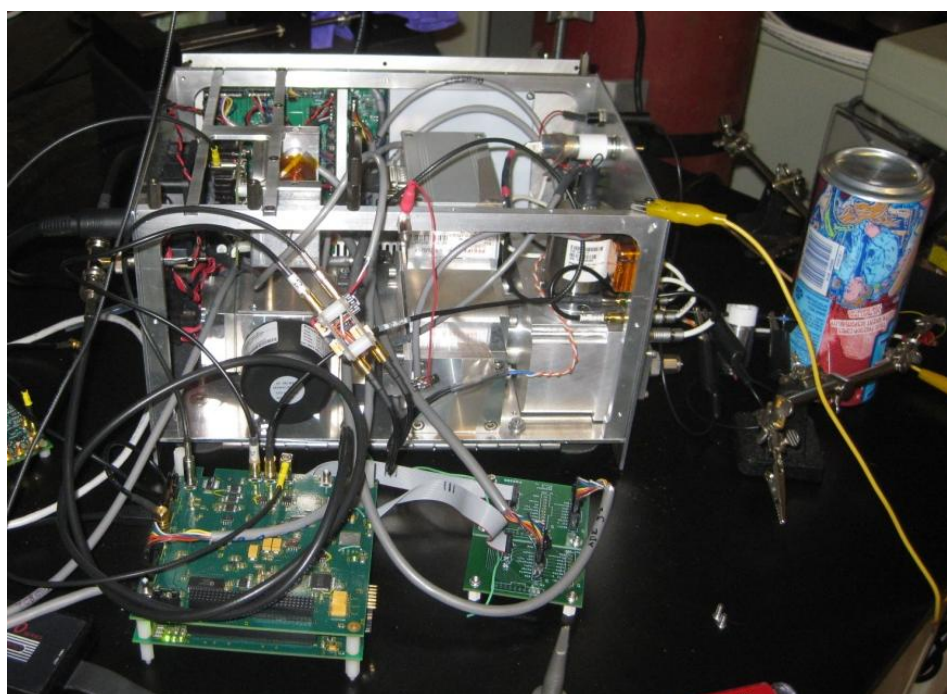


Figure 4-12 - Photo of the Mini11.5 chassis with the Mini12 data acquisition electronics connected to apparatus

4.2. Simulation

A MATLAB Simulink simulation of the RF system was created by incorporating open loop measured results. First, an open loop step response was taken using a Tektronix DPO 4032 oscilloscope. The AM modulated waveform was processed in MATLAB to recover the envelope and then a 3-order polynomial was fitted to the response curve shown in Figure 4-13. Then using the shape of the step response, a 3rd order transfer function was tuned to represent the system plant (Figure 4-14) in MATLAB.

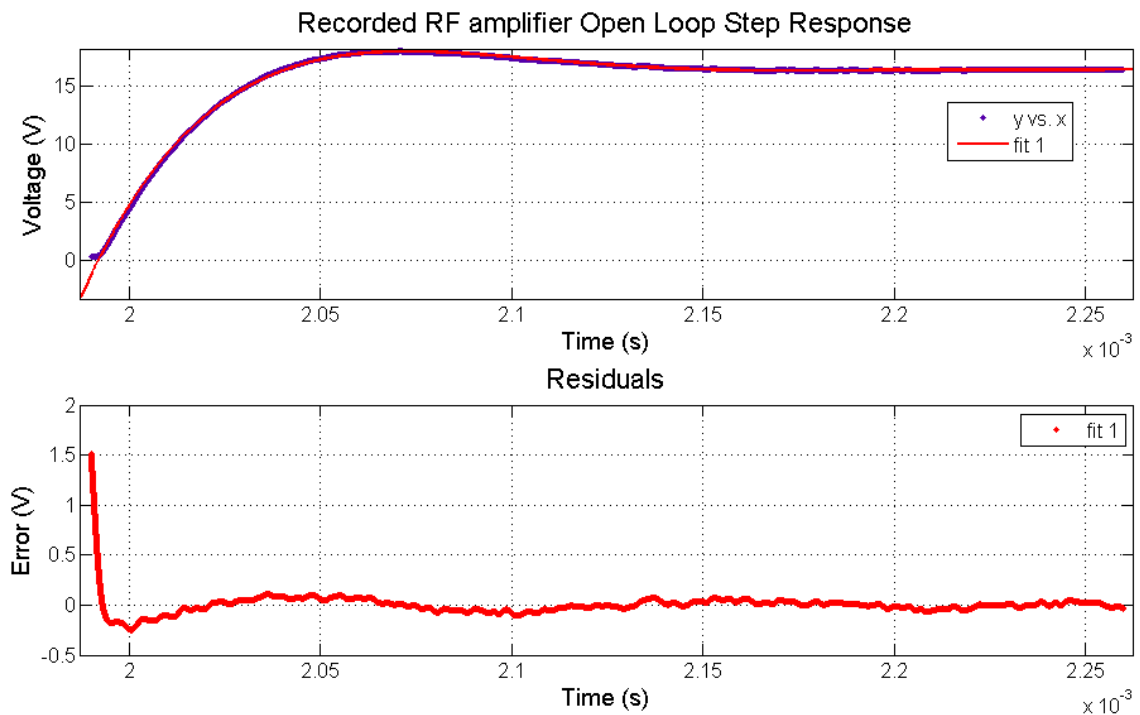


Figure 4-13 – Measured Open Loop step response

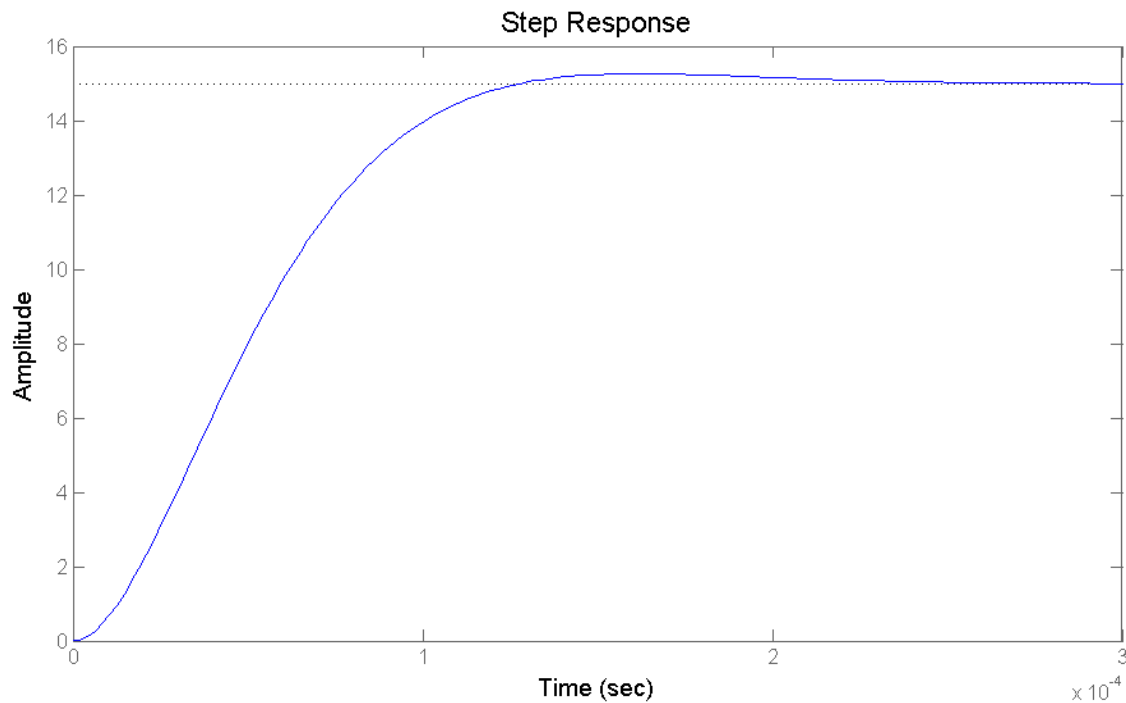


Figure 4-14 – Plant based on measured open loop response

Using the system plant transfer function, a simulation model, shown in Figure 4-15, was designed in Simulink. A 10 μ s transport delay was added to into the feedback path to account for the ADC sample to output delay, feedback circuit phase shift, amplifier phase delay and FPGA signal path delays from demodulation. MATLAB Simulink provides an optimization auto-tune feature in the PID controller block. The output of the optimized tune is shown in Figure 4-16. The gains for the P, I and D terms calculated by the simulation were $K_p = 0.000058$, $K_i = 3.8073$, and $K_d = 0$, so the controller was designed to have 12-bit fractional gain multipliers ranging from 3.999 to 0.00097.

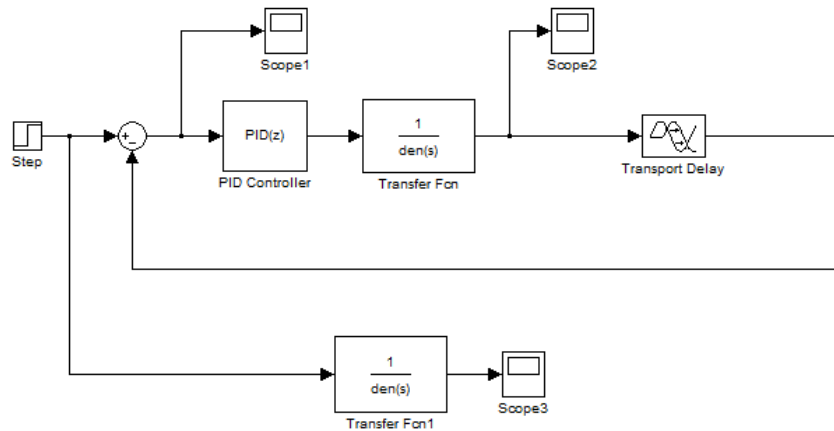


Figure 4-15 – MATLAB Simulink Simulation Diagram

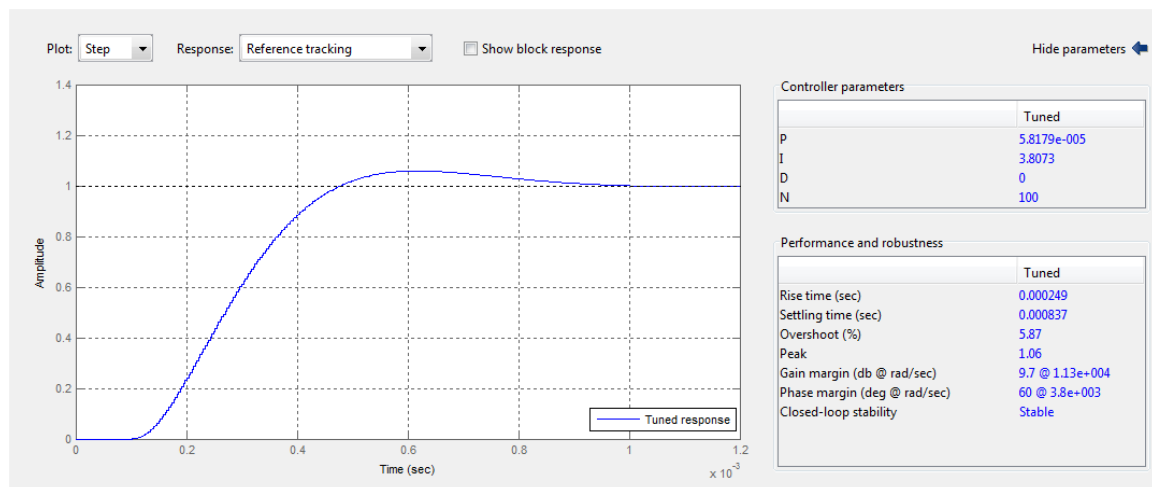


Figure 4-16 – Resulting Simulink PID Tuning results

The digital controller was written in VHDL and operated in the FPGA. The controller was clocked off a 60MHz clock and took 8 states to produce a corrected output signal. The frequency that the controller was operated at was adjustable for changing the T term in Equations 4.4 to 4.6. A full listing of the PID controller VHDL code can be found in the Appendix section. Commands for the user interface were created to adjust gains, timing, offset and enable/disable the controller during operation. Equation 4-4 represents the proportional correction factor where K_p is the gain and $e_{in}(T)$ is the error signal when the

controller was started at time T. Equation 4-5 was used to calculate the integral correction factor by multiplying the integrator gain, K_i , to the incoming error signal $e_{in}(T)$ and then adding the sum of past errors, $e_o(T)$. The derivative term was calculated using Equation 4-6. Its output represented the difference of the previous error, $e_{in-1}(T)$, and the current error $e_{in}(T)$ scaled by a gain factor K_d . A final correction factor C_{out} was calculated as a sum of the proportional term, integral term, derivative term and input set point. The C_{out} term was multiplied by the carrier frequency in the DDS block in the FPGA. A VHDL test bench script was created to verify proper saturation of PID calculations and simulated using Mentor Graphics ModelSim (not shown).

$$P = K_p \cdot e_{in}(T) \quad \text{Eq 4-4}$$

$$I = K_i \cdot e_{in}(T) + \sum K_i \cdot e_o(T) \quad \text{Eq 4-5}$$

$$D = (e_{in}(T) - e_{in-1}(T)) \cdot K_d \quad \text{Eq 4-6}$$

$$C_{out} = P + I + D + Setpoint \quad \text{Eq 4-7}$$

During development of the FPGA VHDL code, simulation of the code using test benches in ModelSim reduced the design troubleshooting time. Each file for the FPGA had a test bench created for it. An example simulation output of the reference ramp generator used in the AC DDS and as the input set point to the PID controller is shown in Figure 4- 18. The digital envelope recovery by the interpolation and peak detection was verified using ModelSim shown in Figure 4-17. Because the RF signal is ideally a sine wave a 4-times interpolation filter was added to better recover the 1MHz signal sampled at 10Msps.

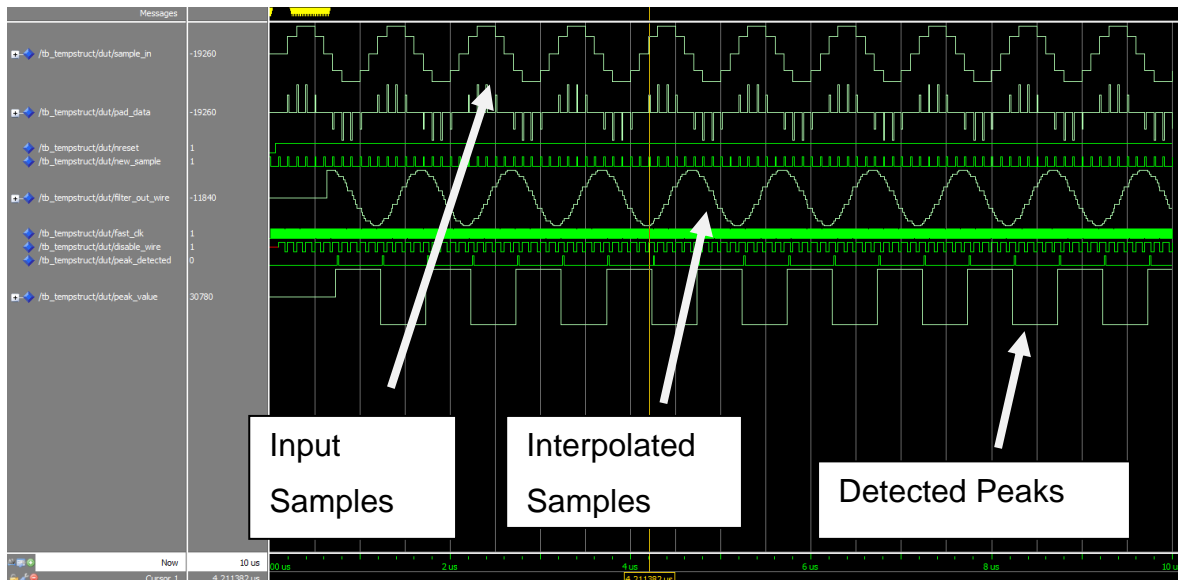


Figure 4-17 - ModelSim Simulation of the RF digital demodulation performed in the FPGA

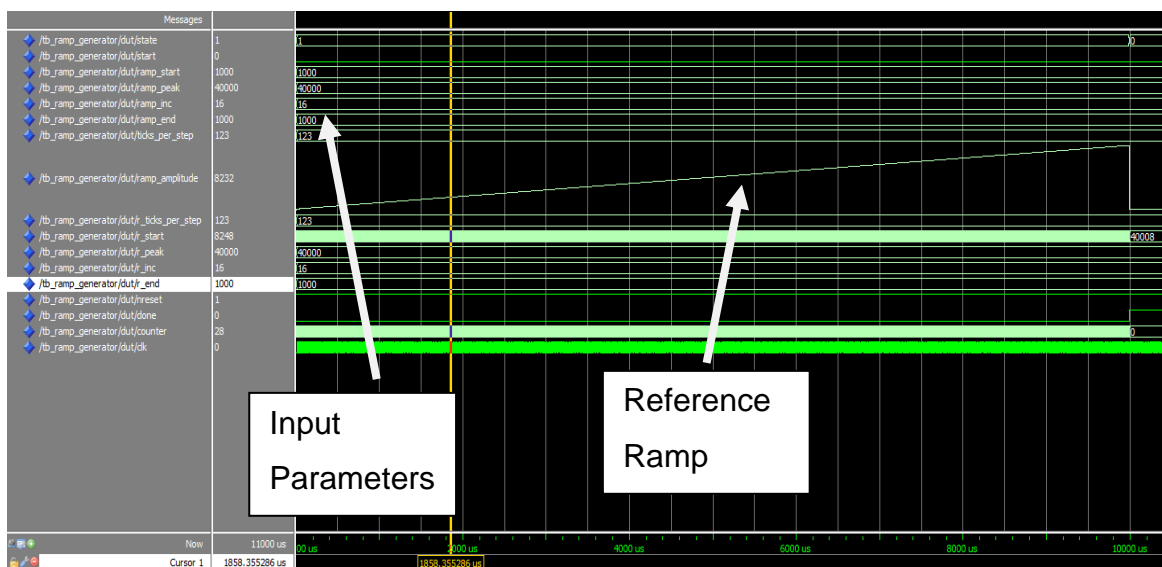


Figure 4-18 – Reference Ramp Generator ModelSim Simulation

After simulation of the controller in Simulink and in ModelSim, the design was synthesized and programmed into the FPGA on the Mini12 electronics. Figure 4-19 shows step responses of the open loop response, simulation PID

gains and manual tuning PID gains. The Simulink simulation results did not create a stable system as shown in the ramp response in Figure 4-20, but was useful for creating a starting point for testing. The ramp response of the manually tuned gains is displayed in Figure 4-21. This was determined by setting all gains to the highest level and decreasing the integrator gain down until minimum envelope oscillations were observed. This combination of gains and operating frequency was held constant throughout the digital controller testing.

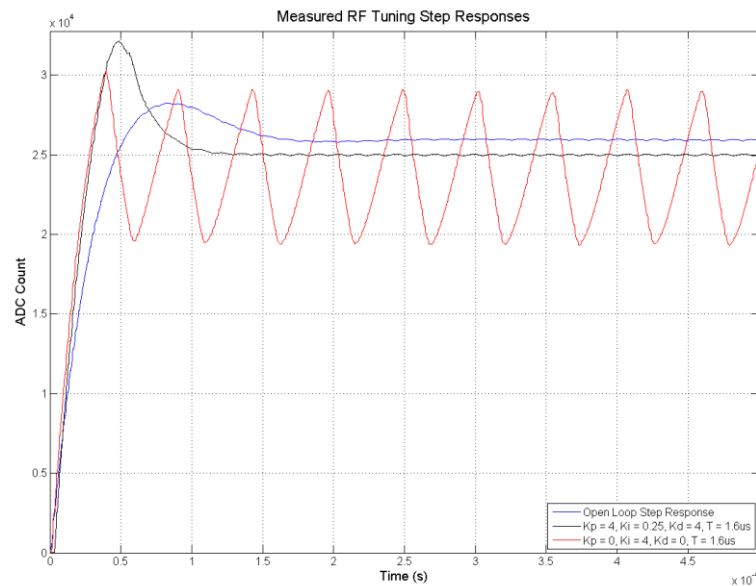


Figure 4-19 – Measured step response of RF amplifier using simulation results and manually tuned gains

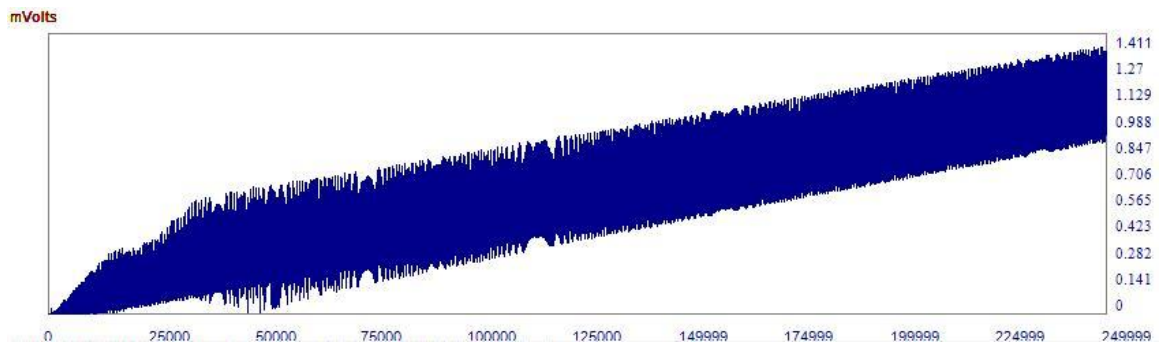


Figure 4-20 – Measure Ramp from 0 to 85% of full scale using gains $K_p = 0$, $K_i = 4$, $K_d = 0$, $T = 1.6\mu s$

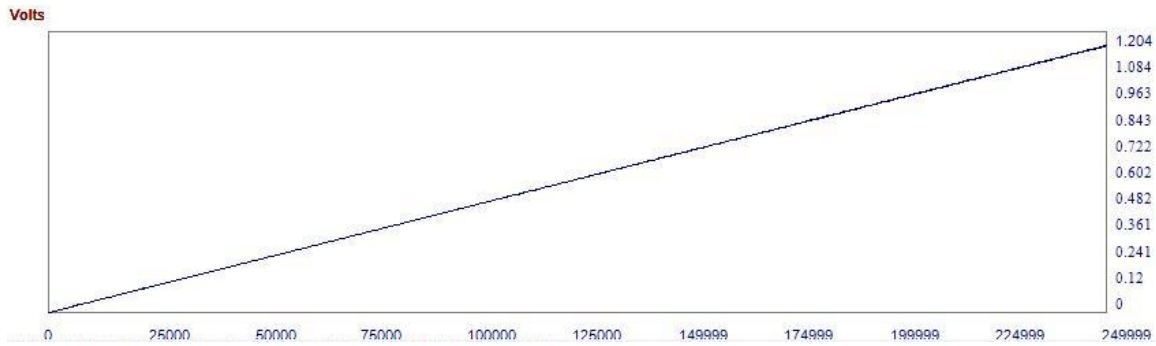


Figure 4-21 – Measure Ramp from 0 to 85% of full scale using gains $K_p = 4$, $K_i = 0.25$, $K_d = 4$, $T = 1.6\mu s$

4.3. Results

Experimental results from the tests outlined in Chapter 3 are presented in the following sub sections

4.3.1. AC and RF Signal Generation Analysis

The purpose of this section is to present the data collected from the outputs of the signal generators before being applied to the RF amplifier and RIT for the Mini 11.5 and Mini 12 data acquisition electronics. First, the accuracy of the RF/AC outputs (Figure 4-22) was measured with an HP 5315A Universal Counter and compared to the output of a Tektronix AFG 3022 Function Generator. An identical positive linear error with frequency was observed on the AC and RF outputs of the Mini12 Data acquisition boards. This error was accounted for in the scan functions by adding a correction in Hz to the desired frequency calculated from the linear regression line shown in Figure 4-22.

Distortion and unwanted frequency noise was measured by collecting 10 million point time domain waveforms sampled at 2.5GS/s captured with a Tektronix DPO 4032 digital oscilloscope. The waveform captures were loaded into MATLAB and converted to the frequency domain by calculating a fast fourier transform (FFT) from the time domain data. The FFT output was used to

calculate magnitude, total harmonic distortion (THD) and spurious free dynamic range (SFDR) for the RF and AC outputs and displayed in Figures 4-14 and 4-15 respectively. SFDR is a measure of the ratio between the center frequency and the next largest magnitude noise or harmonic component. As calculated, a higher SFDR measure indicates a better signal.

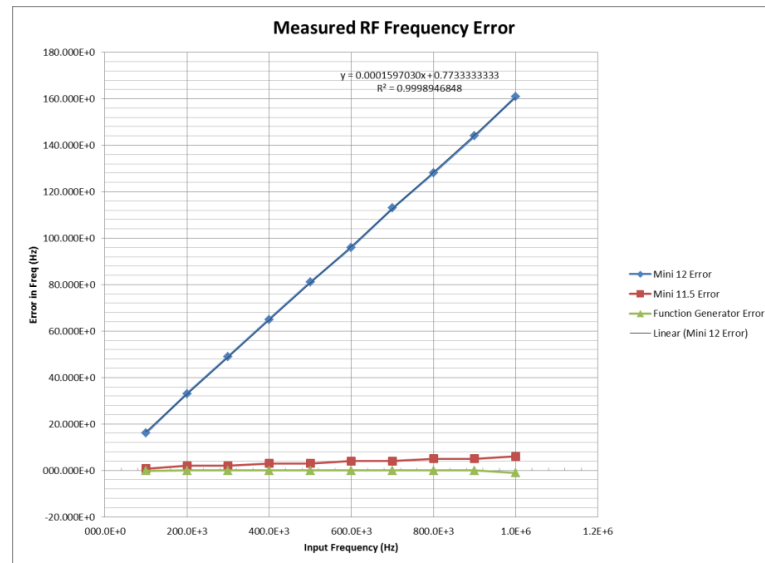


Figure 4-22 – Data acquisition electronics frequency output accuracy

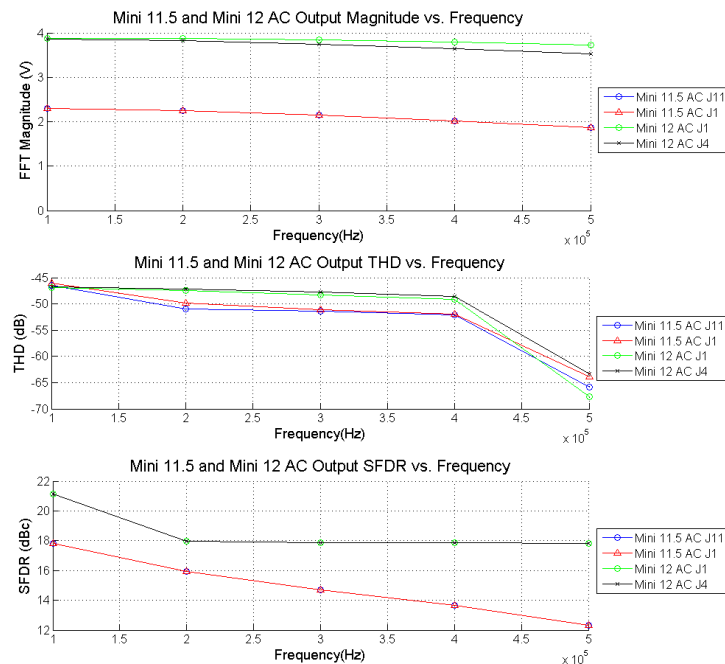


Figure 4-23 – Mini 11.5 and 12 AC output analysis

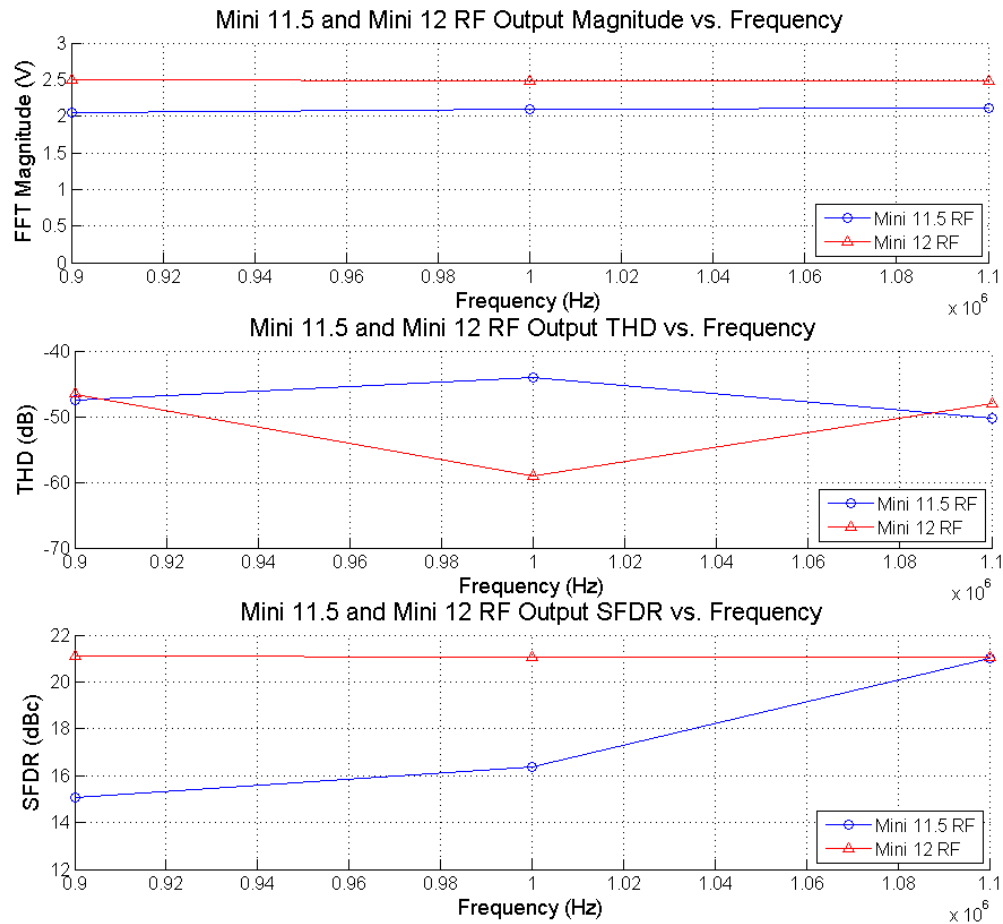


Figure 4-24 - Mini 11.5 and 12 RF output analysis

4.3.2. Controller Comparison

The feedback of the RF amplifier from the three configurations shown in Figure 3-3, 3-2, and 3-3 were connected and monitored with a Tektronix DPO 4032 digital oscilloscope. The resulting 100 ms long AM modulated ramp waveform capture was loaded into MATLAB for frequency and envelope analysis. The waveform capture was sampled at 50MS/s and was 10 million points long ensuring a low loss in information. In order to, remove the carrier frequency from the AM signal, a 100 kHz low pass was applied. Data was normalized and scaled to 2500Vp which was the measured maximum peak output recorded with a Tektronix P6015A high voltage probe. The waveform

capture was taken from the feedback signal rather than the high voltage probe because of the capacitance from the high voltage probe lowers the resonant frequency by 40 kHz. The change in resonance was enough to cause the controllers to be unable to operate at the 998 kHz RF frequency used to collect spectrum.

Finally, the envelope was plotted with a linear regression line drawn along the envelope. A second plot of the residuals from the envelope and regression line was added. The open loop response (Figure 4-25), Mini 12 with digital controller (Figure 4-26), Mini 12 with analog controller (Figure 4-27) and Mini 11.5 with the analog controller (Figure 4-28) were captured and analyzed. Residual analysis shows less variation along the line plot of the RF signal when using the analog controller than the digital controller. The residual plot of the analog controller had an overall non-linear bow shaped error ranging from -15V to 10V whereas the digital controller error was centered on 0V.

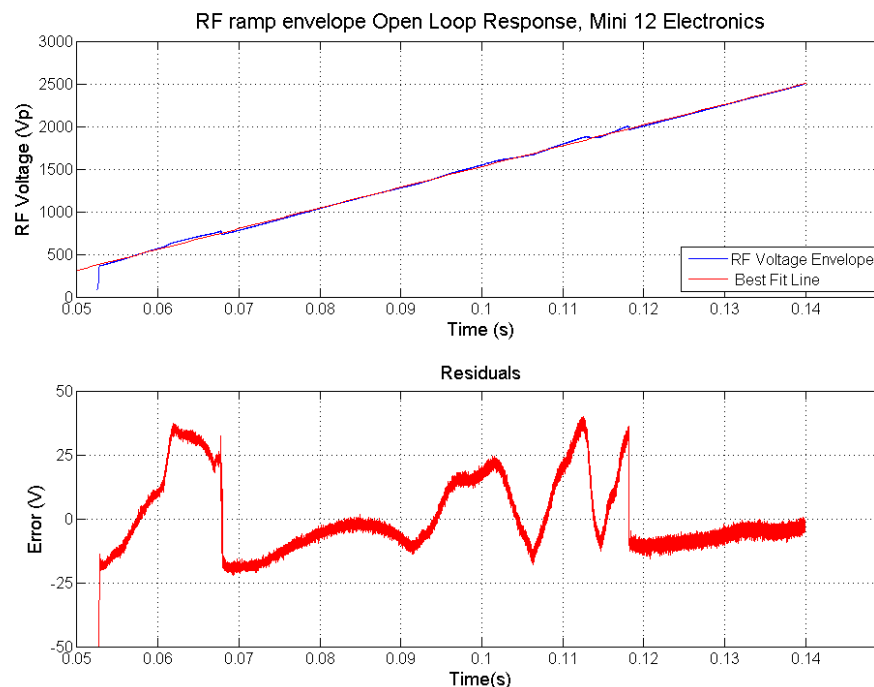


Figure 4-25 – Open loop response of the RF amplifier, 100ms ramp

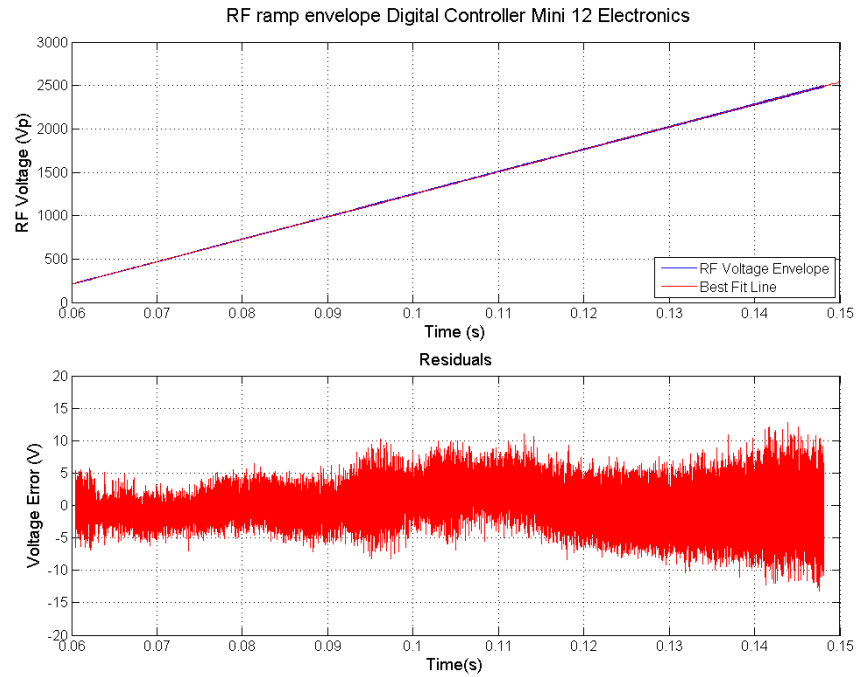


Figure 4-26 – Digital controller response of the RF amplifier, 100ms ramp

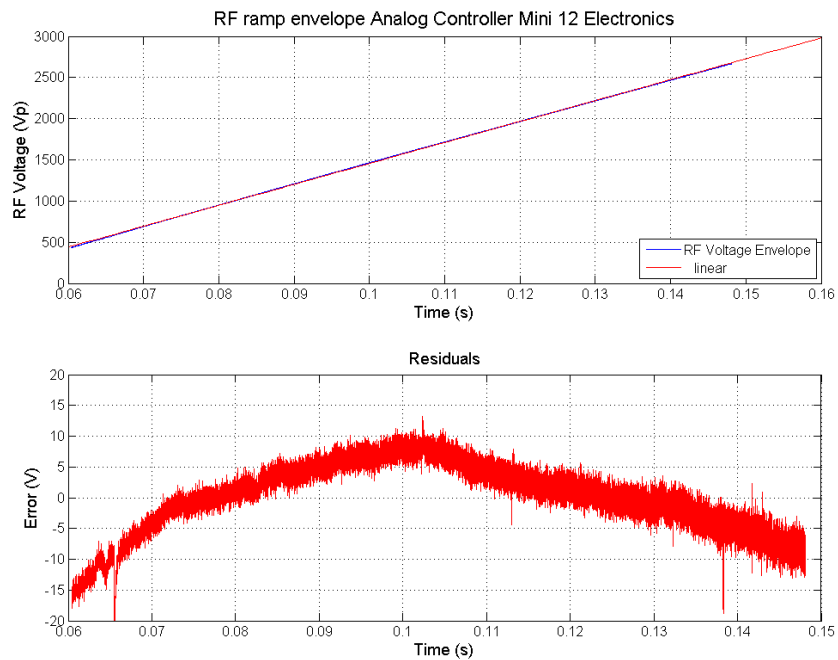


Figure 4-27 – Analog controller response with Mini12 electronics of the RF amplifier, 100ms ramp

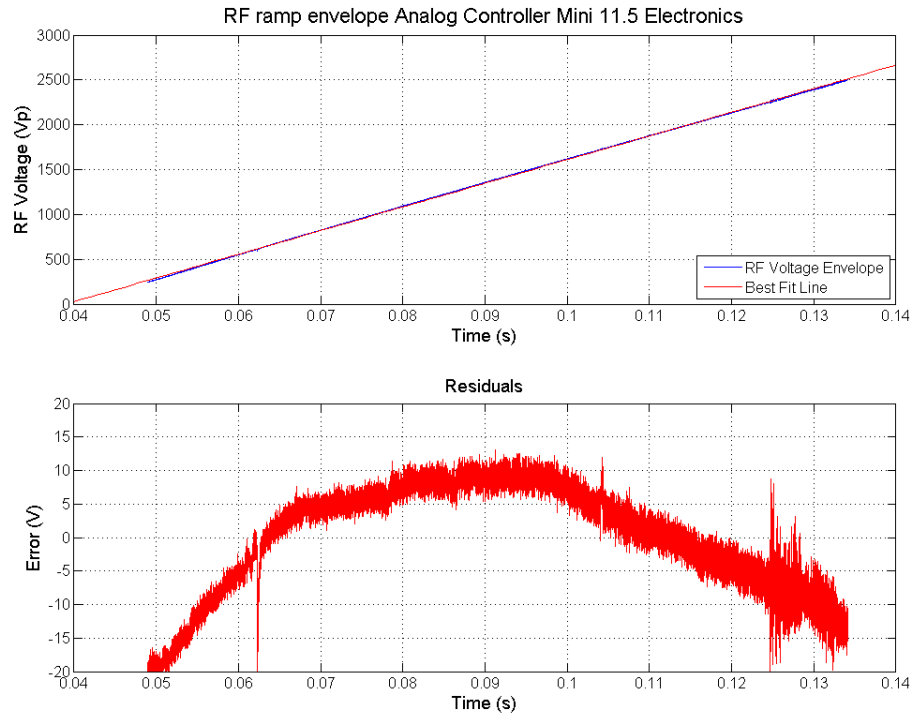


Figure 4-28 - Analog controller response with Mini11.5 electronics of the RF amplifier, 100ms ramp

4.3.3. Spectra

Resonant LC tank circuits are susceptible to stray capacitances from the location of nearby objects. Along with visual inspection of the mechanical setup of the instrument system, daily checks of the RF resonant frequency were done throughout the course of this research to reduce the influence of resonant frequency shifts. The DSP was used to sweep input frequencies from high frequencies to low frequencies while operating the RF amplifier in open loop mode with constant input signal amplitude. Data was collected with Tektronix DPO 4032 oscilloscope and analyzed with MATLAB. An example output of the data can be seen in Figure 4-29. In the case of a change in the resonant frequency, a 10pF tuning capacitor was placed in parallel with the RIT.

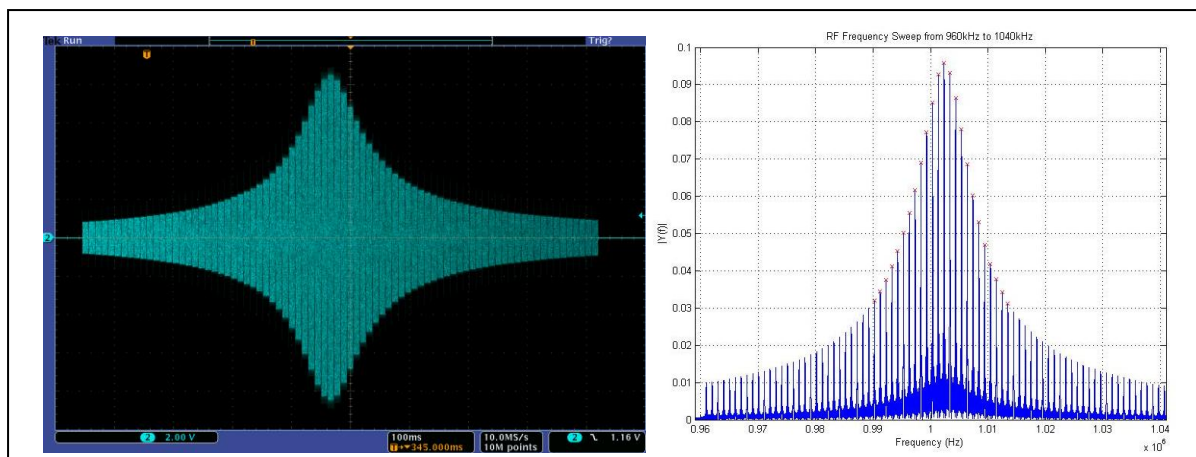


Figure 4-29 – Example RF Resonant Frequency Analysis

Originally Ultramark, cytochrom c and myoglobin, were proposed order to test the instrument's mass accuracy across the spectra x-axis, but these compounds m/z (low mass – to high mass) values were outside the dynamic mass range of the instrument as configured. A change to the RF resonant circuit operating frequency needed to be changed from 998 kHz to 695 kHz would have been needed to change the mass range. Instead, a 10ppm calibration mixture of polyethylene glycol (PEG) was made. The PEG mixture contained mass peaks at m/z 173, 217, 261, 349, 393, 437, 481, and 525 which covered the mass range of the instrument. A nano-ESI ionization method was used to create the sample ions. Three hundred consecutive mass spectra were collected and are shown in Figure 4-30, with peaks displayed by black dots and the average of all spectra displayed as a red line. The Mini 12 electronics were used to collect data and implement the scan function. The RF controller system was configured so that it could be run in analog or digital mode. For each configuration a linear calibration was determined from an average of 10 mass scans of the PEG spectrum. Then mass accuracy was determined by subtracting the exact mass from the measured mass for 300 single scan spectra. The resulting mass accuracy of the digital controller is in Figure 4-31 and for the analog controller, Figure 4-32. The ion detector signal was sampled at 1.25Msps.

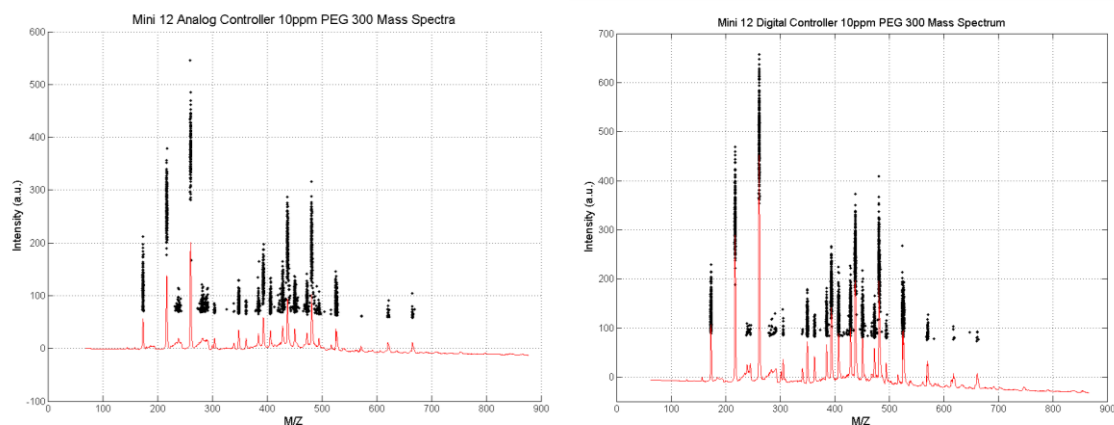


Figure 4-30 – 10ppm nano-ESI PEG mass spectrum

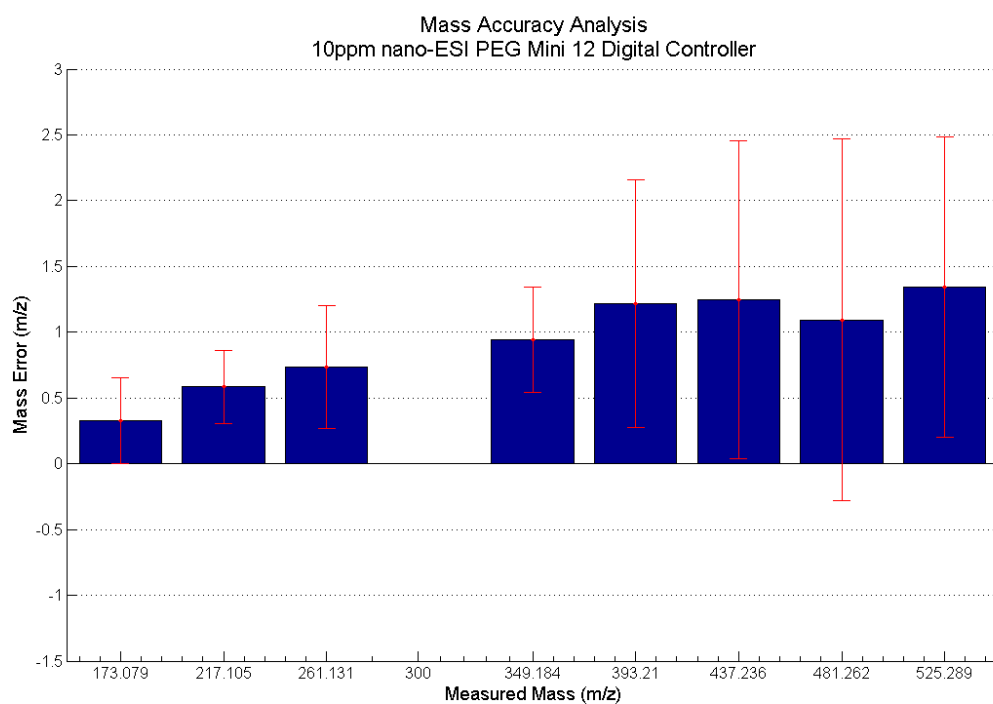


Figure 4-31 – Mass Accuracy of 8 selected peaks from a 10ppm PEG sample for the Mini 12 digital controller

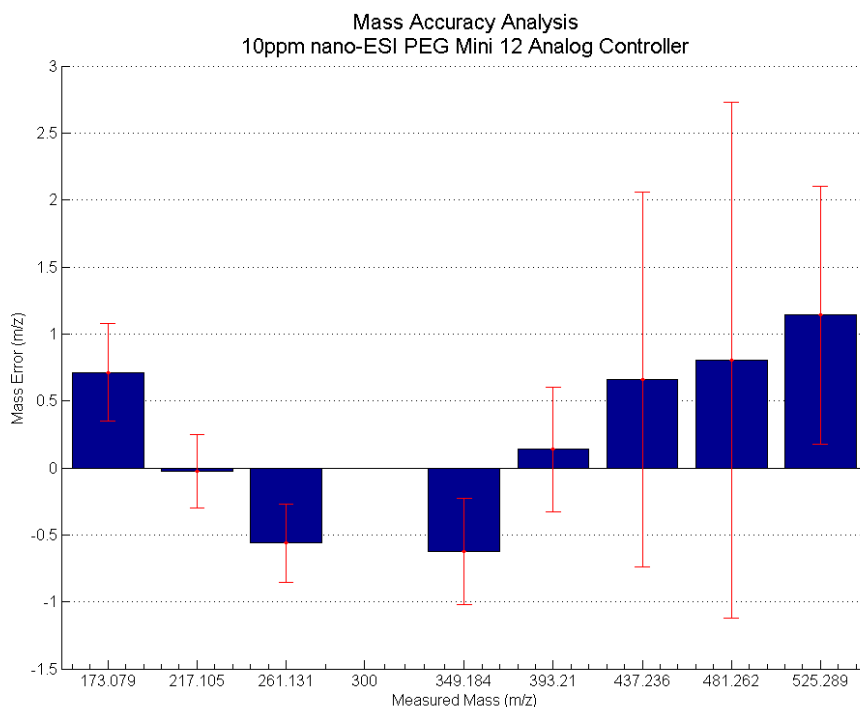


Figure 4-32 – Mass Accuracy of 8 selected peaks from a 10ppm PEG sample for the Mini 12 using the analog controller

Mass drift is an important parameter to characterize, for the purpose of automated analysis. This was done by using a sample of pure Diethyltoluamide (DEET) placed on a cotton swab within 1 inch of the DAPI inlet. An APCI ionization needle was charged to 4800Vdc and also placed within 1 inch of the DAPI inlet. A grounded metal shroud was placed over the DAPI inlet, APCI needle, and cotton swab in order to reduce the effect of airflow which causes variation in the intensity of the spectrum. The Mini instrument had an approximate runtime of 1 hour when operated from batteries and continuously sampled, therefore mass drift was measured for this interval. Mass drift of the Mini 12 equated to approximately 2000 single mass scans when the sampling rate is set to 1.25Msps and scan function from Figure 4-1 is used. Figure 4-33 shows plots of the peak intensity groupings recorded for both the digital and analog controllers over the sampling interval. A single dot was drawn for the peak

intensity detected in each spectrum and an overall average of the spectrum was drawn as a red line. Figure 4-33 shows that there was consistent signal throughout the test. The mass drift analysis is shown in Figure 4-35 and the mass resolving power during the mass drift test is shown in Figure 4-36. The mass resolving power plots show that peak widths were consistent throughout the test. Both controllers exhibited mass drift over time, but the analog controller had a spike in error (1.6 m/z) at the start of the test. Further investigation showed that there was a glitch in the RF signal that was not completely corrected (Figure 4-37 and Figure 4-38). The glitch also appeared in the residual analysis of the analog controller between times 0.06 and 0.07 seconds in Figure 4-27. The amplitude of the glitch was reduced in Figure 4-39, when the digital controller was used and no mass shift was observed.

The Mini 11.5 electronics were also tested with a DEET sample for 30 minutes to highlight differences in the sampling rate and instrument data acquisition throughput (half of the Mini 12). The ion detector sampling rate for the Mini 11.5 is 100 ksps, which is 12.5 times slower than the Mini 12. The effect of the reduced sampling rate resulted in intensity groupings being aligned along the sample intervals in Figure 4-34 below. The low fidelity sample rate contributes error to the recording of the true peak amplitude. The width of the peak is also affected by the sample rate. The Mini 11.5 recorded 12 samples per m/z resulting in a peak width measurement error of ± 0.083 m/z versus ± 0.007 m/z error for the Mini 12 electronics which collects 144 samples per m/z. Also, the Mini 11.5 scan rate could not be lengthened to 1200ms to equal the same number of points per peak because the architecture would not allow for a scan longer than 195ms. For these reasons the Mini 11.5 did not provide an equal comparison between the two controller solutions.

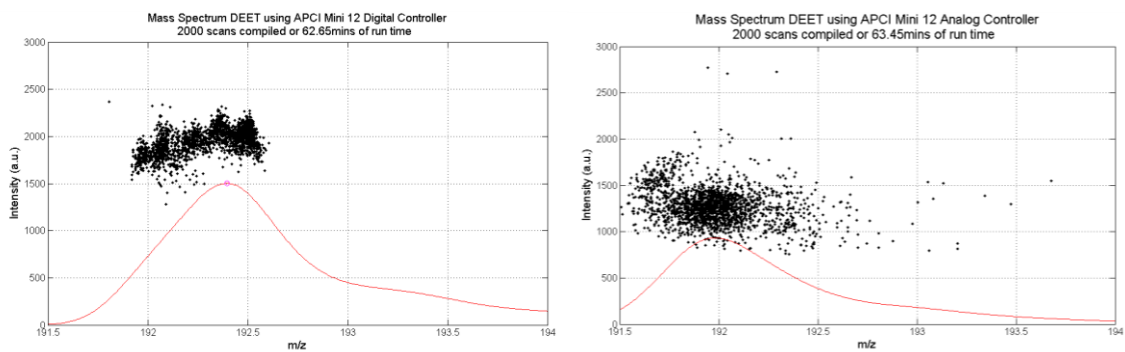


Figure 4-33 – 2000 Mini 12 single scan mass spectrum from the Digital and Analog controller configurations

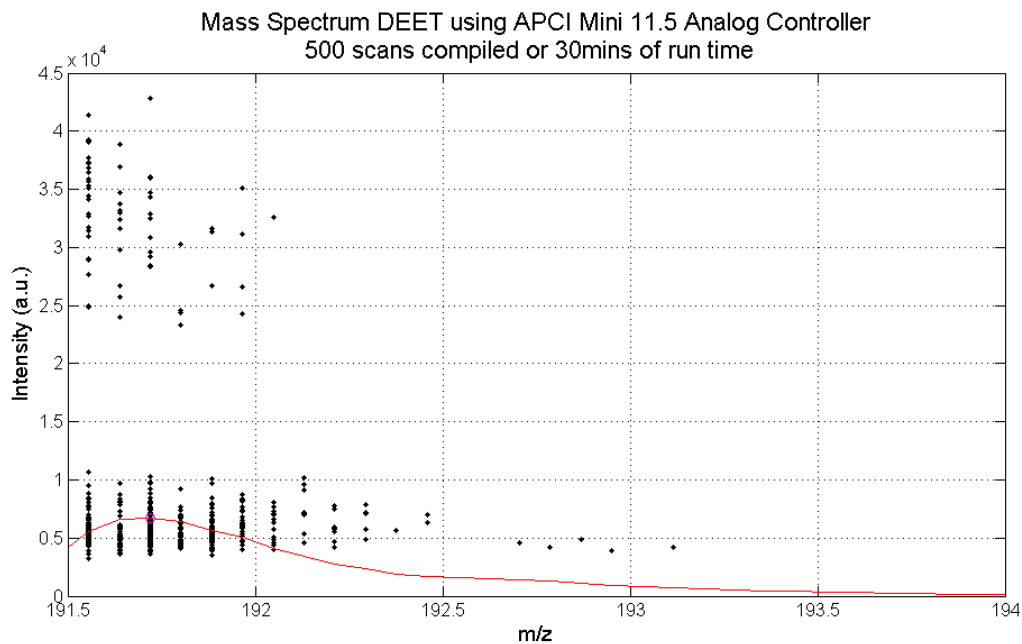


Figure 4-34 – 500 Mini 11.5 spectrum of DEET sampled at 100Ksps

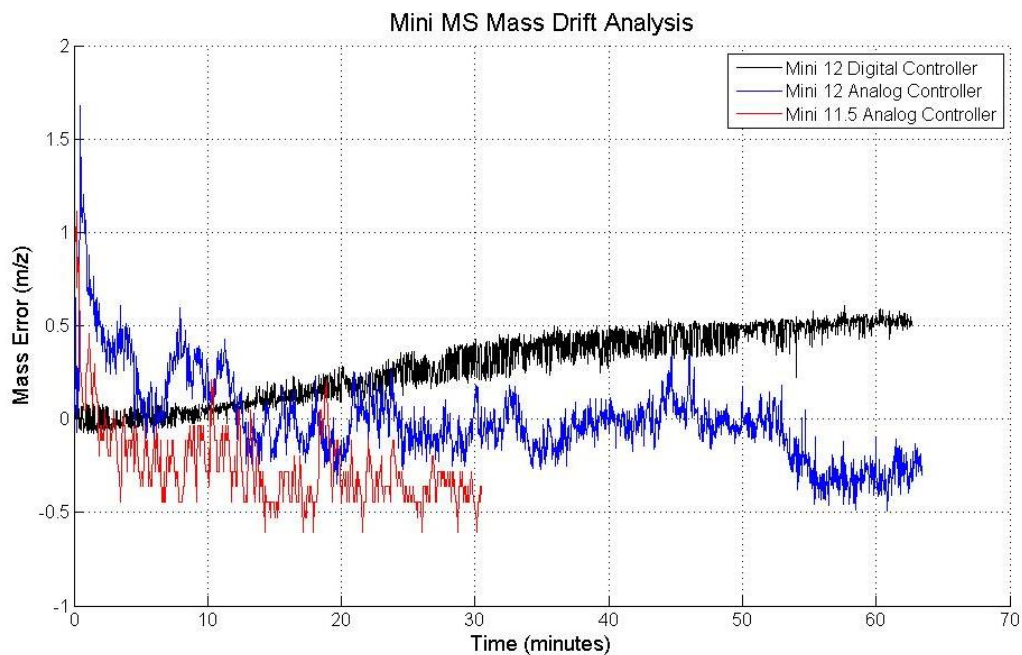


Figure 4-35 – Mass Drift Analysis of DEET over 1 hour of operation

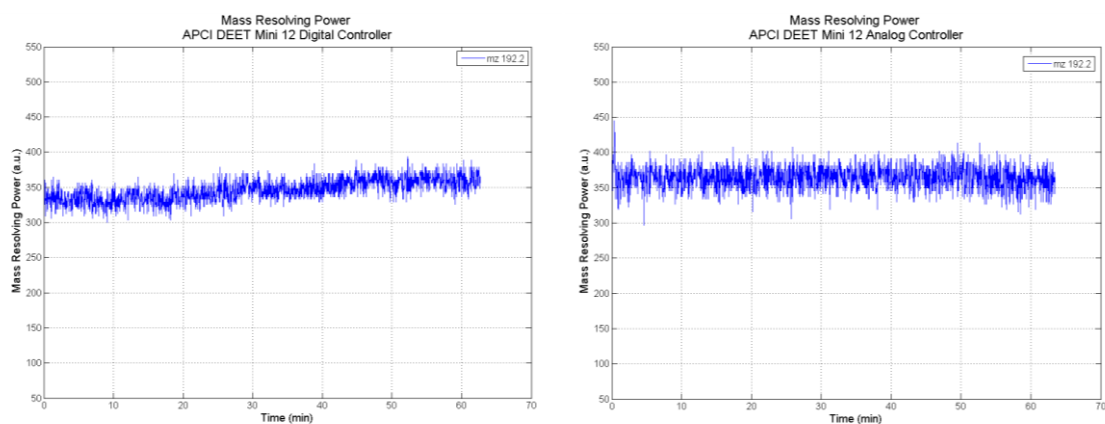


Figure 4-36 – Measured Mass Resolving Power during mass drift test

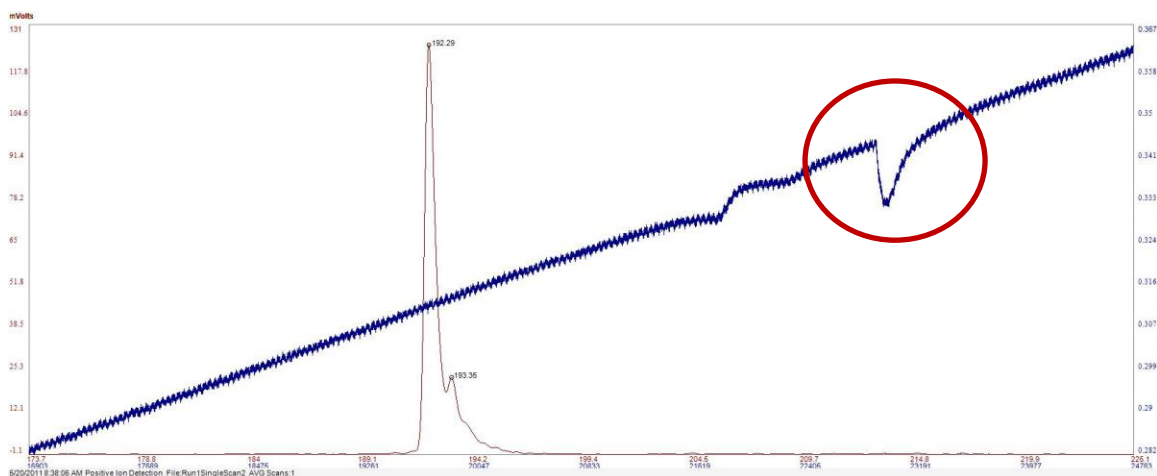


Figure 4-37 – Observed glitch in RF signal (blue line) for DEET Spectrum (red line) captured during the second scan using Mini 12 electronics and the analog controller at the start of the mass drift test.

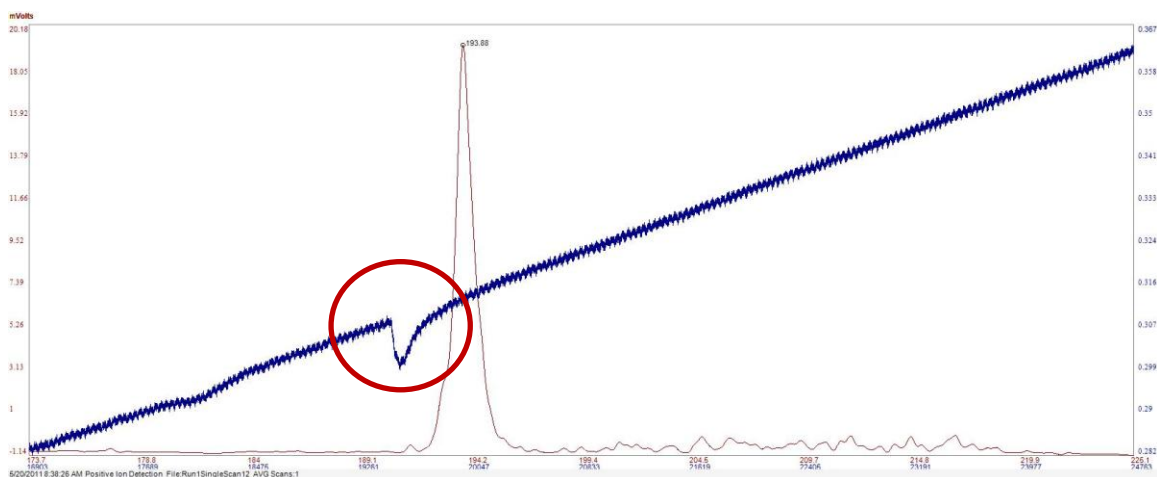


Figure 4-38 - Observed glitch in RF signal (blue line) for DEET Spectrum (red line) captured using Mini 12 electronics and the analog controller after the 12th scan captured during the mass drift test.

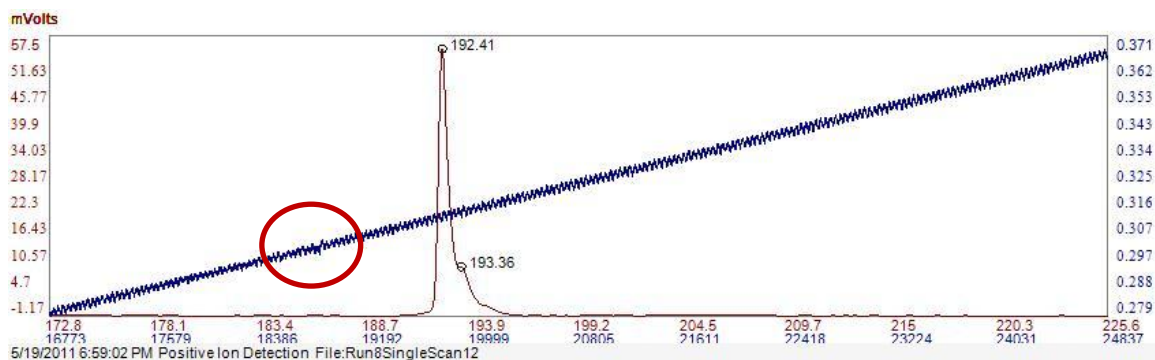


Figure 4-39 - Observed glitch not present in the RF signal (blue line) for DEET Spectrum (red line) captured using Mini 12 electronics and the digital controller after the 12th scan captured during the mass drift test.

Mass resolving power was measured using the definition in Chapter 3 with compounds DEET, methyl salicylate, cocaine, and methamphetamine. DEET and methyl salicylate were ionized using an APCI needle with potential of 4800Vdc applied to it. A nano-ESI source with a potential of 1700Vdc was used to ionized solutions of 10ppm cocaine and 10ppm methamphetamine mixed in 50/50 methanol water. The mass resolving power results from the DEET sample were presented in Figure 4-36 and did not track the fluctuations in mass drift in Figure 4-35 during the test. Note that a representative single scan mass spectrum for each compound and controller (methyl salicylate: Figure 4-40 and 4-42, cocaine: Figure 4-44 and 4-46, and methamphetamine: Figure 4-48 and 4-50) is presented to show that there was high signal intensity and the presence of other chemical compounds was minimized during the test. For the compound of methyl salicylate in Figure 4-41 and 4-43 note the mass resolving power for the peaks m/z 153 and 273.5 was steady throughout the collection of the data and that there little difference between the analog controller and digital controller. In Figure 4-45 and 4-47 notice that the cocaine peak at 304 there were large variations in mass drift and mass resolving power. The methamphetamine sample with peaks at m/z 91 and 150, it can be observed in Figure 4-49 and 4-51 that the digital and analog controller mass resolving power did not fluctuate

during the test. A summary of the mass resolving power measurements for all compound discussed is shown in Figure 4-52. The blue bars in Figure 4-52 represent the average mass resolving power and the red error bars are the standard deviation during the test. For all the compounds, except cocaine, the error bars overlapped indicating that there is not a statistical difference between the analog and digital controllers.

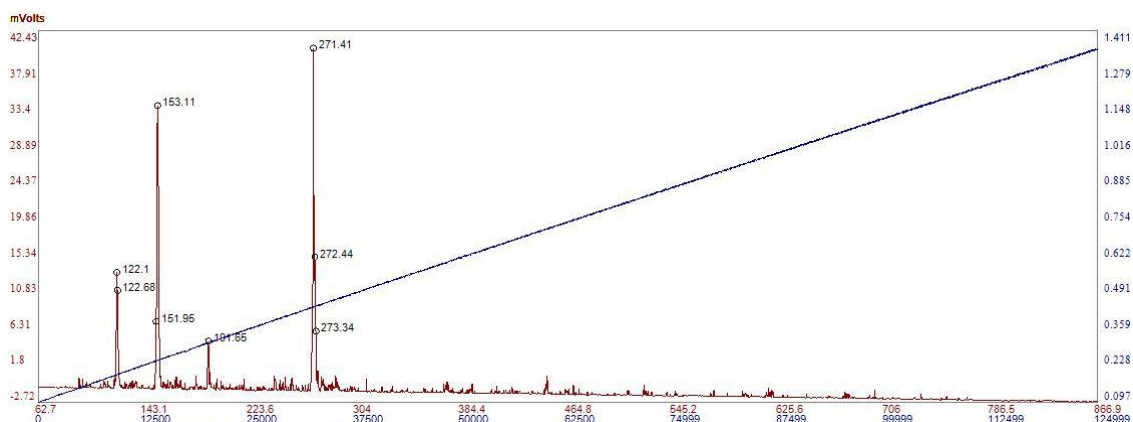


Figure 4-40 - Example Single Scan mass spectra of a 10ppm sample of Methyl Salicylate (m/z 153) collected with the Mini 12 electronics and analog controller

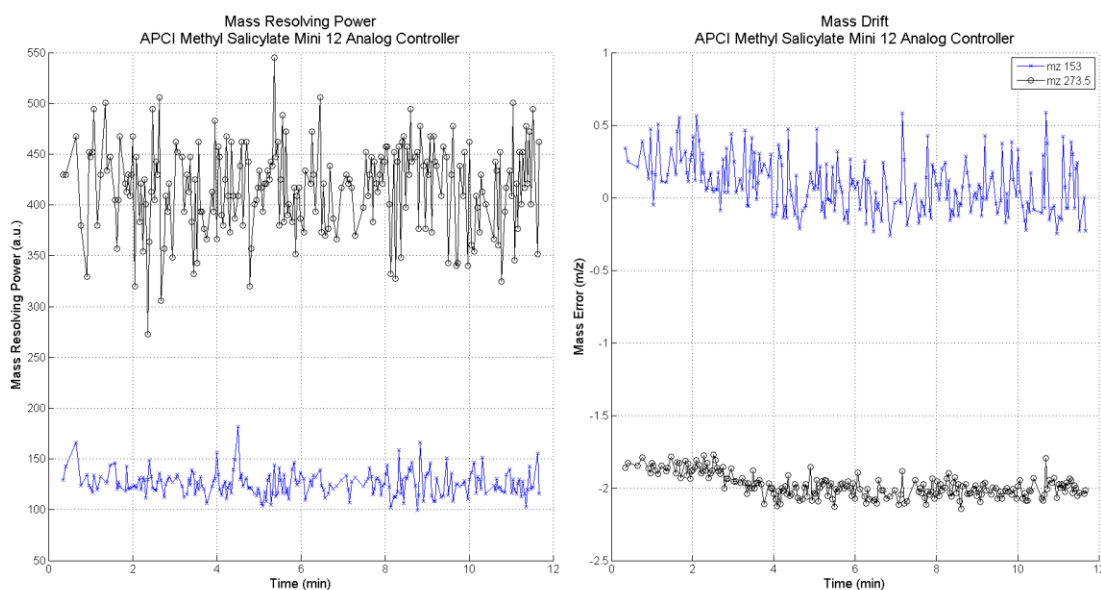


Figure 4-41 - Mass Resolving and Drift recorded using Mini 12 electronics and the analog controller for a 10ppm sample of Methyl Salicylate (m/z 153)

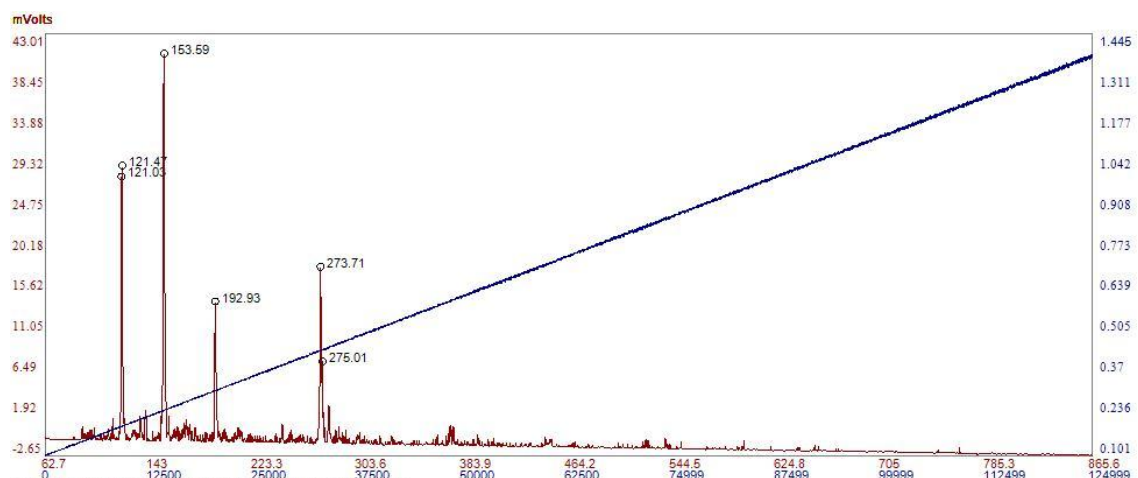


Figure 4-42 - Example Single Scan mass spectra of a 10ppm sample of Methyl Salicylate (m/z 153) collected with the Mini 12 electronics and digital controller

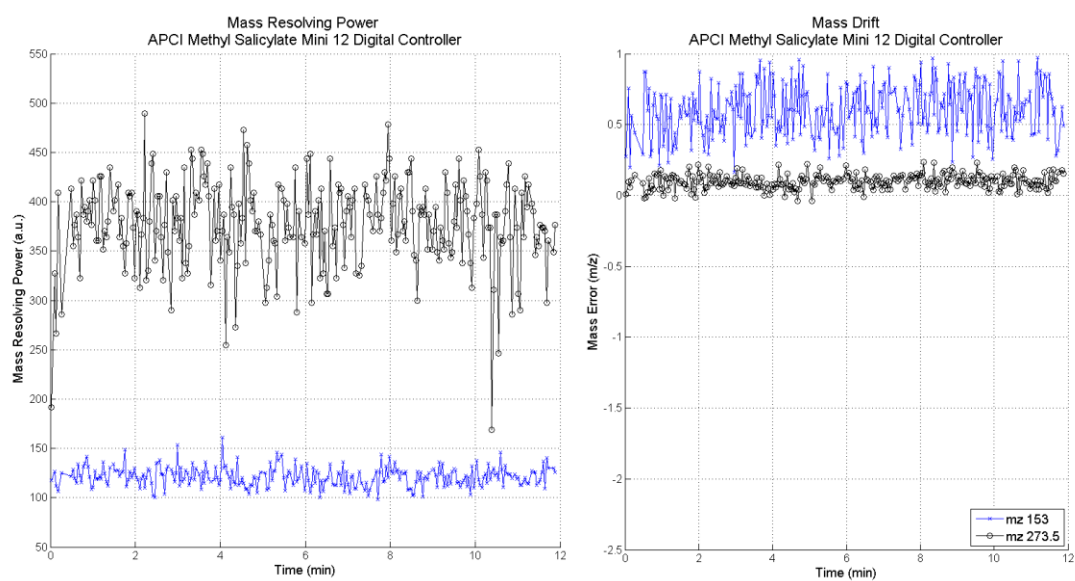


Figure 4-43 - Mass Resolving and Drift recorded using Mini 12 electronics and the digital controller for a 10ppm sample of Methyl Salicylate (m/z 153)

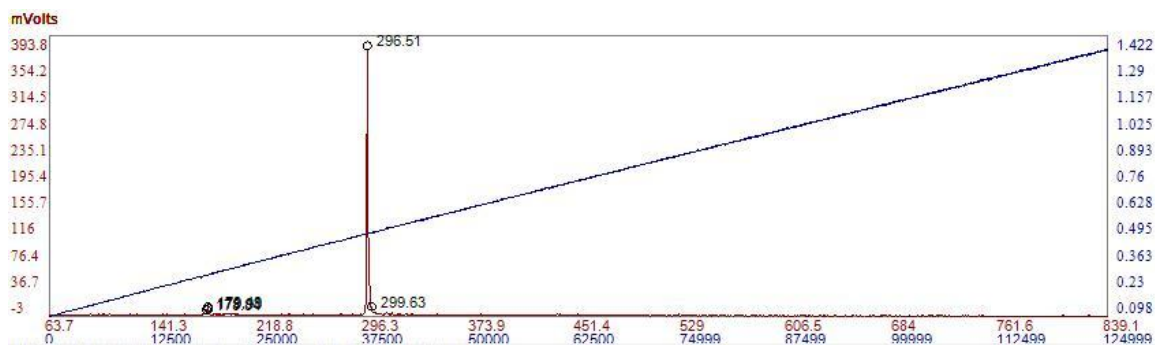


Figure 4-44 - Example Single Scan mass spectra of a 10ppm sample of cocaine (m/z 304.2) collected with the Mini 12 electronics and analog controller, mass calibration correction was corrected in MATLAB

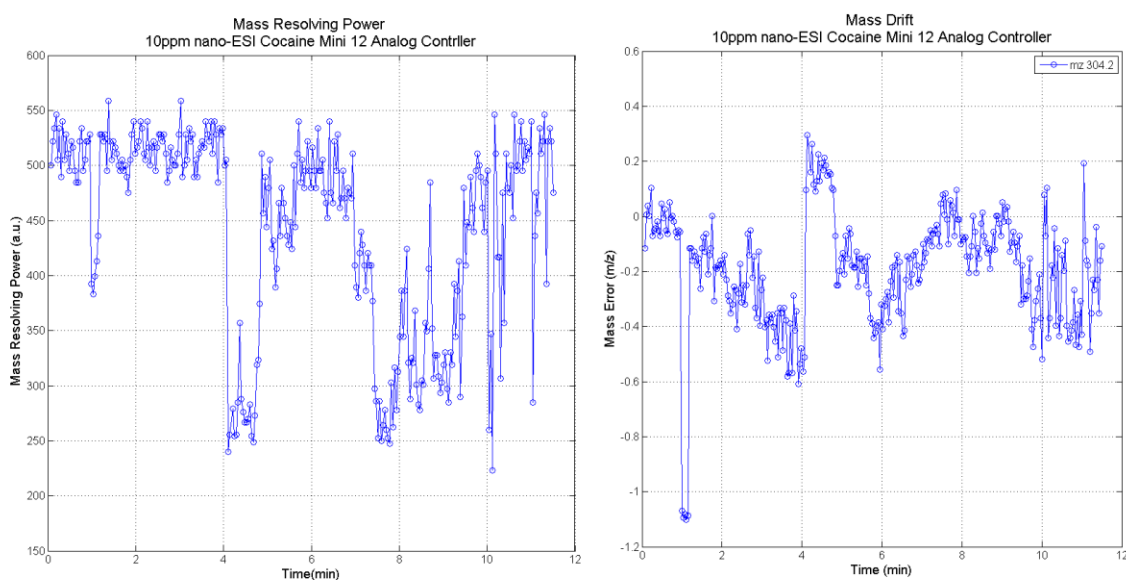


Figure 4-45 - Mass Resolving and Drift recorded using Mini 12 electronics and the analog controller for a 10ppm sample of Cocaine (m/z 304.2)

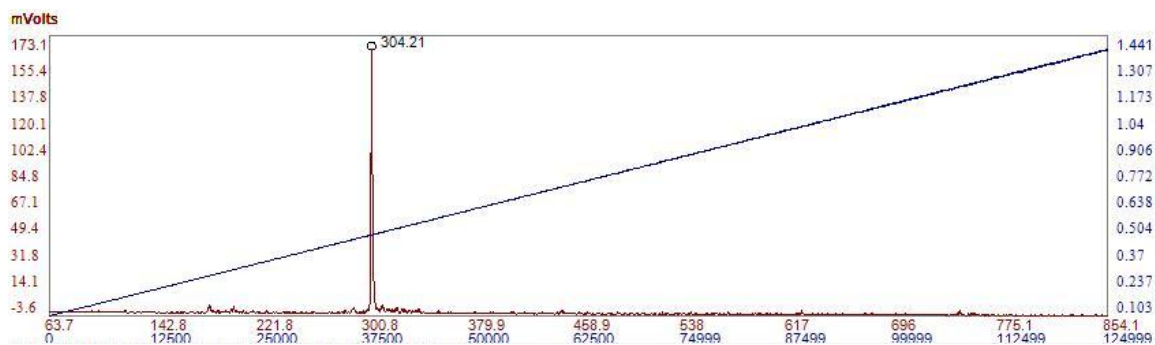


Figure 4-46 - Example Single Scan mass spectra of a 10ppm sample of Cocaine (m/z 304.2) collected with the Mini 12 electronics and digital controller

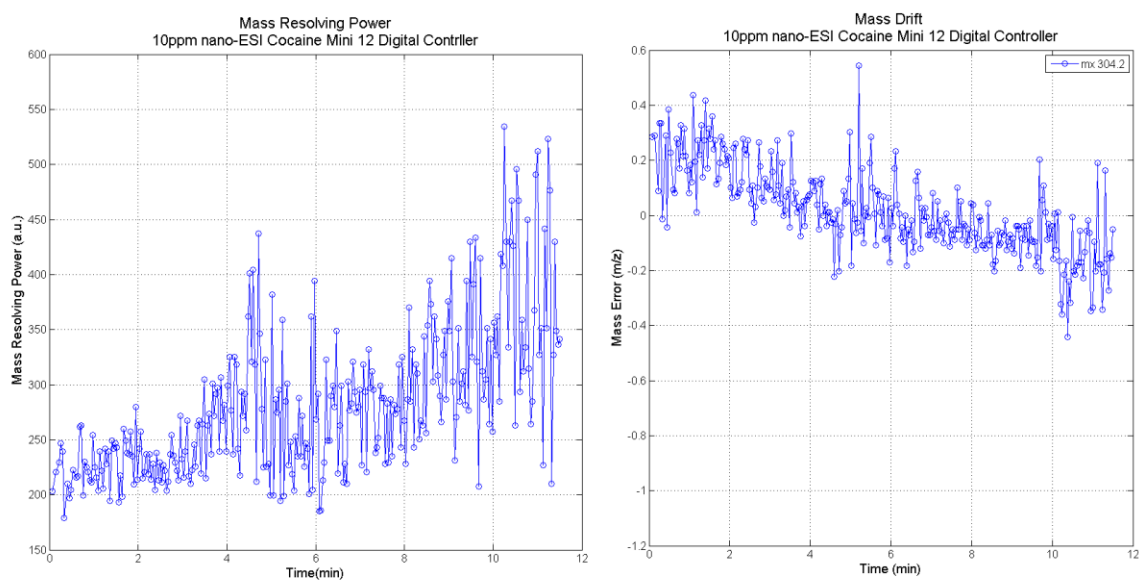


Figure 4-47 - Mass Resolving and Drift recorded using Mini 12 electronics and the digital controller for a 10ppm sample of Cocaine (m/z 304.2)

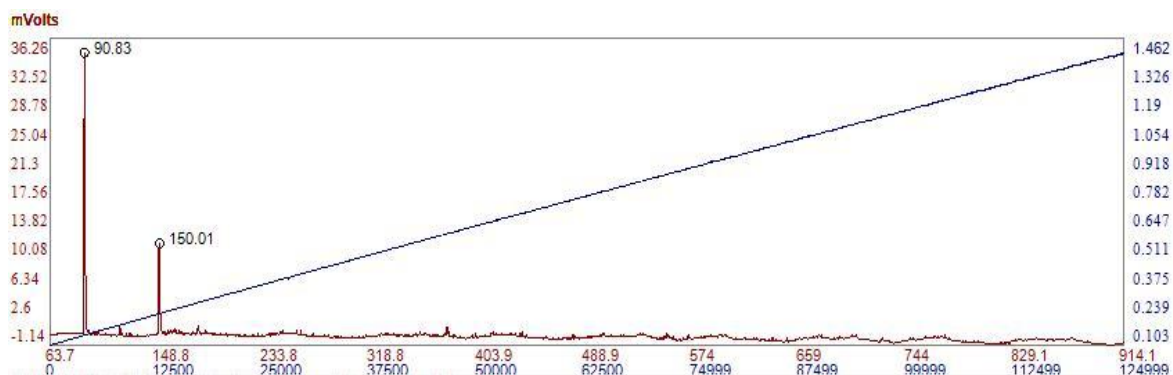


Figure 4-48 - Example Single Scan mass spectra of a 10ppm sample of Methamphetamine (m/z 150, fragment m/z 91) collected with the Mini 12 electronics and analog controller

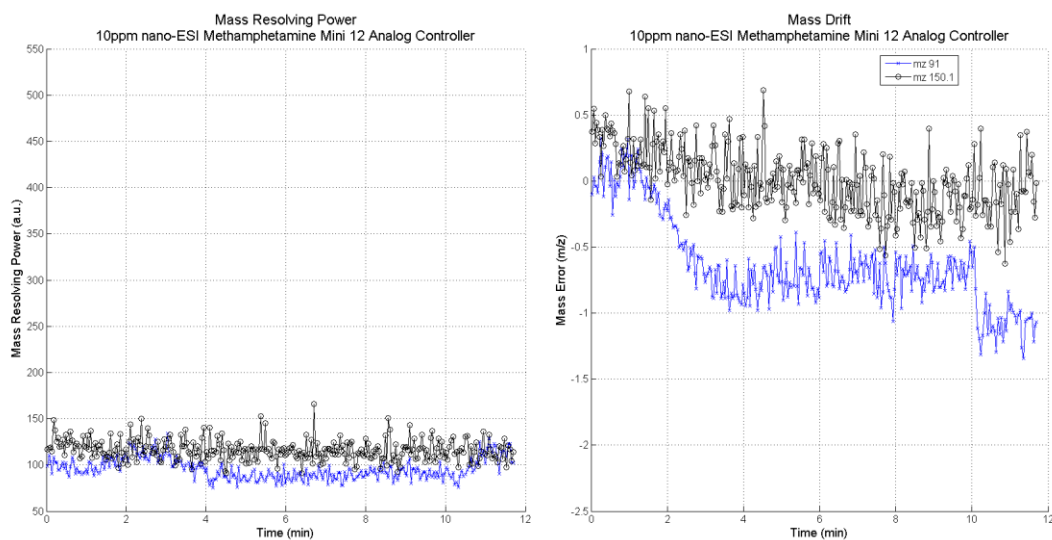


Figure 4-49 – Mass Resolving and Drift recorded using Mini 12 electronics and the analog controller for a 10ppm sample of Methamphetamine (m/z 150, fragment m/z 91)

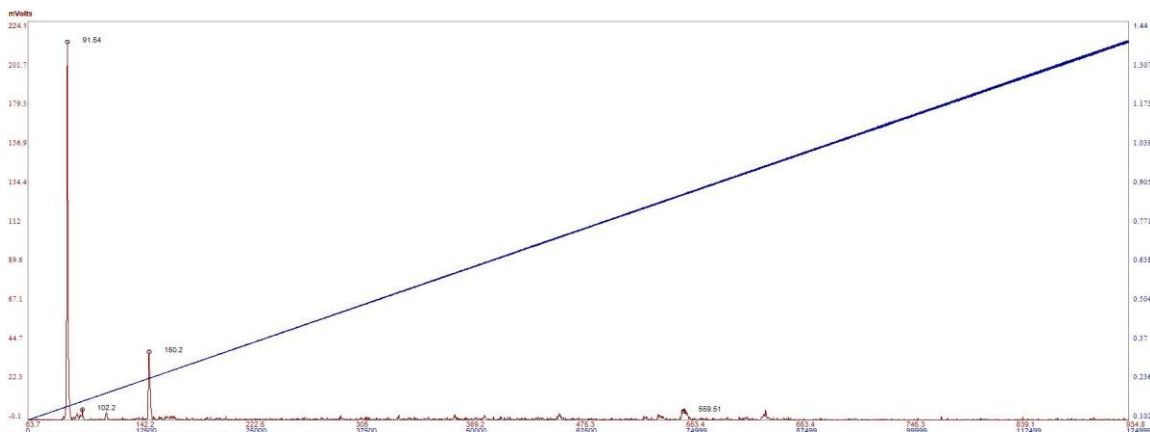


Figure 4-50 – Example Single Scan mass spectra of a 10ppm sample of Methamphetamine (m/z 150, fragment m/z 91) collected with the Mini 12 electronics and digital controller

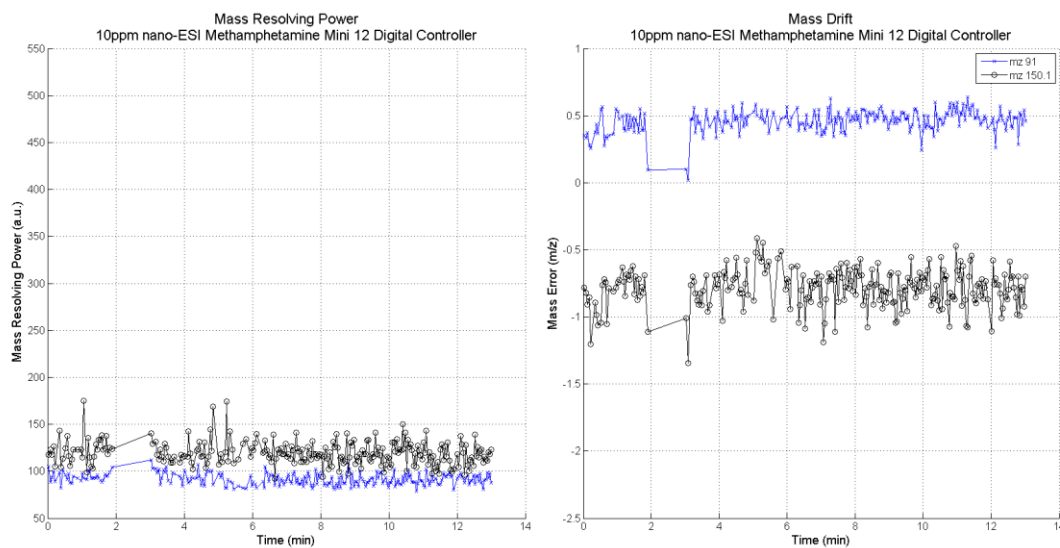


Figure 4-51 - Mass Resolving and Drift recorded using Mini 12 electronics and the digital controller for a 10ppm sample of Methamphetamine (m/z 150, fragment m/z 91)

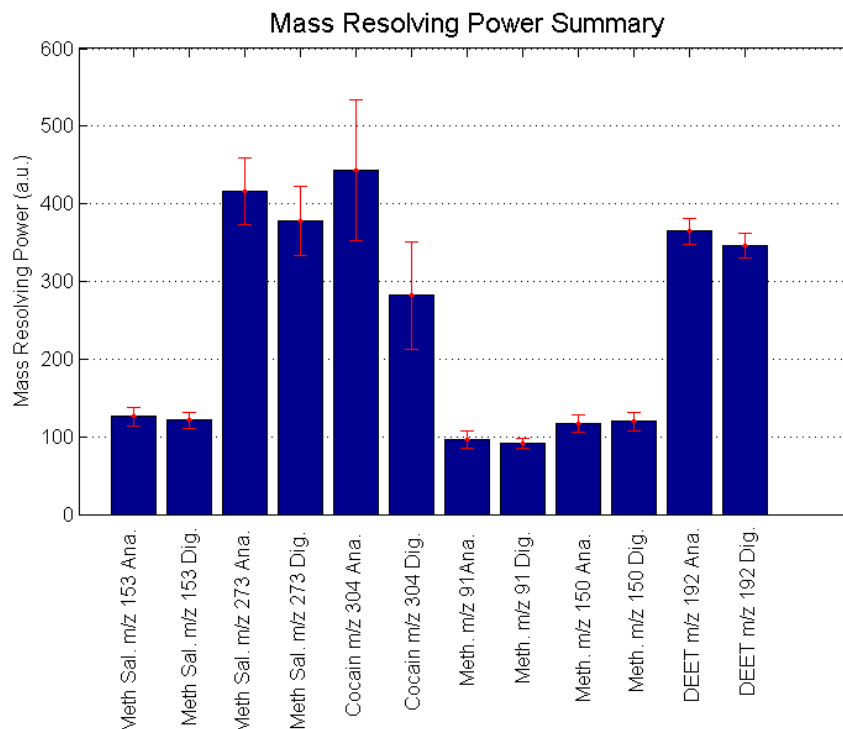


Figure 4-52 – Mass Resolving Power Summary for both Analog and Digital Controller for compounds Methyl Salicylate, Cocaine, Methamphetamine, and DEET

The percentage of peak height to the valley depth used to determine the unit mass resolution was unclear in previous Mini instrument publications. Unit mass resolution was claimed from Figure 5 in the paper written by Gao et al., 2006 on the Mini 10 instrument with the statement: “The peaks due to the molecular ion m/z 92 and the fragment ion m/z 91 are well-separated, indicating unit resolution at this m/z value.” The percentage of the valley to the peak height was estimated to be 18%. Using the 18% valley criteria, a sample of Tamoxifen (m/z 373.5) that had been isotopically labeled with an equal concentration at m/z 375 was ionized with a nano-ESI source and input into the instrument. The resulting spectrum from the digital controller and analog controller is shown in Figure 4-53 below. Only 115 scans were collected from the sample because of the limited quantity available, but the average of the 115 scans confirmed the equal concentration (shown as red line in Figure 4-53). The results of the

MATLAB analysis of the valley between the m/z 373.5 and m/z 375 peaks are shown in Figure 4-54. On average the peak valley using the digital controller was below 18%, but the standard deviation (error bars) is greater than 18%. When using the analog controller the average peak valley percentage increases to an average of 21%. Applying the Chapter 3 mass resolution definition, the Mini 12 electronics with the digital controller on average achieves 1.5 mass resolution. The analog controller degrades the mass resolution degrades to approximately 2.

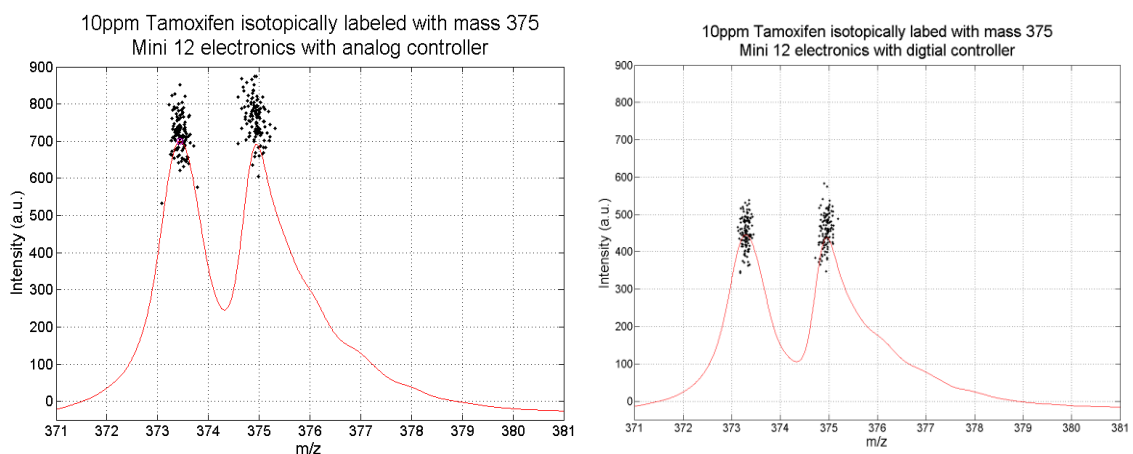


Figure 4-53 – Mass Spectrum of isotopically labeled Tamoxifen

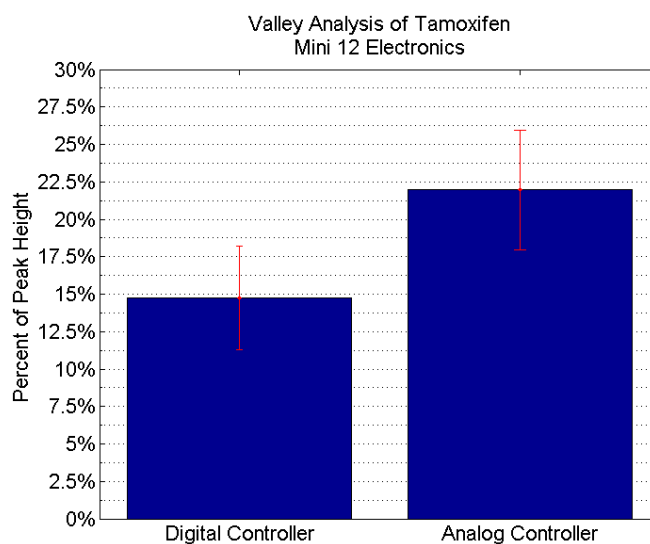


Figure 4-54 – Peak Valley presented as a percentage of peak intensity

4.3.4. Cost Analysis

A cost analysis for the analog and digital controller solutions as implemented in the Mini 12 data acquisition electronics was done. Discrete parts that had costs of less than \$0.10 were excluded from the analysis, leaving the most expensive components. The required electrical parts needed to operate the digital controller in the Mini 12 setup consisted of a high speed 16-bit ADC and the additional circuitry to accompany it. Table 4-1 reflects the \$58.30 additional cost of the ADC circuit needed to sample the RF feedback signal.

The analog controller solution does not need the ADS1610, but did need operational amplifiers to rectify, buffer, mix and correct the RF signal. Table 4-2 shows the cost of these additional blocks to be \$14.55.

Table 4-1 – Digital Controller Cost on Mini 12 electronics

Manufacturer	Part Number	Function	Cost @1000	Quantity	Quote Source	Sub Total
Texas Instruments	ADS1610IPAPT	ADC 10Msps 16-bit	\$ 27.34	1	Mouser	\$ 27.34
Texas Instruments	THS4503CDR	ADC front end op amps	\$ 5.20	1	DigiKey	\$ 5.20
National Semiconductor	LM6172IMX/NOPB	ADC front end op amps	\$ 2.02	2	DigiKey	\$ 4.04
Texas Instruments	THS3092DDA	ADC refernces op amps	\$ 7.75	2	DigiKey	\$ 15.50
Texas Instruments	OPA4227UA	ADC refernces op amps	\$ 6.22	1	DigiKey	\$ 6.22
Total Cost						\$ 58.30

Table 4-2 – Analog Controller Cost on Mini 12 electronics

Manufacturer	Part Number	Function	Cost @1000	Quantity	Quote Source	Sub Total
National Semiconductor	LM6172IMX/NOPB	Precision Rectifier	\$ 2.02	2	DigiKey	\$ 4.04
National Semiconductor	LM6171AIM/NOPB	Controlling Amp	\$ 1.81	1	DigiKey	\$ 1.81
National Semiconductor	LM6172IMX/NOPB	Buffering	\$ 2.02	1	DigiKey	\$ 2.02
Analog Devices	AD8330ACPZ-R7	Mixer	\$ 6.68	1	DigiKey	\$ 6.68
Total Cost						\$ 14.55

4.4. Summary

In this chapter spectral data from compounds DEET, methyl salicylate, cocaine, and methamphetamine have been presented and measured for mass drift and mass resolving power. A solution of PEG was used to demonstrate the mass accuracy across the dynamic operating range of the instrument. Isotopically labeled tamoxifen was used to measure the mass resolution. A cost analysis was done to compare the implementation costs in the Mini 12 data acquisition electronics. RF system simulations were done to facilitate the development and design of the FPGA based digital PID controller. Linearity results were presented for the digital and analog controller. Lastly, signal outputs were measured for total harmonic distortion, accuracy, and spurious free dynamic range.

CHAPTER 5. CONCLUSIONS

Contributions:

- Simulation of RF System
- Simulations of FPGA VHDL design blocks
- Custom designed and programmed Mini 12 data acquisition boards
- A characterized mass spectrometer system
- Double the mass spectral throughput rate while sampling up 25 times faster than the Mini 11.5 data acquisition system
- A comparison of the performance of an analog versus digital RF controller system in a MS

Simulations were created to facilitate in the design of the digital controller and characterize the RF system. These simulations will be important for the portability of the design to new amplifiers or other FPGA devices. Also the FPGA simulations could be used as a tool to visualize the digital controller functionality.

The Mini 12 electronic acquisition board designed during this research has improved upon the previous Mini 11.5 design. It has doubled the mass spectral throughput rate by using the USB 2.0 interface to stream data to the user interface as it was collected during mass analysis. Sustainable data sample rates were also increased to 2.5Msps from 100ksps when sampling a single channel. The sample rate could be divided among the RF envelope and ion detector signals, sampling each at 1.25Msps. The diagnostic information contained in the RF envelope was collected and displayed to the user for the first time in a miniature instrument.

From this study of the RF amplifier control system used in miniature mass spectrometers, an understanding of the controller performance has been gained through experimental results. Measures of quality used to test the resulting mass spectra from both analog and digital controllers were mass resolution, mass resolving power, mass accuracy, and mass drift. Six different compounds were tested.

Linearity testing of the amplified voltage showed that the analog controller on both electrical setups was not completely linearly modulated and not capable of removing all the RF amplifier open loop defects (Figure 4-25, Figure 4-27 and Figure 4-28). The newly designed digital solution as compared to the analog solution had a more linear response and could remove the RF amplifier open loop defects. The non-linear modulated ramp produced with the analog controller did cause mass errors along the x-axis as shown in Figure 4-32. The digital controller did not have zero error as demonstrated by Figure 4-43.

The differences in the signal generation, if significant, would have been most apparent in the mass resolving power measurements. Of the five compounds tested only cocaine showed a significant deviation between the two solutions (Figure 4-52). Mass resolving power in mass spectrometers is most affected by the pressure at scan out and AC signal, which were held constant during this study leaving only the RF amplification and ionization source to account for differences.

The research question asked whether a digital controller is better than the Mini 11.5 analog controller. The application of the instrument plays an important role in determining this because tradeoffs of cost, accuracy, mass range, or throughput. In the case of a miniature mass spectrometer that needs to be small, cheap and repeatable. The digital controller solution offers the ability to change the controller response from a computer interface and RF signal diagnostic information without any external test equipment connected. These attributes will impact the manufacturability of the system and could allow the automation of the

tuning process. Despite being a more expensive solution, the advantages of the digital controller over the analog solution are summarized here:

- Flexibility to change the response behavior in software in under 10 seconds at any time as opposed to more than 2 minutes to change components in a properly equipped laboratory
- Use of the demodulated RF feedback as diagnostic tool to find the resonance operating point in the field or when manufacturing
- Lower mass drift standard deviation: 0.19 versus 0.23 for the analog controller
- Lower mass drift range of 0.7983 versus 2.1704 for the analog controller
- Better mass accuracy across the mass range shown in Figure 4-31 and Figure 4-32
- Improved mass resolution by 0.5 m/z

The lower mass drift and better mass accuracy means that the uncertainty of analytes appearing in a mass spectrum will be lower than that of the analog controller and increasing the number of detectable analytes. The improved mass resolution will aid ascertaining mass spectra with an isotope or mixture of analytes spaced less than 2 m/z apart.

5.1. Future Work

The influence of the RF system on overall system performance was characterized in this research. This together with the development of a digital controller helped moving the mini mass spectrometer a step closer to becoming a device anyone could purchase and use for safety, health and security. There still is work needed to be done, which should be considered next, such as:

1. Automate the entire data collection and analysis
2. Explore a hybrid analog and digital controller

LIST OF REFERENCES

LIST OF REFERENCES

- Bennett, S. (1984). Nicholas Minorsky and the automatic steering of ships. *Control Systems Magazine, IEEE*, 4(4), 10-15.
- Branch, S., Burke, S., Evans, P., Fairman, B., & Wolff Briche, C. S. J. (2003). A preliminary study in determining the geographical origin of wheat using isotope ratio inductively coupled plasma mass spectrometry with ^{13}C , ^{15}N mass spectrometry. *J. Anal. At. Spectrom.*, 18(1), 17-22.
- Bruins, A. P. (1991). Mass spectrometry with ion sources operating at atmospheric pressure. *Mass Spectrometry Reviews*, 10(1), 53-77.
- CAID - Center for Analytical Instrumentation Development. (n.d.). . Retrieved December 11, 2010, from <http://caid.chem.purdue.edu/prototyping.html>
- Campana, J. E. (1987). Time-of-Flight Mass Spectrometry: a Historical Overview. *Instrumentation Science & Technology*, 16(1), 1 - 14.
- Chen, L., Wang, T. C. L., Ricca, T. L., & Marshall, A. G. (1987). Phase-modulated stored waveform inverse Fourier transform excitation for trapped ion mass spectrometry. *Analytical Chemistry*, 59(3), 449-454.
doi:doi: 10.1021/ac00130a016

- El-Faramawy, A., Siu, K. W. M., & Thomson, B. A. (2005). Efficiency of Nano-Electrospray Ionization. *Journal of the American Society for Mass Spectrometry*, 16(10), 1702-1707. doi:doi: 10.1016/j.jasms.2005.06.011
- Gao, L., Cooks, R. G., & Ouyang, Z. (2008). Breaking the Pumping Speed Barrier in Mass Spectrometry: Discontinuous Atmospheric Pressure Interface. *Analytical Chemistry*, 80(11), 4026-4032. doi:doi: 10.1021/ac800014v
- Gao, L., Song, Q., Patterson, G. E., Cooks, R. G., & Ouyang, Z. (2006). Handheld Rectilinear Ion Trap Mass Spectrometer. *Analytical Chemistry*, 78(17), 5994-6002. doi:doi: 10.1021/ac061144k
- Gao, L., Sugiarto, A., Harper, J. D., Cooks, R. G., & Ouyang, Z. (2008). Design and Characterization of a Multisource Hand-Held Tandem Mass Spectrometer. *Analytical Chemistry*, 80(19), 7198-7205. doi:doi: 10.1021/ac801275x
- Harper, J. D., Charipar, N. A., Mulligan, C. C., Zhang, X., Cooks, R. G., & Ouyang, Z. (2008). Low-Temperature Plasma Probe for Ambient Desorption Ionization. *Analytical Chemistry*, 80(23), 9097-9104. doi:doi: 10.1021/ac801641a
- Hoffmann, E. de, & Stroobant, V. (2007). *Mass Spectrometry: Principles and Applications* (3rd ed.). West Sussex, England: John Wiley & Sons, Inc.

- Horning, E. C., Horning, M. G., Carroll, D. I., Dzidic, I., & Stillwell, R. N. (1973). New picogram detection system based on a mass spectrometer with an external ionization source at atmospheric pressure. *Analytical Chemistry*, 45(6), 936-943. doi:doi: 10.1021/ac60328a035
- Hu, Q., Noll, R. J., Li, H., Makarov, A., Hardman, M., & Graham Cooks, R. (2005). The Orbitrap: a new mass spectrometer. *Journal of Mass Spectrometry*, 40(4), 430-443.
- Jeffries, N. (2005). Algorithms for alignment of mass spectrometry proteomic data. *Bioinformatics*, 21(14), 3066-3073. doi:10.1093/bioinformatics/bti482
- Jonscher, K. R., & Yates, J. R. (1997). The Quadrupole Ion Trap Mass Spectrometer--A Small Solution to a Big Challenge. *Analytical Biochemistry*, 244(1), 1-15. doi:doi: DOI: 10.1006/abio.1996.9877
- Julian, R. K., & Cooks, R. G. (1993). Broad-band excitation in the quadrupole ion trap mass spectrometer using shaped pulses created with the inverse Fourier transform. *Analytical Chemistry*, 65(14), 1827-1833. doi:doi: 10.1021/ac00062a006
- Kaiser Jr., R. E., Graham Cooks, R., Stafford Jr., G. C., Syka, J. E. P., & Hemberger, P. H. (1991). Operation of a quadrupole ion trap mass spectrometer to achieve high mass/charge ratios. *International Journal of Mass Spectrometry and Ion Processes*, 106, 79-115. doi:doi: DOI: 10.1016/0168-1176(91)85013-C

- Kaplan, D. A. (2006). *Improvements to the analytical performance of ion trap mass spectrometry*. ProQuest, UMI Dissertations Publishing. Retrieved from <http://search.proquest.com/docview/305297896?accountid=13360>
- Karas, M., Bahr, U., & Dülcks, T. (2000). Nano-electrospray ionization mass spectrometry: addressing analytical problems beyond routine. *Fresenius' Journal of Analytical Chemistry*, 366(6), 669-676.
doi:10.1007/s002160051561
- Keil, A., Talaty, N., Janfelt, C., Noll, R. J., Gao, L., Ouyang, Z., & Cooks, R. G. (2007). Ambient Mass Spectrometry with a Handheld Mass Spectrometer at High Pressure. *Analytical Chemistry*, 79(20), 7734-7739. doi:doi: 10.1021/ac071114x
- Londry, F. A., & March, R. E. (1995). Systematic factors affecting high mass-resolution and accurate mass assignment in a quadrupole ion trap. *International Journal of Mass Spectrometry and Ion Processes*, 144(1-2), 87-103. doi:doi: DOI: 10.1016/0168-1176(95)04153-C
- March, Raymond E. (1997). An Introduction to Quadrupole Ion Trap Mass Spectrometry. *Journal of Mass Spectrometry*, 32(4), 351-369.
- Marshall, A. G. (1985). Fourier transform ion cyclotron resonance mass spectrometry. *Accounts of Chemical Research*, 18(10), 316-322. doi:doi: 10.1021/ar00118a006
- Mulligan, C. C., Talaty, N., & Cooks, R. G. (2006). Desorption electrospray ionization with a portable mass spectrometer: in situ analysis of ambient surfaces. *Chem. Commun.*, (16), 1709-1711.

- Ouyang, Z., & Cooks, R. G. (2009). Miniature Mass Spectrometers. *Annual Review of Analytical Chemistry*, 2(1), 187-214.
- Ouyang, Z., Wu, G., Song, Y., Li, H., Plass, W. R., & Cooks, R. G. (2004). Rectilinear Ion Trap: Concepts, Calculations, and Analytical Performance of a New Mass Analyzer. *Analytical Chemistry*, 76(16), 4595-4605. doi:doi:10.1021/ac049420n
- Paul, W. (1990). Electromagnetic traps for charged and neutral particles. *Rev. Mod. Phys.*, 62(3), 531–540. doi:10.1103/RevModPhys.62.531
- Schaefer, R. T., MacAskill, J. A., Mojarradi, M., Chutjian, A., Darrach, M. R., Madzunkov, S. M., & Shortt, B. J. (2008). Digitally synthesized high purity, high-voltage radio frequency drive electronics for mass spectrometry. *Review of Scientific Instruments*, 79(9), 095107.
- Schwartz, J. C., Senko, M. W., & Syka, J. E. P. (2002). A two-dimensional quadrupole ion trap mass spectrometer. *Journal of the American Society for Mass Spectrometry*, 13(6), 659-669. doi:doi: DOI: 10.1016/S1044-0305(02)00384-7
- Segura, J., Gutiérrez-Gallego, R., Ventura, R., Pascual, J. A., Bosch, J., Such-Sanmartín, G., Nikolovski, Z., et al. (2009). Growth Hormone in Sport: Beyond Beijing 2008. *Therapeutic Drug Monitoring*, 31(1), 3-13. doi:10.1097/FTD.0b013e318194cc94.

- Song, Q., Xu, W., Smith, S. A., Gao, L., Chappell, W. J., Cooks, R. G., & Ouyang, Z. (2010). Ion trap mass analysis at high pressure: an experimental characterization. *Journal of Mass Spectrometry*, 45(1), 26-34.
- Sullivan, C. R., Weidong Li, Prabhakaran, S., & Shanshan Lu. (2007). Design and Fabrication of Low-Loss Toroidal Air-Core Inductors. *Power Electronics Specialists Conference, 2007. PESC 2007. IEEE* (pp. 1754-1759). Presented at the Power Electronics Specialists Conference, 2007. PESC 2007. IEEE.
- Wang, H., Liu, J., Cooks, R. Graham, & Ouyang, Z. (2010). Paper Spray for Direct Analysis of Complex Mixtures Using Mass Spectrometry13. *Angewandte Chemie International Edition*, 49(5), 877-880.
- Yang, M., Kim, T.-Y., Hwang, H.-C., Yi, S.-K., & Kim, D.-H. (2008). Development of a Palm Portable Mass Spectrometer. *Journal of the American Society for Mass Spectrometry*, 19(10), 1442-1448. doi:doi: DOI: 10.1016/j.jasms.2008.05.011

APPENDIX

APPENDIX

Figure A-1 – VHDL PID Controller Code Listing

```

1  -----
2  -- Function      : PID_Controller
3  -- Coder         : Matthew A Kirlis
4  -- Date          : 4/14/2011
5  -- Translator    :
6  -----
7  library ieee;
8  use ieee.std_logic_1164.all;
9  use ieee.std_logic_unsigned.all;
10 use ieee.std_logic_arith.all;
11
12 entity PID_Controller is
13 port (
14     set_point      : in std_logic_vector (15 downto 0);
15     error           : in std_logic_vector (15 downto 0);
16     max_correct     : in std_logic_vector (15 downto 0);
17     min_operate     : in std_logic_vector (15 downto 0); --Deadband where not to operate
18     p_gain          : in std_logic_vector (11 downto 0);
19     i_gain          : in std_logic_vector (11 downto 0);
20     d_gain          : in std_logic_vector (11 downto 0);
21     new_error_in    : in std_logic;
22     corrected_ready : out std_logic; -- pulses high when new signal is ready
23     corrected       : out std_logic_vector (15 downto 0);
24     i_vector        : out std_logic_vector (15 downto 0);
25     p_vector        : out std_logic_vector (15 downto 0);
26     enable          : in std_logic;
27     nRESET           : in std_logic; -- async reset.
28     clk             : in std_logic -- Input clock
29 );
30 end entity;
31
32 architecture behave of PID_Controller is
33     signal error_in : signed (15 downto 0) := x"0000";
34     signal set_in   : signed (15 downto 0) := x"0000";
35     signal last_error : signed (15 downto 0) := x"0000";
36     signal diff_error : signed (15 downto 0) := x"0000";
37     signal sum_error  : signed (15 downto 0) := x"0000";
38     signal last_sum_error : signed (15 downto 0) := x"0000";
39     signal p          : signed (28 downto 0) := '0' & x"00000000";

```

```

40 signal I      : signed (28 downto 0) := '0' & x"00000000";
41 signal D      : signed (28 downto 0) := '0' & x"00000000";
42 signal error_adj : signed (15 downto 0) := x"0000";
43 signal temp1_adj : signed (15 downto 0) := x"0000";
44 signal temp2_adj : signed (15 downto 0) := x"0000";
45 SIGNAL state    : INTEGER RANGE 0 TO 9 := 0;
46 signal i_test : signed (15 downto 0) := x"0000"; --test vector
47 signal p_test : signed (15 downto 0) := x"0000"; --test vector
48 begin
49
50   PID_Loop: process (clk, nRESET, set_point, min_operate, new_error_in, enable, error,
max_correct) begin
51     if (nReset <= '0') then
52       corrected <= (others => '0');
53       corrected_ready <= '0';
54       error_in <= (others => '0');
55       last_error <= (others => '0');
56       diff_error <= (others => '0');
57       sum_error <= (others => '0');
58       last_sum_error <= (others => '0');
59       state <= 0;
60     elsif (rising_edge(clk)) then
61       if (set_point > min_operate) and enable = '1' then
62         ----- To create an output correction
63         --0 Wait for new_sample and latch in error_in/set_point with it arrives
64         --1 Calculate slope (subtract) and apply Ki to error_in (16-bit signed)
65         --2 saturate if needed
66         --3 multiply Kp, Kd (3.99 to 0) with P and D error signals and sum of I error
signal (16-bit signed output)
67         --4 saturate if needed
68         --5 Calculate the Correction Sum of the P, I, D
69         --6 Saturate if needed and ensure less than max correction
70         --7 Calculate correction value of Correction Sum + Set point
71         --8 saturate if needed and mult by 2 (external) to make (unsigned 16-bit)
indicate correction_ready
72
73       if state = 0 then
74         if (new_error_in = '1') then
75           error_in <= signed(error);

```

```

76     set_in <= signed(set_point);
77     state <= 1;
78     end if;
79     corrected_ready <= '0';
80     end if;
81
82     if state = 1 then
83         diff_error <= error_in - last_error;
84         I <= error_in * signed('0' & i_gain); --new
85         state <= 2;
86     end if;
87
88     if state = 2 then
89         last_error <= error_in;
90         if diff_error(15) = '1' and last_error(15) = '1' and error_in(15) = '0' then
91             diff_error <= x"7FFF";
92         elsif diff_error(15) = '0' and last_error(15) = '0' and error_in(15) = '1' then
93             diff_error <= x"8000";
94         end if;
95
96         if (I(28 downto 10) < -32768) and error_in(15) = '1' then
97             I(25 downto 10) <= x"8000";
98         elsif (I(28 downto 10) > 32767) and error_in(15) = '0' then
99             I(25 downto 10) <= x"7FFF";
100        end if;
101
102        state <= 3;
103    end if;
104
105    if state = 3 then
106        p <= error_in * signed('0' & p_gain);
107        sum_error <= last_sum_error + I(25 downto 10);
108        D <= diff_error * signed('0' & d_gain);
109
110
111        state <= 4;
112    end if;
113
114    if state = 4 then

```

```

115 --starate P,I,D calc
116 if (P(28 downto 10) < -32768) and error_in(15) = '1' then
117     P(25 downto 10) <= x"8000";
118 elseif (P(28 downto 10) > 32767) and error_in(15) = '0' then
119     P(25 downto 10) <= x"7FFF";
120 end if;
121
122 if sum_error(15) = '1' and last_sum_error(15) = '0' and I(25) = '0' then
123     sum_error <= x"7FFF";
124     last_sum_error <= x"7FFF";
125 elseif sum_error(15) = '0' and last_sum_error(15) = '1' and I(25) = '1' then
126     sum_error <= x"8000";
127     last_sum_error <= x"8000";
128 else
129     last_sum_error <= sum_error;
130 end if;
131
132 if (D(28 downto 10) < -32768) and diff_error(15) = '1' then
133     D(25 downto 10) <= x"8000";
134 elseif (D(28 downto 10) > 32767) and diff_error(15) = '0' then
135     D(25 downto 10) <= x"7FFF";
136 end if;
137
138 state <= 5;
139 end if;
140
141 if state = 5 then
142     i_test <= sum_error; --new
143     p_test <= P(25 downto 10);
144     temp1_adj <= P(25 downto 10) + set_in;
145     temp2_adj <= sum_error + D(25 downto 10);
146     state <= 6;
147 end if;
148
149 if state = 6 then --intermediate saturation
150     if (temp1_adj(15) = '1' and P(25) = '0' and set_in(15) = '0') or
151         (temp2_adj(15) = '1' and sum_error(15) = '0' and D(25) = '0') then
152         error_adj <= x"7FFF";
153     elseif (temp1_adj(15) = '0' and P(25) = '1' and set_in(15) = '1') or

```



```

154 (temp2_adj(15) = '0' and sum_error(15) = '1' and D(25) = '1') then
155   error_adj <= x"0000";
156   else
157     error_adj <= temp1_adj + temp2_adj;
158   end if;
159   state <= 7;
160   end if;
161
162   if state = 7 then --Final Saturation
163     if error_adj(15) = '1' and temp1_adj(15) = '0' and temp2_adj(15) = '0' then
--pos overflow set_in(15) will always be 0
164       error_adj <= x"7FFF";
165       elsif error_adj(15) = '0' and temp1_adj(15) = '1' and temp2_adj(15) = '1' then
--neg overflow
166         error_adj <= x"0000";
167         elsif error_adj(15) = '1' then --neg overflow
168           error_adj <= x"0000";
169         end if;
170         state <= 8;
171       end if;
172
173       if state = 8 then
174         corrected <= std_logic_vector(error_adj);
175         corrected_ready <= '1';
176         state <= 0;
177       end if;
178
179     elsif (set_point <= min_operate) and enable = '1' then
--don't adjust
180       corrected_ready <= '0';
181     corrected <= set_point;
182   elsif (set_point > min_operate) and enable = '0' then
--reset to initial conditions
183     corrected_ready <= '0';
184     error_in <= (others => '0');
185     last_error <= (others => '0');
186     diff_error <= (others => '0');
187     sum_error <= (others => '0');
188     last_sum_error <= (others => '0');
189
190

```

```

191         corrected <= set_point;
192     elsif (set_point <= min_operate) and enable = '0' then
193         --reset to initial conditions
194         corrected_ready <= '0';
195         error_in      <= (others => '0');
196         last_error    <= (others => '0');
197         diff_error    <= (others => '0');
198         sum_error     <= (others => '0');
199         last_sum_error <= (others => '0');
200         corrected <= set_point;
201     end if;
202 end if;
203 end process PID_Loop;
204
205 i_vector <= std_logic_vector(i_test);
206 p_vector <= std_logic_vector(p_test);
207
208 end architecture;
209

```